A Detailed Investigation of the Reaction of 5,9-Diphenylbenz[*a*]azulene with Dialkyl Acetylenedicarboxylates Leading to Dialkyl 8,12-Diphenylbenzo[*a*]heptalene-6,7-dicarboxylates

by **Anthony Linden**, **Markus Meyer**[1]), **Peter Mohler**[2]), **Andreas J. Rippert**, and **Hans-Jürgen Hansen***

Organisch-chemisches Institut der Universität Zürich, Winterthurerstrasse 190, CH-8057 Zürich

The synthesis of 5,9-diphenylbenz[*a*]azulene (**1**) from 1,3-diphenylcyclopent[*a*]indene-2,8-dione (**4**) and cyclopropene has been re-investigated. The reduction of the decarbonylated cycloadduct **5** with $LiAlH_4/AlCl_3$ in Et_2O leads not only to the expected 7,10-dihydrobenz[*a*]azulene **6**, but also to small amounts of the cyclopropa[*b*]fluorenes *exo*-**7** and *endo*-**7** (*cf. Scheme 2*), the structures of which have been determined by X-ray crystal-structure analysis (*cf. Fig. 1*). The reaction of **1** with dialkyl acetylenedicarboxylates (ADR) in MeCN at 100° in the presence of 2 mol-% of catalysts such as $[RuH_2(PPh_3)_4]$ results mainly in the formation of the expected 8,12-diphenylbenzo[*a*]heptalene-6,7-dicarboxylates **3**. A thorough investigation of the reaction mixture of **1** and dimethyl acetylenedicarboxylate (ADM) revealed the presence of a number of intermediates and side products (*Scheme 5*). Most important was the isolation and identification of the cyclobutene intermediate **9a** (*cf. Fig. 4*), which is formed by a zwitterionic rearrangement of the primary adduct **2a** of **1** and ADM and represents the direct precursor of the heptalene-diester **3a**. Compounds of type **9a** have so far only been postulated as necessary intermediates in the thermal reaction of azulenes and ADR to give corresponding heptalenedicarboxylates. Compound **9a** is photochemically unstable and undergoes rearrangement even under the influence of normal laboratory light into a mixture of *trans*-**10a** and *cis*-**10a** (*Scheme 8*). Both diastereoisomers are also found in the original reaction mixture of **1** and ADM, but not when the reaction is performed under exclusion of light. On heating in MeCN at 100°, or better in DMF at 150°, *trans*-**10a** and *cis*-**10a** undergo rearrangement to the fluoranthene-1,2-dicarboxylate **11a** (*Scheme 9*), which is also present in the original reaction mixture of **1** and ADM. The catalysts do not accelerate the reaction of **1** and ADR, but they lead to better yields of the benzo[*a*]heptalene-6,7-dicarboxylates **3**, especially in the reaction of **1** with diisopropyl acetylenedicarboxylate (ADiP) (*cf. Tables 1* and *2*).

1. Introduction. – Recently, we have shown that 5,9-diphenylbenz[*a*]azulene (**1**) reacts with excess dimethyl acetylenedicarboxylate (ADM) in the presence of catalytic amounts of $[RuH_2(PPh_3)_4]$ in MeCN to yield the tricyclic intermediate **2a** and the benzo[*a*]heptalene-6,7-dicarboxylate **3a** (*Scheme 1*) [1]. Both products, **2a** and **3a**, are also formed when **1** and ADM are heated at 100° in supercritical CO_2 [2].

In the context of our interest in the synthesis of optically active bis-phosphanes with the backbone of **3** [3], we studied the formation of **3a**, as well as its alkyl analogues **3b**–**3d** (**b**: E_{Et}, **c**: $E_{i\text{-}Pr}$, and **d**: $E_{t\text{-}Bu}$), from **1** and the corresponding dialkyl acetylenedicarboxylates in the presence of catalysts such as $[RuH_2(PPh_{3)4}]$, $[RhH(PPh_3)_4]$, and $[Rh(cod)Cl]_2$ (cod = (*Z*,*Z*)-cycloocta-1,5-diene), or without a catalyst. We also re-investigated the synthesis of the starting azulene **1** [4], specifically with respect to its optimization and to clarify the formation of side products that we had observed in the course of the synthesis. In the following sections, we will discuss our

---

[1]) Part of the diploma thesis of *M. M.*, University of Zurich, 1995.

[2]) Part of the Ph. D. thesis of *P. M.*, University of Zurich, 1999.

Scheme 1

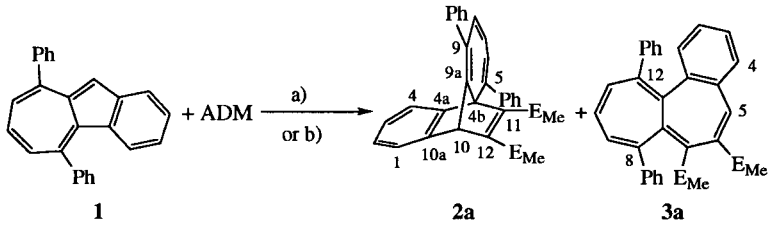

a) $[RuH_2(PPh_3)_4]$, 100°, MeCN [1]. b) 150 bar CO_2, 100° [2].

results that also corroborate our proposed mechanism for the formation of heptalene-dicarboxylates from azulenes and dialkyl acetylenedicarboxylates (*cf.* [5–7]).

2. Synthesis of 5,9-Diphenylbenz[*a*]azulene (1). – We precisely followed the procedure described by *Kapicak* and *Battiste* [4]. The reaction of the diphenylcyclopent[*a*]indene-dione **4**, which is readily available from ninhydrine and dibenzyl ketone [8], with cyclopropene, generated *in situ* from allyl chloride and $NaNH_2$ [9] and transferred with a stream of N_2 into the CH_2Cl_2 solution of **4**, took place smoothly at room temperature (*Scheme 2*)[3]). We obtained the decarbonylated *Diels-Alder* adduct **5** in yields up to 83%. The reduction of **5** with $LiAlH_4/AlCl_3$ in Et_2O gave 7,10-dihydrobenz[*a*]azulene **6** as yellow-to-orange-colored crystals[4]). Careful and repeated chromatography on silica gel with hexane/Et_2O mixtures finally yielded **6** as colorless crystals (in total 66%) and, in addition, an orange-colored fraction, from which *endo*-**7** was separated as orange crystals, which were contaminated with yellow-colored needles. Mechanical separation of the two crystalline forms showed that the yellow needles consisted of *exo*-**7**. The total yield of *endo*-**7** amounted to 5.2% and that of its diastereoisomer *exo*-**7** to 0.5%.

The prolonged chromatographic separation of the mixture of **6**, and *endo*-**7** and *exo*-**7** had already produced small amounts of the blue benz[*a*]azulene **1** – presumably as a result of dehydrogenation of **6** in air. However, a better method was to ionically dehydrogenate **6** with tritylium tetrafluoroborate, followed by treatment with Et_3N in CH_2Cl_2 (*cf.* [4]). This procedure led to pure **1** in yields of up to 52%.

Experiments with *endo*-**7** showed that treatment with *t*-BuOK in *t*-BuOH at 50° transforms it – at least partially – into **6**. Irradiation of hexane solutions of *endo*-**7** and *exo*-**7** with the 366-nm light from a fluorescent tube showed that *exo*-**7** could be partially transformed into *endo*-**7** whereas *endo*-**7** was stable under irradiation at the chosen concentration.

The ^{1}H-NMR spectrum ($CDCl_3$, 300 MHz) of **5** at 295 K exhibited for $CH_2(7)$ two broad signals at 3.13 and 2.20 ppm, which could be resolved at 263 K to a *td* signal with $^2J = 12.3$, and $^3J = 7.9$ and 6.6 Hz, respectively, in accordance with the non-planarity of the seven-membered ring in **5**. The coalescence temperature of the signals of $CH_2(7)$

---

[3]) The average yield of cyclopropene from allyl chloride and $NaNH_2$ amounted to 6–7%, in accordance with the investigations of *Closs* and *Krantz* [9], who reported that their yields of cyclopropene did not exceed 10%.

[4]) *Kapicak* and *Battiste* [4] described **6** as a non-crystalline glass.

Scheme 2

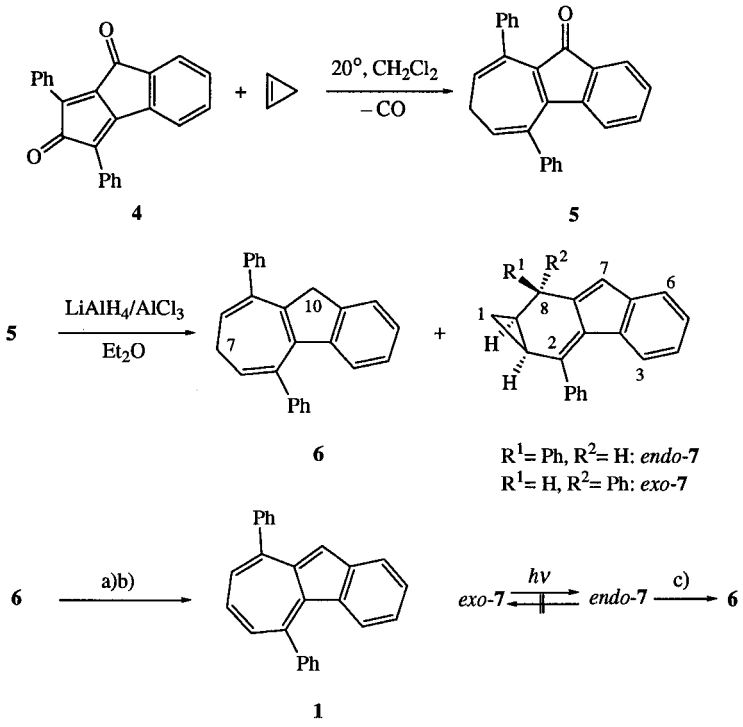

a) $Ph_3C^+BF_4^-$, 20°, CH_2Cl_2. b) Et_3N, 20°, CH_2Cl_2. c) *t*-BuOK/*t*-BuOH, 50°.

was found to be 320 K, which, with $\Delta\nu = 292.0$ Hz, corresponds to a free enthalpy of activation $\Delta G^{\ddagger}_{320} = (61.3 \pm 0.1)$ kJ · mol^{-1} for the ring-inversion process of the seven-membered ring. Similarly, the ^{1}H-NMR spectrum ($CDCl_3$, 300 MHz) of **6**, at 295 K, showed two signals for $CH_2(10)$, as well as for $CH_2(7)$, with coalescence temperatures of 296 and 300 K, respectively. The derived $\Delta G^{\ddagger}_{296}$ values of (57.8 ± 0.1) kJ · mol^{-1} for $CH_2(10)$ ($\Delta\nu = 164.9$ Hz) and (57.3 ± 0.1) kJ · mol^{-1} for $CH_2(7)$ ($\Delta\nu = 299.3$ Hz) indicate that both figures stand for the same exchange process, namely the inversion of the non-planar seven-membered ring in **6** (*Scheme 3*). The slightly lower $\Delta G^{\ddagger}$ value for the ring-inversion process in **6** compared with that of **5** ($\Delta\Delta G^{\ddagger} = -3.7$ kJ · mol^{-1}) might be due to the different states of hybridization of C(10) in **6** (sp^3) and **5** (sp^2), leading to

Scheme 3

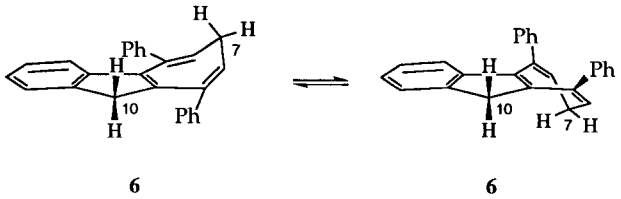

a higher transition-state strain in the cyclopentadienone substructure of **5** compared with the transition-state strain in the cyclopentadiene substructure of **6**. The observed $\Delta G_T^{\ddagger}$ values for the inversion of the seven-membered ring in **5** and **6** are within the range of that for other substituted, as well as benzo-anellated, cycloheptatrienes (*cf.* [10]).

The ^{1}H-NMR spectra of *endo*-**7** and *exo*-**7** were very similar, indicating that both compounds might represent diastereoisomers. Signals of coupled H-atoms in the range of 2.0 to 0.6 ppm were in agreement with the presence of a cyclopropane ring. However, the final structures of *endo*-**7** and *exo*-**7** were obtained from an X-ray crystal-structure analysis of both compounds (see *Fig. 1,a* and *b*). The dihedral angles

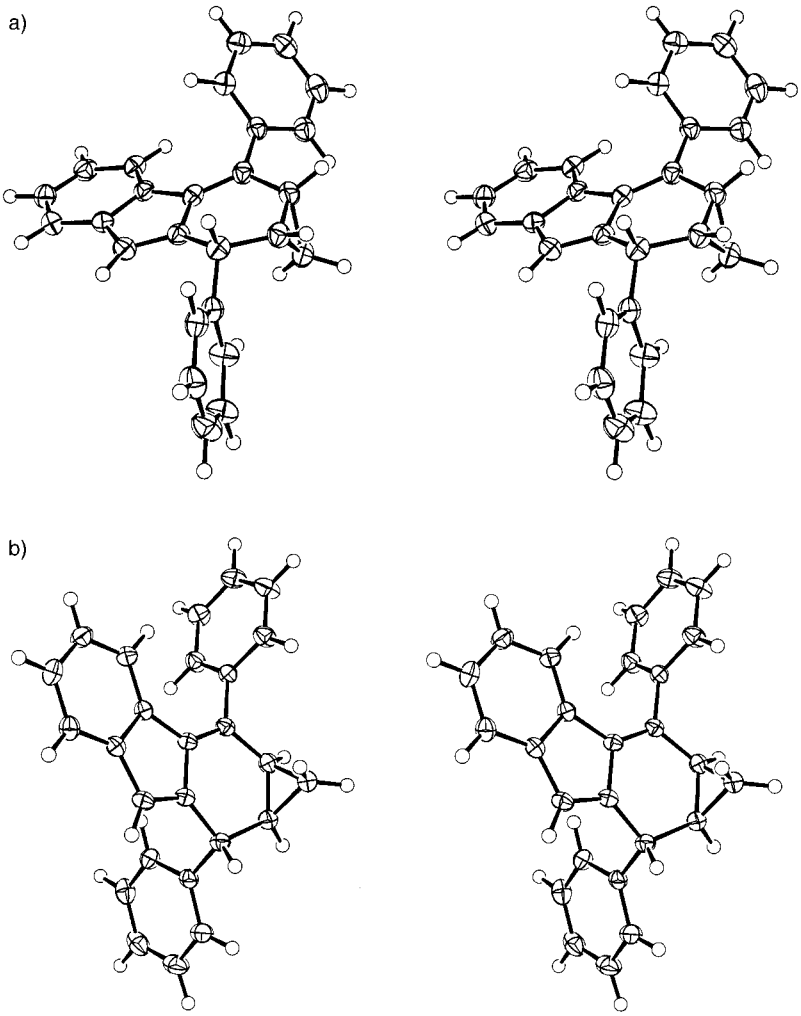

Fig. 1. *Stereoscopic views of the molecular structures of* a) endo- *and* b) exo-*1a,8a-dihydro-2,8-diphenyl-1*H,*8*H-*cyclopropa[*b*]*fluorene* (*endo*-**7** and *exo*-**7**, resp.)

H–C(1a)–C(8)–H amount to 48(2)° [37°][5]) for *endo*-**7** and to 82(2)° [89°] for *exo*-**7**. According to the *Karplus* equation (*cf.*, *e.g.*, [11]), one would expect vicinal coupling constants between H–C(1a) and H–C(8) in the range of 3–6 Hz for *endo*-**7** and 0–1 Hz for *exo*-**7**. The observed values of 5.1 Hz (*endo*-**7**) and 0.9 Hz (*exo*-**7**) are within these ranges.

We assume that **6**, *endo*-**7**, and *exo*-**7** are formed from the same intermediate cation **a**, which may be further reduced directly to **6**, or *via* its cyclized form **b**, to give *endo*-**7** and *exo*-**7** (*Scheme 4*). The observed *endo*/*exo* ratio of 10:1 is in agreement with the *exo*-face of cation **b** being much less sterically shielded against the approach of the reducing agent than its *endo*-face.

Scheme 4

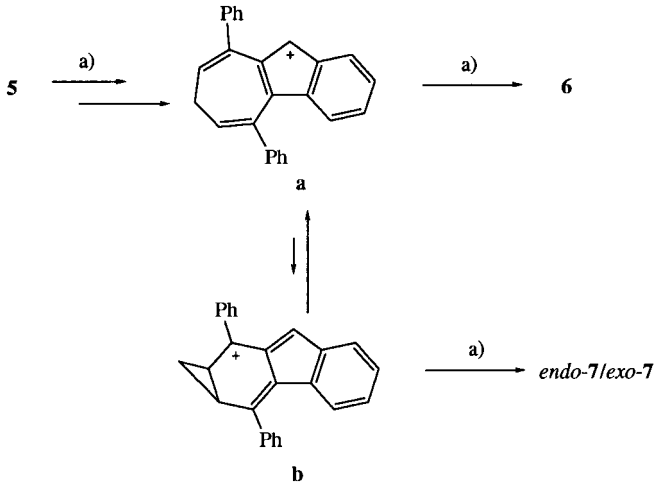

a) $LiAlH_4/AlCl_3$, Et_2O.

The ^{1}H-NMR spectrum ($CDCl_3$) of **1** shows two clearly different vicinal coupling constants of 8.8 and 11.4 Hz for the H-atoms at the seven-membered ring. Their size is in agreement with a distinct accentuation of the heptafulvene substructure in **1**, as we have recently discussed in detail [12].

3. Formation of Dialkyl 8,12-Diphenylbenzo[*a*]heptalene-6,7-dicarboxylates 3 from 1 and Dialkyl Acetylenedicarboxylates. – 3.1. *Product Pattern of the Reaction*. In our earlier experiments [1], we found that **1** reacted with a fourfold molar excess of ADM in the presence of 2 mol-% of $[RuH_2(PPh_3)_4]$ in MeCN at 100° to yield the benzo-anellated tricycle **2a** and the benzo[*a*]heptalene-6,7-dicarboxylate **3a** (*cf. Scheme 1*). Heating **2a** in DMF at 150° yielded mainly **3a** and small amounts of **1** [1]. The chromatographic workup of a large-scale reaction mixture of **1** and ADM revealed the presence of a number of further products (*Scheme 5*) which could be obtained in pure form. The composition of the reaction mixture was not changed significantly in the presence of other catalysts or without any catalyst (*Table 1*).

---

[5]) The corresponding dihedral angles from AM1 calculations are in brackets.

Scheme 5

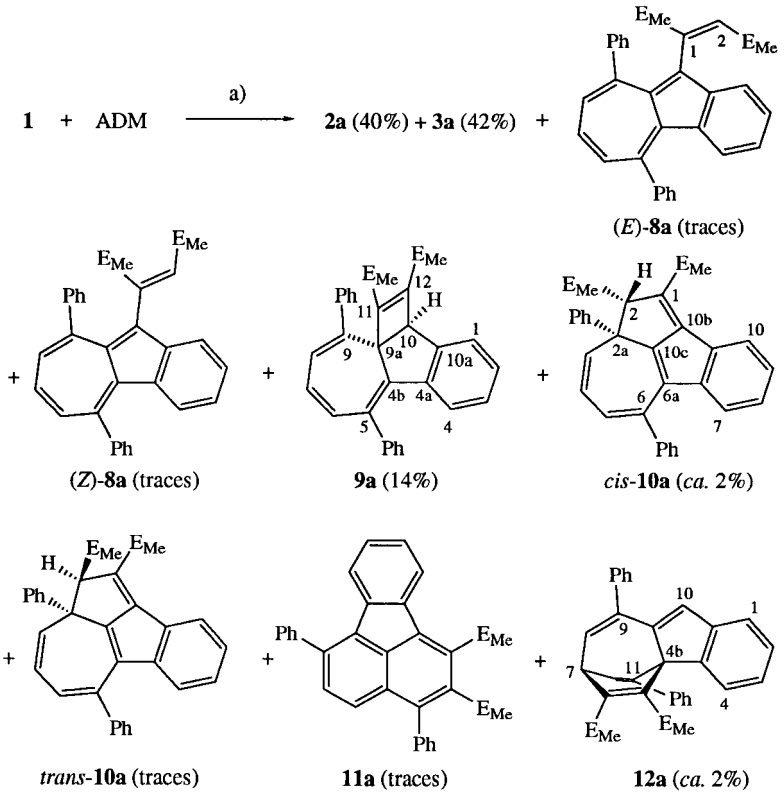

a) Azulene **1** was reacted with 3 mol-equiv. of ADM in the presence of 2 mol-% of $[RuH_2(PPh_3)_4]$, 100°/18 h, MeCN. The composition of the reaction mixture was determined by ^{1}H-NMR analysis. 'Traces' means that the relative amount of the corresponding compound was < 2%. The yield of pure and recrystallized **3a** amounted to 81% after heating the reaction mixture at 150°/1 h, DMF.

Table 1. *Thermal Reactions of* **1** *and ADM in MeCN in the Presence of Different Catalysts*[a])

Entry	Catalyst	Yields [%][b])		
		Tricycle **2a**	Tricycle **9a**	Heptalene **3a**[c])
1	$[RhH(PPh_3)_4]$	40	13	41 (91)
2	$[RhCl(cod)]_2$	33	3	53 (87)
3	$[RuH_2(PPh_3)_4]$	35	12	37 (81)
4	none	46	15.5	38 (83)

[a]) 3 Mol-equiv. of ADM were reacted in the presence of 2 mol-% of the catalyst at 100°/18 h. [b]) Relative yields determined by ^{1}H-NMR spectroscopy of the raw reaction mixtures. Trace amounts of the other products (*cf. Scheme 5*) were also recognizable. [c]) In parentheses, isolated yields of pure **3a** after heating the reaction mixtures in DMF, 150°/1 h.

Further experiments showed that the catalysts had no distinct influence on the reaction rates in MeCN[6]). On the other hand, reaction of **1** with diethyl, diisopropyl, or di(*tert*-butyl) acetylenedicarboxylate (ADE, ADiP, and AD*t*B, resp.) revealed that at least $[RuH_2(PPh_3)_4]$ had a clear influence on the composition of the reaction mixture in that the formation of side-products was much more suppressed in the presence of the catalyst (*Table 2*). For example, the reaction of **1** and diisopropyl acetylenedicarboxylate led to the formation of appreciable amounts of (*E*)-**8c** and (*Z*)-**8c** in addition to the main products **2c** and **3c**, whereas in the presence of $[RuH_2(PPh_3)_4]$ under the same conditions the tricycle **2c**, the precursor of **3c**, was formed predominantly. The same effect was observed when **1** and 3 mol-equiv. ADiP were reacted in MeCN in the presence of 20 mol-% of LiBr. Therefore, we assume that both the Ru^{II} complex and LiBr favor the zwitterionic rearrangement of the primary intermediate **2c** into the secondary tricycle **9c**, which then undergoes electrocyclic ring opening to give the final product **3c** (*cf.* [7])[7])[8]). However, a clear acceleration of the thermal rearrangement of **2c** to **9c** and then **3c** in the presence of 20 mol-% LiBr is not recognizable, since the first-order rate constants (MeCN, 100°) k_1(**2c**) = $(8.46 \pm 0.35) \cdot 10^{-6}\ s^{-1}$ and k_1(**2c**, LiBr) = $(9.24 \pm 0.45) \cdot 10^{-6}\ s^{-1}$ are still within the margins of error.

Table 2. *Yields of Dialkyl Heptalene-6,7-dicarboxylates* **3** *from the Reactions of* **1** *with Different Dialkyl Acetylenedicarboxylates*[a])

$E_R-C\equiv C-E_R$	ADM		ADE		ADiP		AD*t*B	
	A	*B*	*A*	*B*	*A*	*B*	*A*	*B*
Yield [%][b])	81	83	82	77	71	28	30	25
No.	**3a**		**3b**		**3c**		**3d**	

[a]) 3 Mol-equiv. of the acetylenedicarboxylates in the presence (*A*) or absence (*B*) of 2 mol-% of $[RuH_2(PPh_3)_4]$ were applied in MeCN, 100°/18 h (**3a** and **3b**) and 100°/40 h (**3c** and **3d**). [b]) Yields of pure heptalene-dicarboxylates **3** after heating the raw reaction mixture in DMF, 150°/1 h.

Most importantly, the secondary tricyclic intermediate **9a**, which is the direct precursor of the heptalene-6,7-dicarboxylate **3a**, could be observed and, for the first time, isolated, as well as characterized (see later). Kinetic experiments revealed that it is indeed the thermal rearrangement product derived from the primary tricyclic intermediate **2a**. *Fig. 2* shows the temporal course of the rearrangement of **2a** in MeCN at 100°. The secondary intermediate **9a** appears and vanishes again to yield the final product, the heptalene-6,7-dicarboxylate **3a**. The presence of very small amounts of (*E*)-**8a** and (*Z*)-**8a**, *cis*-**10a**/*trans*-**10a**, and **11a** (altogether $< 0.2\%$) were also observed by HPLC analysis. However, the tricycle **12a** was not found. It is present only in the original reaction mixture of **1** and ADM. The thermal rearrangement of **9a** under the same conditions led only to the formation of **3a**, and none of the other products could be observed, *i.e.*, **9a** is formed irreversibly from **2a** under the applied conditions. This clearly indicates an uncatalyzed, thermal electrocyclic ring opening of **9a**. The

---

6) We found this effect also with other azulenes and ADM (*cf.* [14]).

7) The Rh^I complex exerts no recognizable influence over product formation from **1** and ADiP in MeCN.

8) The reaction of azulenes with dialkyl acetylenedicarboxylates takes another course in the presence of strong *Lewis* acids such as Et_2AlCl [15].

rearrangement of **2a** and **9a** follow first-order kinetics with calculated rates at 100° in MeCN k_1 (**2a**) $= (1.68 \pm 0.10) \cdot 10^{-5}\ s^{-1}$ and k_1 (**9a**) $= (1.56 \pm 0.07) \cdot 10^{-5}\ s^{-1}$, respectively. The thermal rearrangement of **2a** to **9a** at 100° is twice as fast as that of **2c** to **9c** (*vide supra*). This rate effect is in agreement with heterolysis of the C(4a)–C(11) bond of the primary intermediates **2** (*cf. Scheme 1*) in the rate-determining step. The developing negative charge at C(11) in the course of the formation of the zwitterions should be better stabilized by a MeOCO than by an i-PrOCO residue at C(11) due to the smaller destabilizing σ-donor effect of the Me group compared with the i-Pr group.

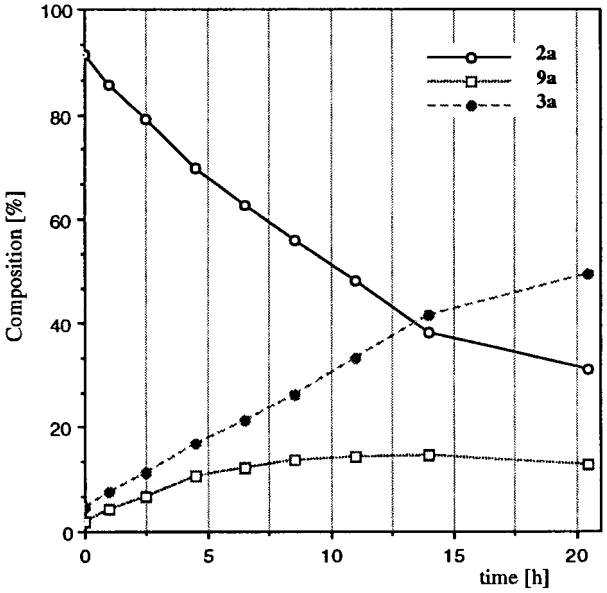

Fig. 2. *Course of the rearrangement of the primary tricyclic intermediate* **2a** *in MeCN at 100°*.The amounts of **2a**, **3a**, and **9a** were determined by HPLC (see *Exper. Part*). After 14 h, the amounts of **2a** and **3a** are not fully reliable due to the long reaction time.

The almost clean thermal rearrangement of **2a** to **9a** and then **9a** to **3a** in MeCN demonstrates that all other products observed in the reaction of **1** with ADM must originate from side reactions of **1** and ADM, or from other sources. Compounds of type (*E*)-**8a** and (*Z*)-**8a** are generally found in small amounts when azulenes are reacted with ADM, and they may become the main products in the presence of *Brønsted* acids or protic solvents [16][17]. Similarly, tricyclic compounds of type **12a** are often formed in the thermal reactions of azulenes with ADM. They represent *Diels-Alder* adducts of ADM with the seven-membered ring of azulenes, resulting from a SHOMO(azulene) controlled reaction [5][18][19].

Compounds of type *cis*-**10a** and *trans*-**10a**, as well as **11a**, have so far been observed only when azulenes are reacted with ADM at temperatures > 200° in apolar solvents [16], or in polar solvents (MeCN) at 110° in the presence of $[RuH_2(PPh_3)_4]$ [21]. One route for the formation of *cis*-**10a** and *trans*-**10a** could be a HOMO(azulene)-controlled [8 + 2] cycloaddition of **1** and ADM [20] as is generally observed with heptafulvenes [22]. Indeed, the heptafulvene substructure in benz[*a*]azulenes is

distinctly accentuated [12]. A prototropic shift in the primary adduct **13a** would then lead to the formation of *trans*-**10a** and *cis*-**10a** (*Scheme 6*). This view is supported by AM1 calculations of the parent structure of **13a** and those of *cis*-**10a** and *trans*-**10a**, which show that the latter compounds are energetically favored by $\Delta\Delta H_f^0 = -4.7$ kcal · mol^{-1}. That this ΔH_f^0 difference is attributable to a change in the basal skeletons and not to a change of the substitution patterns of **13a**, and *cis*-**10a** and *trans*-**10a** is evidenced by a comparison of the AM1-calculated ΔH_f^0 values for the three actual compounds, which again leads to a mean $\Delta\Delta H_f^0 = -4.4$ kcal · mol^{-1} (*Scheme 7*).

Scheme 6

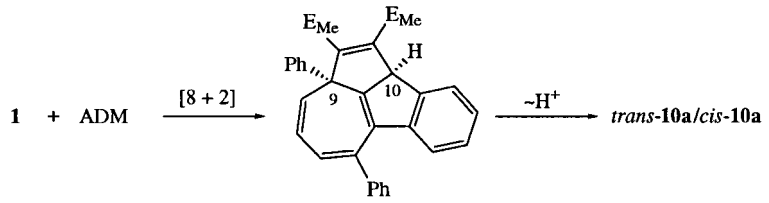

Scheme 7

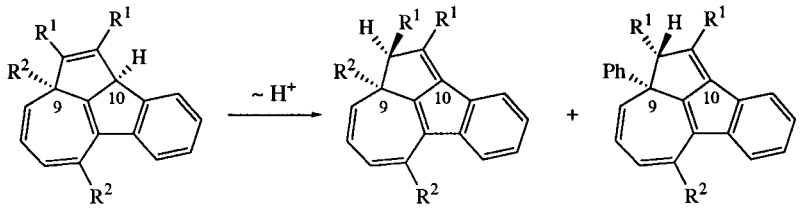

$R^1 = R^2 = H$[a])	114.80	110.07	
$R^1 = E_{Me}$, $R^2 = Ph$[b])	19.01 (**13a**)	13.53 (*trans*-**10a**)	15.75 (*cis*-**10a**)

[a]) The numbers represent the AM1-calculated ΔH_f^0 values in kcal · mol^{-1}. [b]) The numbers represent the AM1-calculated ΔH_f^0 values in kcal · mol^{-1} of the lowest-energy conformations.

The base-catalyzed equilibration of *cis*-**10a** and *trans*-**10a** ($NaHCO_3$/MeCN) at ambient temperature resulted in a *cis*-**10a**/*trans*-**10a** ratio of 0.10, which is quite close to 0.025 derived from $\Delta\Delta H_f^0$ (*cis*-**10a** – *trans*-**10a**) = 2.2 kcal · mol^{-1}, assuming similar ΔS_f^0 values for the diastereoisomers. However, we found another way by which *trans*-**10a**/*cis*-**10a** can be formed. We observed that fractions containing the yellow colored **9a**, when exposed to normal laboratory light, turned orange after a short time. The same color change was recognized on the surface of the yellow crystals of **9a** when kept under normal laboratory light. Control experiments revealed that irradiation of the *Dewar* heptalene **9a** at room temperature in benzene solution with the 366-nm light from a fluorescent tube leads quantitatively to a 1 : 1 mixture *cis*-**10a**/*trans*-**10a** (*Scheme 8*)[9]).

[9]) After short times of irradiation, when large amounts of **9a** are still present, the *cis*-**10a**/*trans*-**10a** ratio was 0.7 : 1.

Scheme 8

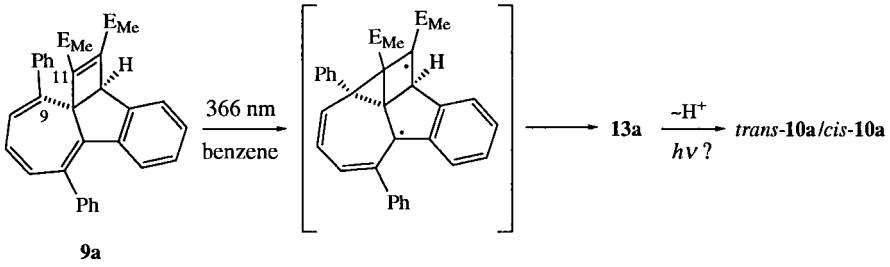

We assume that the formation of *trans*-**10a** and *cis*-**10a** from **9a** is, in the first step, the result of a di-π-methane rearrangement of **9a**, which leads, in a second step, to the formation of **13a**, which is then rearranged to *cis*-**10a** and *trans*-**10a** by a prototropic 1,3-shift. It might be that, in this case, the 1,3-H shift is also photochemically induced due to a change in the acidity of H–C(6a) in the excited singlet state of **13a**. Most of the *cis*-**10a** and *trans*-**10a** that is found in the original reaction mixture must have been formed by this photochemical pathway from **9a**, since the reaction of **1** and ADM at 100° in MeCN under strict exclusion of light resulted only in the formation of trace amounts of **11a**. The precursors of the fluoranthene-dicarboxylate are *cis*-**10a** and *trans*-**10a** (or **13a**; *cf.* [16][21]), since heating *trans*-**10a** or *cis*-**10a** in MeCN at 100° led slowly to the formation of **11a**. This rearrangement could be appreciably accelerated by heating *trans*-**10a** or *cis*-**10a** in DMF at 150°, whereupon the fluoranthene-dicarboxylate **11a** was formed quantitatively from both diastereoisomers within 1 h. On the other hand, no rearrangement occurred when *trans*-**10a** or *cis*-**10a** was heated at 150° in cumene. This observation indicates a polar mechanism for the discussed rearrangement (*Scheme 9*). Thermally allowed disrotatory ring closure of *trans*-**10a** and *cis*-**10a** will lead to the cyclopropane ring in **14a**. Heterolysis of the most strained bond in the

Scheme 9

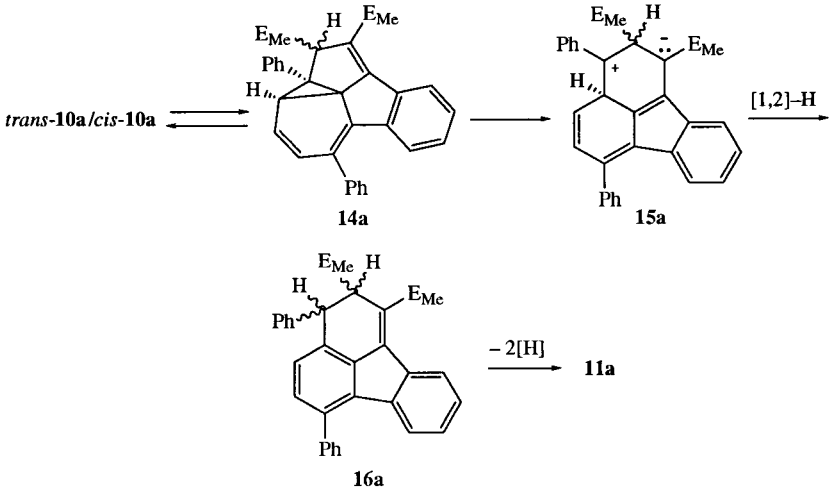

cyclopropane ring will then yield the zwitterion **15a**, which can balance its charges by a sigmatropic [1,2]-H shift ($\rightarrow$ **16a**). Thermal dehydrogenation of **16a** will then provide the observed fluoranthene-dicarboxylate **11a**.

3.2. *Structure Elucidations.* 3.2.1. *Primary Tricyclic Intermediates* **2**. We isolated compound **2a** (see also [1]), as well as **2c**, from the corresponding reaction mixtures. No suitable crystals of **2a** for an X-ray crystal-structure analysis could be obtained, but compound **2c** crystallized well from CH_2Cl_2/hexane or benzene/hexane. The solid-state molecular structure of **2c** is shown in *Fig. 3*. Some of the geometric data are collected

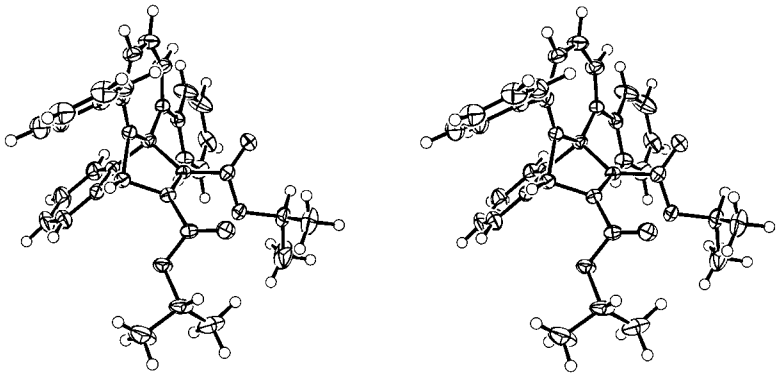

Fig. 3. *Stereoscopic view of the molecular structure of diisopropyl 5,9-diphenyl-4b,10-etheno-10*H*-benz[*a*]azulene-11,12-dicarboxylate* (**2c**)

in *Table 3* and compared with those of a non-benzo-anellated structure **17** (*cf.* [7]). The crucial bond that has to be cleaved heterolytically for the rearrangement to the secondary tricyclic intermediates **9** is the C(4b)–C(11) bond. It is, as in other tricycles of this type (*cf.* **17** and [7]), the longest $C(sp^2)-C(sp^3)$ bond in the molecule (*cf.* also *Table 4*), and the benzo-anellation does not alter this feature. The second longest bond in **2c**, as well as in **17**, is the C(4a)–C(4b) bond. However, in contrast to the tricycles of type **17**, this bond is not cleaved under normal thermal conditions, and, therefore, a retro-*Diels-Alder* reaction to produce a corresponding azulene-1,2-dicarboxylate (*cf.* [5]), due to the benzo-anellation, does not take place. In other words, the E_a value for the formation of 1,2-didehydrobenzene is much too high to compete with that for the heterolysis of the C(4b)–C(11) bond, which leads to the zwitterionic intermediates that collapse to form the secondary intermediates of type **9** and to all the other compounds formed in trace amounts.

The seven-membered ring in **2c** is, as in **17** and the other tricycles of this type (*cf.* [7]), perfectly planar. The UV absorption of the planar cycloheptatriene substructure of **2c** is characterized by two broad shoulders in the region of 350–400 nm. These absorptions are bathochromically shifted in comparison with **17** (*cf.* [7]) due to the presence of the two Ph substituents in **2c**. The planarity of the seven-membered ring in **2c** is also expressed in the vicinal coupling constants of H–C(6–8) which amount to 12.0 Hz across the C=C bond and 8.7 Hz across the C–C bond. They are quite similar to those of other tricycles of this type (*cf.* [7]). Typical for the discussed tricycles is also the chemical shift of the bridgehead H-atom. Its signal appears for tricycles of type **17**

Table 3. *Characteristic Geometric Parameters from the Crystal Structures of* **2c** *and Dimethyl 2,3,4,6,8-Pentamethyl-1,3a-etheno-1*H*-azulene-9,10-dicarboxylate*[a]) (**17**), *and the AM1-Calculated Parent Structure* **18**

Geometric parameter	**2c**[c])	**17**[b])	**18**
Bond lengths *d* [pm]			
C(4b)–C(11)	157.2(2)		154.7
C(3a)–C(10)		157.5(2)	
C(4a)–C(4b)	156.6(3)		153.3
C(3)–C(3a)		157.8(2)	
C(10)–C(10a)	152.1(3)		152.2
C(1)–C(2)		153.9(2)	
C(10)–C(12)	153.0(3)		153.6
C(1)–C(9)		153.1(2)	
C(4b)–C(5)	151.6(2)		146.3
C(3a)–C(4)		150.5(2)	
C(4b)–C(9a)	155.8(3)		154.5
C(3a)–C(8a)		154.4(2)	
C(5)–C(6)	134.8(3)		134.0
C(4)–C(5)		134.1(2)	
C(6)–C(7)	145.6(3)		143.9
C(5)–C(6)		146.5(3)	
C(7)–C(8)	134.0(3)		135.5
C(6)–C(7)		134.4(3)	
C(8)–C(9)	145.9(3)		143.9
C(7)–C(8)		146.9(2)	
C(9)–C(9a)	133.7(3)		132.9
C(8)–C(8a)		133.2(2)	
C(9a)–C(10)	153.4(3)		154.6
C(8a)–C(1)		152.5(2)	
Bond angles δ [°]			
C(4b)–C(5)–C(6)	123.9(2)		129.0
C(3a)–C(4)–C(5)		126.3(2)	
C(5)–C(6)–C(7)	133.4(2)		130.6
C(4)–C(5)–C(6)		133.5(2)	
C(6)–C(7)–C(8)	131.2(2)		130.3
C(5)–C(6)–C(7)		127.8(2)	
C(7)–C(8)–C(9)	128.6(2)		128.8
C(6)–C(7)–C(8)		130.5(2)	
C(8)–C(9)–C(9a)	124.8(2)		126.3
C(7)–C(8)–C(8a)		125.5(2)	
C(9)–C(9a)–C(4b)	135.0(2)		133.6
C(8)–C(8a)–C(3a)		134.0(1)	
C(9a)–C(4b)–C(5)	123.0(2)		121.5
C(8a)–C(3a)–C(4)		122.4(1)	
C(4b)–C(9a)–C(10)	96.2(1)		96.2
C(3a)–C(8a)–C(1)		95.2(1)	
Torsion angles Θ [°]			
C(4b)–C(5)–C(6)–C(7)	– 0.2(4)		– 0.3
C(3a)–C(4)–C(5)–C(6)		– 0.5(3)	
C(5)–C(6)–C(7)–C(8)	– 0.9(5)		1.3
C(4)–C(5)–C(6)–C(7)		0.7(3)	
C(6)–C(7)–C(8)–C(9)	– 1.1(4)		0.0
C(5)–C(6)–C(7)–C(8)		1.2(3)	
C(7)–C(8)–C(9)–C(9a)	2.1(4)		– 1.3

Table 3 *(cont.)*

Geometric parameter	**2c**[c])	**17**[b])	**18**
C(6)–C(7)–C(8)–C(8a)		–2.3(3)	
C(8)–C(9)–C(9a)–C(4b)	0.5(4)		0.0
C(7)–C(8)–C(8a)–C(3a)		0.9(3)	
C(9)–C(9a)–C(4b)–C(5)	–3.5(3)		1.6
C(8)–C(8a)–C(3a)–C(4)		1.1(3)	
C(9a)–C(4b)–C(5)–C(6)	2.9(3)		–1.6
C(8a)–C(3a)–C(4)–C(5)		–1.1(3)	
C(6)–C(5)–(Ph plane)	–9.4(3)	–	–
C(8)–C(9)–(Ph plane)	–58.8(3)	–	–

[a]) In [7], named *dimethyl 2,4,6,11,12-pentamethyltricyclo[6.2.2.0^{1,7}]dodeca-2,4,6,9,11-pentaene-9,10-dicarboxylate* (**17**).

[b]) C-atom numbering:

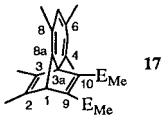

17

18

[c]) For C-atom numbering, see *Scheme 1*.

Table 4. *Comparison of the Ring Geometries in the Crystal Structures of* **2c** *and* ***17*** *with the Ring Geometry of the AM1-Calculated Parent Structure* **18**[a])

Parameter	**2c**	**17**	**18**
$\Sigma\delta$(7-ring) [°][b])	899.9(5)	900.0(5)	900.1
$\Sigma\lvert\Theta\rvert$(7-ring) [°]	11.2 (1.1)	0.0	6.5
Deviation [%] of *d*			
(C(4b)–C(11))A[c])	+2.7	+2.9	+0.7
(or C8(a)–C(10))			
B[d])	+1.6	+1.8	–
C[e])	+1.9	+2.1	+1.3
(C(4a)–C(4b)) A[f])	+3.0	+2.5	+0.7
(or C(3)–C(3a))			
B[d])	+2.2	+2.9	–
C[e])	+1.6	+2.3	+0.4

[a]) See footnotes in *Table 3*. [b]) Calculated for an *n*-membered polygon: $180° \cdot (n-2)$; *i.e.*, 900.0° for a planar seven-membered ring. [c]) With respect to *d* of the opposite C(10)–C(12) or C(1)–C(9) bond. [d]) With respect to the calculated value of the parent structure. [e]) With respect to the average value of *d* for all C(sp^2)–C(sp^3) bonds (*cf. Table 3*) at the considered tricycle. [f]) With respect to *d* of the opposite C(10)–C(10a) or C(1)–C(2) bond.

with a Me group at C(12), which corresponds to C(10a) in **2a** (*cf. Scheme 1*), at 4.28 ppm (C_6D_6) [7]. It is strongly deshielded in **2a** and its analogues by the benzoanellation, and emerges as a sharp *singlet* at 4.84 ppm.

3.2.2. *Secondary Tricyclic Intermediates* **9**. For the first time, we were able to isolate a candidate of these postulated 'missing links' from the thermal reaction of azulenes with acetylenedicarboxylates to give heptalene-dicarboxylates. Compound **9a** could be crystallized from Et_2O/hexane, and its solid-state molecular structure, as determined by X-ray crystallography, is shown in *Fig. 4*. As expected (*cf.* [7]), the seven-membered

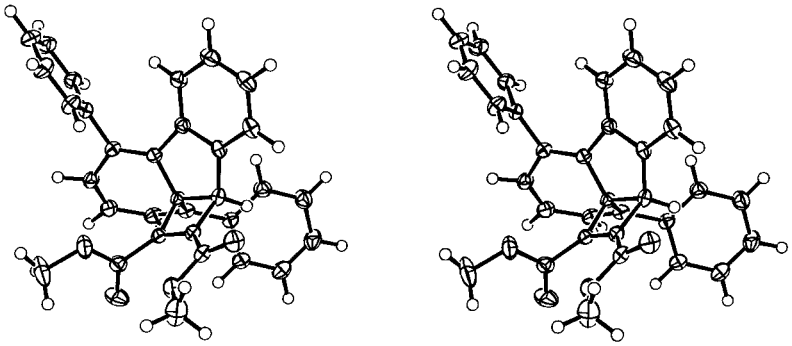

Fig. 4. *Stereoscopic view of the molecular structure of dimethyl 5,9-diphenyl-9a,10-etheno-10*H*-benz[*a*]azulene-11,12-dicarboxylate* (**9a**)

ring of **9a** is no longer planar as in **2c**. The torsion angles found for the seven-membered ring (*cf. Table 5*) of **9a** are typical for a distorted C_s symmetry of the boat conformation of cycloheptatrienes.

The corresponding values for the lowest-conformational-energy AM1-calculated structure of **9a** and its parent structure **19** are very similar (*cf. Table 5*). The non-planarity of the seven-membered ring in **9a** can also be seen from the vicinal coupling constants of H–C(6–8), which amount to 11.5 Hz across the C=C bond and 6.4 Hz across the C–C bond. In agreement with these findings is the UV spectrum (hexane) of **9a**, which shows a hypsochromic shift for the long-wavelength absorption band compared with that of **2a** (*cf.* the discussion in [7]).

The solid-state geometrical parameters of the cyclobutene ring in **9a** are comparable with those of an analogous compound **20** which is formed in the thermal reaction of indene and ADM (*cf.* [23]). The ester groups at C(11) and C(12) have no influence on the bond lengths of the cyclobutene ring, since the calculated parent structure of **9a** shows very similar bond lengths (*cf. Table 5*). The interatomic distance for C(9)···C(11) is 261.5(2) pm, so that bonding can occur in the excited S_1 state to induce the postulated di-π-methane rearrangement (*cf. Scheme 7*).

3.2.3. *Benzo[*a*]heptalene-6,7-dicarboxylates* **3**. Characteristic for the ^{1}H-NMR spectra ($CDCl_3$) of **3a**–**3d** is the strongly low-field shifted signal for H–C(5), which appears in the range of 8.42 (**3a**)–8.20 ppm (**3d**) as a *singlet*. Also quite typical is the large chemical shift difference ($\Delta\delta = 0.7–1.0$ ppm) for H–C(4), which emerges as a *doublet* with fine structure at 7.6–7.3 ppm, and for H–C(1), also present as a *doublet*, with fine structure, at 6.6 ppm due to the shielding effect of the neighboring Ph group at C(12). This conclusion can be drawn from the observation that dimethyl 8-phenylbenzo[*a*]heptalene-6,7-dicarboxylate (**21a**; *cf. Table 6*)[10]), which does not possess a Ph group at C(12), shows the signal for H–C(1) at *ca.* 7.15 ppm, whereas the signal of H–C(4) still appears at 7.68 ppm. The vicinal coupling constants for the H-atoms on the seven-membered ring of **3a**–**3d** are again very typical for heptalene-dicarboxylates

[10]) Heptalene-dicarboxylate **21a** was prepared from 9-phenylbenz[*a*]azulene [12] and ADM in MeCN at 100°/18 h, followed by removal of MeCN and heating of the residual reaction mixture in DMF at 150°/1 h (see *Exper. Part*).

Table 5. *Comparison of the Characteristic Geometric Parameters from the Crystal Structures of* **9a** *and Tetramethyl (1*R**,2*R**,4a*S**,8*S**,8a*S**)-5,8-Dibromo-1,8a-etheno-2,4a-methano-1,2,4a,5,8,8a-hexahydronaphthalene-3,4,9,10-tetracarboxylate* (**20**) *with Those Obtained from the AM1 Calculations of* **9a**, *and the Parent Structure* **19**[a])

Geometric Parameter	**9a**[b])	**19**[c])	**20**[d])
Bond lengths *d* [pm]			
C(4b)–C(5)	136.4(2) [135.3]	134.5	–
C(5)–C(6)	145.6(2) [145.1]	143.9	–
C(6)–C(7)	135.1(2) [134.5]	134.7	–
C(7)–C(8)	144.8(3) [143.8]	144.1	–
C(8)–C(9)	135.1(2) [135.0]	134.2	–
C(9)–C(9a)	151.2(2) [148.0]	146.9	–
C(9a)–C(4b)	151.8(2) [150.9]	150.0	–
C(9a)–C(11)	154.1(2) [154.7]	153.6	153(2)
C(10)–C(12)	151.7(2) [152.5]	152.5	151(2)
C(11)–C(12)	133.9(2) [135.7]	135.3	134(2)
C(9a)–C(10)	158.5(2) [161.9]	161.9	159(2)
Bond angles δ [°]			
C(9a)–C(4b)–C(5)	122.3(1) [124.4]	126.2	–
C(4b)–C(5)–C(6)	122.9(2) [124.3]	126.0	–
C(5)–C(6)–C(7)	128.3(2) [127.3]	126.8	–
C(6)–C(7)–C(8)	127.7(2) [127.0]	127.0	–
C(7)–C(8)–C(9)	126.4(2) [126.5]	127.0	–
C(8)–C(9)–C(9a)	119.8(2) [123.0]	125.4	–
C(9)–C(9a)–C(4b)	113.5(1) [114.8]	114.8	–
C(4b)–C(9a)–C(11)	112.6(1) [114.9]	115.6	115(1)
C(10a)–C(10)–C(12)	118.8(1) [116.9]	116.0	115(1)
Torsion angles Θ [°]			
C(4b)–C(5)–C(6)–C(7)	–26.6(3) [–30.7]	–27.0	–
C(5)–C(6)–C(7)–C(8)	1.2(3) [0.9]	0.0	–
C(6)–C(7)–C(8)–C(9)	29.1(3) [30.2]	27.7	–
C(7)–C(8)–C(9)–C(9a)	4.9(3) [2.5]	2.7	–
C(8)–C(9)–C(9a)–C(4b)	–61.2(2) [–55.0]	–50.0	–
C(9)–C(9a)–C(4b)–C(5)	66.0(2) [55.4]	50.6	–
C(9a)–C(4b)–C(5)–C(6)	–11.3(3) [–2.4]	–3.2	–
C(10)–C(9a)–C(11)–C(12)	2.0(1) [0.5]	0.0	4(1)
C(9a)–C(10)–C(12)–C(11)	2.1(1) [0.5]	0.0	4(1)
C(11)–C(9a)–C(10)–C(12)	–1.8(1) [–0.8]	0.0	–4(1)
C(4b)–C(5)–(Ph-plane)	–64.0(2) [–87.4]	–	–
C(8)–C(9)–(Ph-plane)	–59.0(2) [–71.2]	–	–

[a])

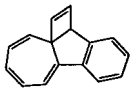

19

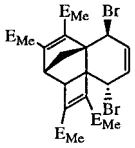

20

[b]) AM1 Parameters in square brackets. [c]) For C-atom numbering, see *Scheme 5*. [d]) See [23]; for comparison purposes, C-atom numbering analogous to that of **9a** was chosen.

with four *peri*-substituents: ^3J(H–C(9),H–C(10)) amounts to 6.3–6.6 Hz and ^3J(H–C(10),H–C(11)) to 10.7–11.3 Hz. The coupling constants across the C(9)–C(10) bond are compatible with a torsion angle Θ(H–C(9)–C(10)–H) of 30–35°. The X-ray crystal-structure analysis of **3a** (*Fig. 5* and *Table 6*) displays a corresponding torsion angle Θ(C(8)–C(9)–C(10)–C(11)) = 31.8(2)° in good agreement with the estimated Θ value from the vicinal H,H-coupling constants. Other geometrical parameters in this structure are similar to those of dimethyl 1,2,6,8,10-pentamethylheptalene-4,5-dicarboxylate (**22**), which possesses a comparable substitution pattern for the seven-membered ring carrying the ester groups. The magnitudes of the torsion angles at the central σ-bond (C(7a)–C(12a) and C(5a)–C(10a), resp.) of both heptalene types are similar and fully comparable with other heptalene-4,5-dicarboxylates carrying four *peri*-substituents (*cf.* [25]). These findings indicate that the anellated benzo ring at the *a*-side of the heptalene ring does not markedly influence the general geometry of the heptalene core (see also [26]).

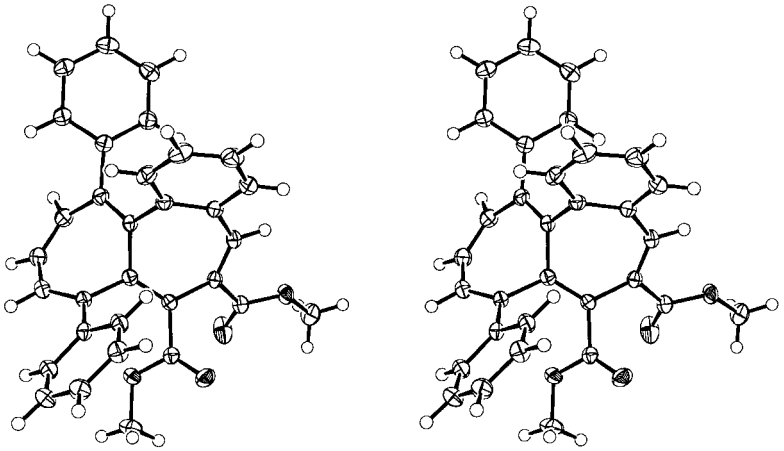

Fig. 5. *Stereoscopic view of the molecular structure of dimethyl 8,12-diphenylbenzo[*a*]heptalene-6,7-dicarboxylate* (**3a**)

Since we were interested in the optical resolution of **3a**, which can be achieved, at least on an analytical scale, on a *Chiralcel OD* column (*cf.* [1]), we attempted to improve the chromatographic separation of the antipodes of the diesters **3a**–**3d**. *Table 7* contains the separation factors α of the antipodes of the four diesters under constant conditions on the analytical column. As one can see, **3a** possesses the largest α value, followed by **3c**. The dicarboxylates **3b** and **3d** are less suited for the separation of their antipodes. Since the diisopropyl dicarboxylate **3c** was more soluble than **3a** in the employed mixture of eluants (hexane/i-PrOH 95:5), we separated a larger amount of **3c** into the enantiomers on a semi-preparative *Chiralcel OD* column (see *Exper. Part* and [2][26]). We included the 8-phenyl derivative **21a** and the non-substituted dicarboxylate **23a** [20] in our evaluations of optical resolutions of benzo[*a*]heptalene-6,7-dicarboxylates on the analytical *Chiralcel OD* column. The separation factors α for these compounds are also collected in *Table 7*. The effect of the substituents on α-values is amazing. Whereas **3a** and **21a** show similar α values, an

Table 6. *Comparison of Some Characteristic Geometric Parameters of the Benzo[*a*]heptalene-6,7-dicarboxylates* **3a**, **21a**, *and* **23a** *with Those of Dimethyl 1,2,6,8,10-Pentamethylheptalene-4,5-dicarboxylate* (**22**)[a])

Heptalene	Torsion angles[b]) [°]				Bond angles[c]) [°]		Bond lengths[d]) [pm]		
No.	Θ_1	Θ_2	Θ_3	Θ_4	δ_1	δ_2	d_1	d_2	d_3
3a	−110.3(1)	64.7(2)	33.4(4)	−40.2(1)	124.1(3)	117.6(2)	149.0(3)	146.1(4)	135.4(4)
21a	121.1(1)	−57.2(3)	32.2(5)	41.7(2)	125.2(5)	119.1(2)	149.4(3)	145.8(4)	134.9(4)
23a[e])	−115.9(2)	57.9(4)	34.0(8)	−44.0(3)	124.8(7)	118.3(4)	148.1(5)	145.9(7)	135.0(7)
22[f])	112.1(2)	−65.3(3)	34.1(6)	33.2(2)	124.0(6)	117.4(2)	148.7(3)	146.0(4)	135.0(5)

[a])

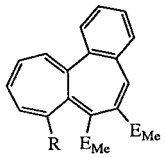

21a R = Ph
23a R = H

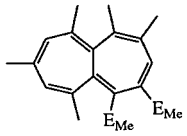

22

[b]) Θ_1 = Torsion angle of the three sequential σ-bond vectors; Θ_2 = average torsion angle of the two *ac*-conformations at the C(7a)–C(12a) or C(5a)–C(10a) bonds, respectively; Θ_3 = average magnitude of the torsion angles at the four σ-bonds of the two seven-membered rings; Θ_4 = torsion angle at the two carboxylate groups. [c]) δ_1 = Average value of the bond angles at the seven-membered rings with the exception of the angles at C(7a) and C(12a), or C(5a) and C(10a), respectively; δ_2 = average value of the internal angles at C(7a) and C(12a), or C(5a) and C(10a), respectively. [d]) d_1 = Average length of the three sequential σ-bonds; d_2 = average length of the four residual σ-bonds in the perimeter; d_3 = average length of the five and six π-bonds, respectively. [e]) Data from [20]. [f]) See also [5][21b].

extreme increase is observed for the non-substituted form **23a**. We assume that this extraordinary effect is due to the flatter and more flexible heptalene core of **23a** compared with the other two compounds[11]). These effects seem to enable a better differentiation of the binding sites in the *Chiralcel OD* material by the antipodes of **23a**.

Table 7. *Separation Factors* α *of the Benzo[*a*]heptalene-6,7-dicarboxylates* **3**, **21a**, *and* **23a** *on an Analytical* Chiralcel OD *Column*[a])

Eluant[b])	α-Values					
	3a	**3b**	**3c**	**3d**	**21a**	**23a**
Hexane/i-PrOH 93 : 7	1.48	–	–	–	2.19	8.11
Hexane/i-PrOH 95 : 5	1.55	1.09	1.42	1.07	–	–
Hexane/EtOH 97 : 3	1.45	1.08	1.23	1.0	–	–

[a]) For details, see *Exper. Part.* [b]) Volume ratio.

3.2.4. *Tricyclic Compounds of Type* **12**. As already mentioned, this product type arises from a SHOMO(azulene) and LUMO(ADR) interaction and leads to an irreversible addition – at least under the applied reaction conditions – of ADR at the seven-membered ring of the azulenes (*cf.* [5][18][19]). Compounds of type **12** were present in small amounts in all reaction mixtures of **3a**–**3d** and ADR. However, only in

11) The X-ray crystal-structure analysis of **23a** supports this view [20]. The average torsion angle of the two *ac*-conformations at the central σ-bond is reduced by 8° compared with **3a**.

the reaction between **1** and ADM, a compound of type **12**, *i.e.*, **12a** was isolated in almost pure form and characterized by its ^{1}H-NMR spectrum ($CDCl_3$). Typical for **12a** is the *dd* signal of H–C(7) that appears at 4.63 ppm, while none of the other compounds in the reaction mixture (*cf. Scheme 5*) show a similar signal. The coupling constants ^3J(H–C(7),H–C(8)) = 8.5 and ^3J(H–C(7),H–C(12)) = 6.9 Hz are very characteristic for compounds of this type [5][27]. The H-atom H–C(10) gives rise to a *singlet* at 6.69 ppm, next to the *doublet* of H–C(12) at 6.66 ppm. The benzo-anellation of **12a** prevents the [1,5]-sigmatropic C-shifts that we have observed with other tricyclic compounds of this type (*cf.* [5][27]).

3.2.5. *Fumarate- and Maleate-Type Compounds* **8**. Both stereoisomers of type **8** exhibit a deep green color, so they are easy to detect in the reaction mixtures by TLC. The two forms (*E*)-**8a** and (*Z*)-**8a** could be obtained in a crystalline state. Whereas (*E*)-**8a** crystallized as dark green prisms with a black shimmer, which were suitable for an X-ray crystal-structure analysis (see below), (*Z*)-**8a** crystallized as green needles. Both diastereoisomers show significant differences in their ^{1}H-NMR spectra ($CDCl_3$; see also [17]). For example, the sharp *singlet* for H–C(2) appears for (*E*)-**8a** at 6.63 ppm and for (*Z*)-**8a**, strongly shifted, at 5.80 ppm, due to the orthogonal conformation around the C(1)–C(10′) bond, placing it above the benz[*a*]azulene ring. The opposite shift behavior is observed for the signals of the MeO groups of the ester functions. Since the MeO group of MeOCO–C(2) is placed above the benz[*a*]azulene ring in (*E*)-**8a**, the corresponding *singlet* appears at 3.48 ppm, *i.e.*, at highest field compared with the MeO *singlet* of MeOCO–C(1) (3.60 ppm) and those of (*Z*)-**8a** (3.68 and 3.66 ppm, resp.). The three neighboring H-atoms at the seven-membered ring of (*E*)-**8a** and (*Z*)-**8a** exhibit different vicinal coupling constants ((*E*)-**8a** [(*Z*)-**8a**]: ^3J(H–C(7′),H–C(8′)) = 8.8 [8.4] and ^3J(H–C(8′),H–C(9′)) = 11.1 [11.4] Hz), in agreement with an accentuation of the heptafulvene substructure in these compounds, as is also found in the starting azulene **1** (*cf.* [12]). As discussed already, the tricyclic intermediate **2c**, the X-ray crystal-structure analysis of which revealed a perfectly planar seven-membered ring (*cf. Fig. 3* and *Table 3*), has vicinal coupling constants of 12.0 Hz across the localized C=C bond and 8.7 Hz across the C–C bond. Since these coupling constants are similar to those of (*E*)-**8a** and (*Z*)-**8a**, we cannot differentiate between planarity or non-planarity of the seven-membered rings in both forms of **8a** on the basis of their ^{1}H-NMR spectra. Nevertheless, the X-ray crystal structure of (*E*)-**8a** reveals that, indeed, its seven-membered ring is not completely planar (*Fig. 6*). The torsion angle Θ(C(6′)–C(7′)–C(8′)–C(9′)) amounts to 9.9(4)° (*cf. Footnote 17* in the *Exper. Part*; AM1 calculation: 15.5° for (*E*)-**8a** and 19.2° for (*Z*)-**8a**). In other words, the accentuation of the heptafulvene structure in (*E*)-**8a** and (*Z*)-**8a**, and possibly also in **1**, leads to a flat boat-like conformation of the seven-membered ring in these benz[*a*]azulenes. This view is fully supported by the complementary torsion angle Θ(C(4′b)–C(5′)–C(6′)–C(7′)) of –14.0(4)° in the crystal structure of (*E*)-**8a** (AM1 calculation: –15.7° for (*E*)-**8a** and –25.3° for (*Z*)-**8a**).

The deep green color of both diastereoisomers of **8a** is caused by similar large torsion angles around the C(1)–C(10′) bond that links the benz[*a*]azulene chromophore with the MeOCO-substituted ethene chromophore. The X-ray crystal-structure analysis of (*E*)-**8a** shows that Θ(C(2)–C(1)–C(10′)–C(9′a)) = –53.4(3)° and the complementary torsion angle Θ(C(2)–C(1)–C(10′)–C(10′a)) = 123.6(2)° (AM1

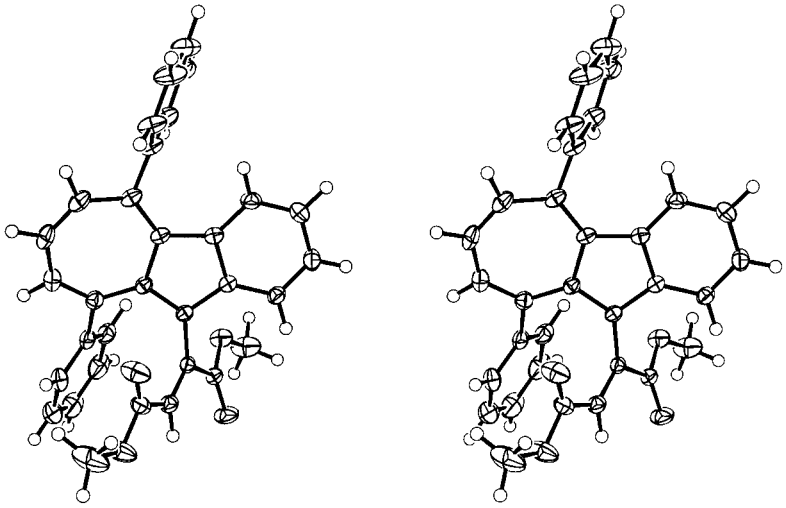

Fig. 6. *Stereoscopic view of the molecular structure of dimethyl* (E)*-(5,9-diphenylbenz[*a*]azulen-10-yl)ethene-1,2-dicarboxylate* ((*E*)-**8a**)

calculation (for the lowest energy conformations; in square brackets for the conformation corresponding to the crystal structure): $-116.2°[-66.8°]/65.5°[112.3°]$ for (*E*)-**8a** and $-111.9°/70.0°$ for (*Z*)-**8a**). Both compounds show, beside the weak long-wavelength azulene absorption bands, a strong UV absorption band at *ca.* 400 nm ((*E*)-**8a**: 383 nm ($\log \varepsilon = 3.95$); (*Z*)-**8a**: 410 nm ($\log \varepsilon = 3.08$); see *Exper. Part*), which, together with the azulene bands, causes the green color[12]).

3.2.6. *2,2a-Dihydrobenzo[*a*]cyclopent[*cd*]azulene-1,2-dicarboxylates* **10**. We observed this class of compounds for the first time in the reaction mixtures of **1** and ADM ($\rightarrow$ *trans*-**10** and *cis*-**10a**). The main source of *trans*-**10a** and *cis*-**10a** in this case is the efficient photochemical rearrangement of the *Dewar*-heptalene **9a** that occurs even under the influence of normal laboratory light. Their analogues are present in small amounts in the reaction mixtures of **1** with the other acetylenedicarboxylates (ADE, ADiP, and AD*t*B). However, aside from *trans*-**10a** and *cis*-**10a**, we only isolated *cis*-**10c**. This product type is also found in amounts of up to 20% in the reaction mixtures of benz[*a*]azulene (**24**) itself and ADM or ADE (see *Exper. Part*). In the latter two cases, the formation must be the result of a thermally allowed $[8+2]$ cycloaddition, followed by a 1,3-prototropic shift (*cf. Schemes 6*, *7*, and *11*).

The thermal rearrangement of *trans*-**10a** and *cis*-**10a** to **11a** proved chemically that both compounds represented structurally related isomers that were further connected to **9a** by the observed photochemical transformation. All three compounds exhibited in their ^{1}H-NMR spectra ($CDCl_3$) a characteristic *singlet* at *ca.* 4.5 ppm of a non-coupled H-atom that originally could only stem from H–C(10) of **1**. Indeed, when the *singlet* of **9a** at 4.37 ppm was irradiated, the corresponding *d* of H–C(4) of the benzo ring showed a ^{1}H-NOE effect. However, such ^{1}H-NOE effects were not observed with *trans*-**10a** or *cis*-**10a**. Instead, the *singlet* of *trans*-**10a**, when irradiated, displayed a weak ^{1}H-NOE

[12]) For a more detailed discussion, see [17].

effect with a *doublet* ($J = 10.3$ Hz) at 5.94 ppm from an H-atom in an olefinic position that was obviously coupled with a second H-atom in an olefinic position *via* a C=C bond. Similar effects were observed when the *singlet* of *cis*-**10a** was irradiated; however the ^{1}H-NOE effect on the *doublet* ($J = 10.0$ Hz) of an H-atom in an olefinic position (6.51 ppm) was much stronger in this case. These main observations, together with the general similarities of the ^{1}H-NMR spectra of both compounds, demonstrated that *trans*-**10a** and *cis*-**10a** were diastereoisomers. This view was strongly supported by the observed chemical-shift differences of the *singlet* signals of the two MeOCO groups of both isomers. They appeared for *trans*-**10a** close together at 3.87 and 3.82 ppm; however, for *cis*-**10a**, a $\Delta\delta$ value of 0.76 ppm (3.90 and 3.14 ppm) was observed. The latter effect can be attributed to the *cis*-relationship of the Ph group at C(2a) and the MeOCO group at C(2), which leaves the reverse relative *trans*-configuration for the other diastereoisomer.

Since both isomers crystallized well, we performed an X-ray crystal-structure analysis of both forms to corroborate the spectroscopically established structures of *trans*-**10a** and *cis*-**10a** (*cf. Fig. 7*). Some of the solid-state geometrical parameters of *trans*-**10a** and *cis*-**10a** are listed together with those from AM1 calculations in *Table 8*. Both diastereoisomers embody a benzofulvene substructure defined by the atoms from C(1), C(10b), and C(10a) around to C(10c). The benzofulvene substructure has an almost planar indenylidene moiety with a mean deviation of 2.1 and 2.0 pm from the least-squares plane for *trans*-**10a** and *cis*-**10a**, respectively; it is only the '*exo*-methylene' C-atom (C(1)) that deviates markedly from this plane. This deflection from the plane is distinctly smaller for *trans*-**10a** (10.1 pm) than for *cis*-**10a** (20.8 pm) and can mainly be attributed to the anellation of the cycloheptatriene ring and the Ph substituent at C(2a), as is evidenced by the somewhat larger deviation from planarity of *cis*-**10a**, which carries Ph and MeOCO groups at C(2a) and C(2), respectively, in the sterically demanding *cis*-relationship. Indeed, the two *ortho*-C-atoms of Ph–C(2a) and the two O-atoms of MeOCO–C(2) are oriented nearly perfectly parallel to each other in the crystal structure of *cis*-**10a** (*cf. Fig. 7,b*) and also according to the AM1 calculation of the structure. The strain of anellation in both molecules causes a small torsion of the fixed s-*trans*-conformation of the central 1,3-diene fragment C(1)=C(10b)–C(10c)=C(6a), leading to torsion angles of Θ(*trans*-**10a**) = –176.9(2)° [–170.6°] and Θ(*cis*-**10a**) = –172.5(1)° [–167.6°]. The larger strain in *cis*-**10a** compared with *trans*-**10a** is also reflected in the torsion angles of the s-*cis*-conformation of the 1,3-diene subunit, C(3)=C(4)–C(5)=C(6), of the cycloheptatriene ring, *i.e.*, Θ(*trans*-**10a**) = 26.0(5)° [29.8°] and Θ(*cis*-**10a**) = 30.0(3)° [31.5°]. In total, on the basis of the torsion angles Θ(C(3)=C(4)–C(5)=C(6)) and Θ(C(5)=C(6)–C(6a)=C(10c)) (Θ(*trans*-**10a**) = 26.0(5)°/–21.8(4)°; Θ(*cis*-**10a**) = 30.0(3)°/–26.7(3)°), the cycloheptatriene ring displays a fixed, but only weakly distorted C_s-symmetric boat conformation. The '*exo*-methylene' C-atom, of the benzofulvene substructure is, as a result of being embedded in the additional five-membered ring, markedly 'in-plane' distorted compared with benzofulvene itself. The AM1 calculation of the latter relaxed structure yields bond angles of 127.9° and 126.8° at the methylene group, whereas the observed [calculated] bond angle C(1)–C(10b)–C(10c) is 109.8(2)° [110.0°] for *trans*-**10a** and 109.4(1)° [109.9°] for *cis*-**10a**. In general, the AM1-calculated geometric parameters of *trans*-**10a** and *cis*-**10a** are in good-to-excellent agreement with the data from the X-ray

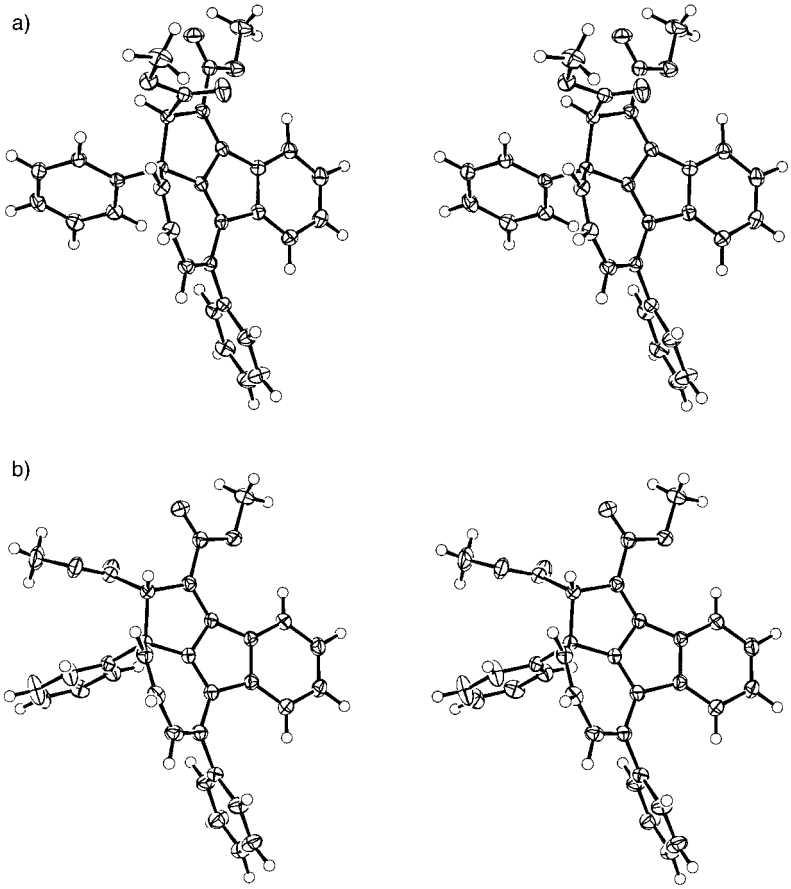

Fig. 7. *Stereoscopic views of the molecular structures of* a) *dimethyl (2*R**,2a*R**)- and* b) *dimethyl (2*R**,2a*S**)-2,2a-dihydro-2a,6-diphenylbenzo[*a*]cyclopent[*cd*]azulene-1,2-dicarboxylate* (*trans*-**10a** and *cis*-**10a**, resp.)

crystal-structure analyses with the exception of the calculated parameters of the C(10b)–C(10c) region, where most of the skeletal strain has to be compensated. For example, the calculated bond length of C(10b)–C(10c) is *ca.* 4 pm longer than found experimentally for both isomers. Moreover, the parent structure also shows this deviation, which indicates that the skeletal strain is overestimated by the AM1 program.

The more or less planar benzofulvene substructure in *trans*-**10a** and *cis*-**10a** accounts for the deep orange color of both diastereoisomers, which show the longest wavelength absorption (hexane) as a shoulder at 349 nm (*trans*-**10a**) and 346 nm (*cis*-**10a**), on the flank of a strong absorption band at 319 nm (log ε 4.04) exhibited by both forms. The small bathochromic shift of the longest-wavelength band of *cis*-**10a** compared with that of *trans*-**10a** is in agreement with the greater deviation of C(1) from the otherwise planar benzofulvene substructure in *cis*-**10a**.

3.2.7. *Fluoranthene-1,2-dicarboxylates* **11**. – This product type is often found in small amounts in the reaction mixtures of ADR with azulenes [16][21]. For **11a**, we have

Table 8. *Comparison of the Characteristic Geometric Parameters from the Crystal Structures of* trans-**10a** *and* cis-**10a** *with Those Obtained from the AM1 Calculations of the Two Diastereoisomers, and Their Parent Structure*

Geometric Parameter	*trans*-**10a**[a])	Parent structure[b])	*cis*-**10a**[a])
Bond lengths d [pm]			
C(5)–C(6)	136.4(3) [135.9]	135.1	136.7(2) [135.9]
C(6)–C(6a)	145.0(3) [144.1]	143.1	145.2(2) [144.1]
C(4)–C(5)	145.1(3) [144.1]	144.5	145.1(3) [144.2]
C(3)–C(4)	134.3(3) [134.4]	134.4	134.7(2) [134.4]
C(2a)–C(3)	151.2(3) [149.7]	148.3	151.7(2) [149.8]
C(2)–C(2a)	159.0(3) [159.0]	155.9	160.1(2) [158.7]
C(2a)–C(10c)	150.6(3) [148.9]	148.0	150.0(2) [149.1]
C(1)–C(2)	151.9(3) [151.8]	151.3	152.0(2) [151.9]
C(1)–C(10b)	135.0(3) [135.1]	134.7	135.4(2) [135.1]
C(10b)–C(10c)	145.4(3) [149.3]	149.3	144.9(2) [149.3]
C(6b)–C(10a)	142.4(3) [144.6]	144.8	142.3(2) [144.6]
C(6a)–C(10c)	135.4(3) [136.5]	136.2	135.7(2) [136.5]
Bond angles δ [°]			
C(4)–C(5)–C(6)	129.4(2) [129.2]	129.0	128.7(2) [129.0]
C(6)–C(6a)–C(10c)	125.3(2) [123.9]	123.9	125.1(2) [123.8]
C(5)–C(6)–C(6a)	121.6(2) [121.4]	123.3	120.8(2) [121.2]
C(3)–C(4)–C(5)	131.4(2) [130.9]	130.9	130.4(2) [130.6]
C(2a)–C(3)–C(4)	125.0(2) [126.0]	125.8	124.0(2) [125.9]
C(2)–C(2a)–C(3)	115.3(2) [114.9]	116.0	112.1(1) [111.2]
C(3)–C(2a)–C(10c)	108.2(2) [108.2]	110.6	106.6(1) [107.8]
C(1)–C(2)–C(2a)	104.7(2) [106.2]	106.3	105.8(1) [106.2]
C(2a)–C(10c)–C(10b)	111.3(2) [110.7]	110.3	112.9(1) [110.7]
C(2a)–C(10c)–C(6a)	136.8(2) [138.2]	138.0	134.6(2) [137.9]
C(2)–C(2a)–C(10c)	100.9(2) [102.2]	102.8	100.4(1) [102.0]
C(2)–C(1)–C(10b)	110.8(2) [110.6]	110.7	111.1(1) [110.6]
C(10b)–C(10c)–C(6a)	111.9(2) [110.8]	111.4	112.4(1) [110.8]
C(10a)–C(10b)–C(1)	143.7(2) [143.9]	145.0	144.1(2) [143.7]
C(1)–C(10b)–C(10c)	109.8(2) [110.0]	109.3	109.4(1) [109.9]
Torsion angles Θ [°]			
C(3)–C(4)–C(5)–C(6)	26.0(5) [29.8]	27.0	30.0(3) [31.5]
C(6)–C(6a)–C(10c)–C(2a)	–4.9(5) [1.6]	–2.0	–5.3(3) [–5.9]
C(5)–C(6)–C(6a)–C(10c)	–21.8(4) [–26.0]	–20.6	–26.7(3) [–27.0]
C(2a)–C(3)–C(4)–C(5)	7.3(4) [0.7]	3.6	5.5(3) [0.0]
C(4)–C(5)–C(6)–C(6a)	–3.5(4) [0.6]	–4.6	–2.0(3) [–2.0]
C(2)–C(2a)–C(3)–C(4)	–157.4(2) [–154.2]	–156.0	–159.1(2) [–152.8]
C(4)–C(3)–C(2a)–C(10c)	–45.3(3) [–40.8]	–39.8	–50.2(2) [–41.8]
C(1)–C(2)–C(2a)–C(3)	131.7(2) [123.0]	128.3	118.1(1) [121.8]
C(3)–C(2a)–C(10c)–C(6a)	47.1(4) [44.6]	41.2	53.7(2) [45.4]
C(2a)–C(2)–C(1)–C(10b)	–14.9(3) [–4.3]	–4.7	–2.7(2) [–4.5]
C(2)–C(2a)–C(10c)–C(10b)	–12.0(2) [–6.0]	–8.0	–6.5(2) [–7.6]
C(2)–C(1)–C(10b)–C(10c)	7.6(3) [0.4]	–0.3	–1.4(2) [–0.3]
C(1)–C(2)–C(2a)–C(10c)	15.4(2) [6.2]	7.6	5.3(2) [7.2]
C(1)–C(10b)–C(10c)–C(6a)	–176.9(2) [170.6]	–169.7	–172.5(1) [–167.6]
C(10a)–C(10b)–C(10c)–C(6a)	0.4(3) [–175.2]	–3.3	3.1(2) [5.7]

[a]) Values from AM1 calculations in brackets. [b]) *Cf. Scheme 11*; E_{Me} = H in *trans*-**31a** or *cis*-**31a**.

unequivocally demonstrated that it is formed in a polar rearrangement from *trans*-**10a** and *cis*-**10a**, followed by a dehydrogenation step (*cf. Scheme 9*)[13]). The precursor of *trans*-**10a** and *cis*-**10a**, *i.e.*, **13a** (*cf. Scheme 6*), may also rearrange thermally into **11a**. If dehydrogenation reactions are already possible for intermediates of type **13a**, the polar rearrangement to acenaphthylene-1,2-dicarboxylates or their benzo analogues may be suppressed in favor of the formation of cyclopent[*cd*]azulenedicarboxylates or their benzo derivatives. An instructive example is the thermal behavior of benz[*a*]azulene (**24**) in the presence of ADM. Besides dimethyl benzo[*a*]heptalene-6,7-dicarboxylate (**23a**), appreciable amounts of benzo[*a*]cyclopent[*cd*]azulene-6,7-dicarboxylate **26a** are also formed (*cf. Scheme 10*) [2][13] (for further examples, see [24]).

Scheme 10

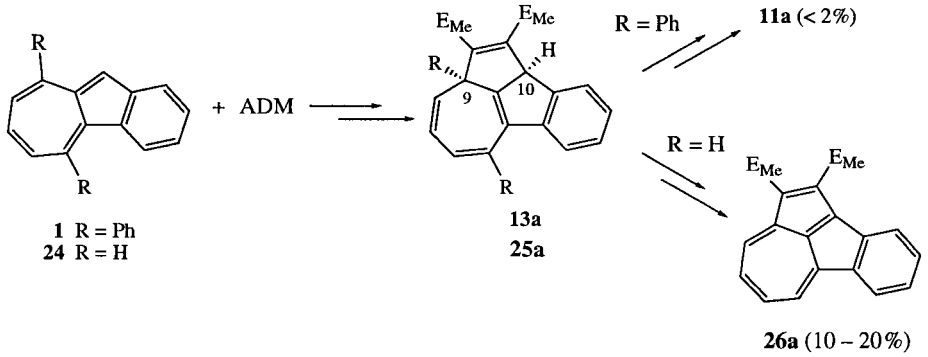

In the present investigation, we found **11a** in the reaction mixture of **1** with ADM (*cf. Scheme 5*). Its analogues **11b** – **11d** were not found in detectable amounts (TLC) in the corresponding reaction mixtures with ADR. The UV spectra of fluoranthene derivatives are very characteristic with at least two equally intense absorption bands >300 nm. For **11a** (hexane), these maxima are found at 374 nm (log ε 3.92) and 342 nm (log ε 3.88) (*cf. Fig. 8*). Fluoranthene (isooctane) itself shows the absorption maxima at 359 (log ε 3.97) and 341 nm (log ε 3.91) with further maxima at 323 nm (log ε 3.78) and 308 nm (3.60) [29]. The ^{1}H-NMR spectrum ($CDCl_3$) of **11a** only allowed the identification of a benzo-anellated structure with a strongly deshielded *doublet* with fine structure at 8.03 ppm (H–C(10)), followed by a further signal of this type at 7.37 ppm (H–C(7)) and two *doublet* × *triplet* signals at 7.30 and 7.16 ppm (H–C(9) and H–C(8), respectively). The important signals of H–C(4) and H–C(5) were completely hidden under the resonance lines of the two Ph rings (7.6–7.4 ppm). Therefore, we determined the structure of **11a** by an X-ray crystal-structure analysis (*Fig. 9*) that removed any doubt about the substitution pattern of **11a**. As expected, the fluoranthene skeleton is perfectly planar, but the planes of both ester groups and the Ph substituents are substantially turned out of the fluoranthene plane by $>43°$.

---

13) π-Donor substituents, such as MeO, on the azulenes may favor this reaction path. For example, 7,8-dimethoxybenz[*a*]azulene reacts with ADM in MeCN or toluene at temperatures $>60°$ to give, in this case by loss of MeOH in the final step, 4-methoxyfluoranthene-1,2-dicarboxylate as the sole product in yields up to 55% [28].

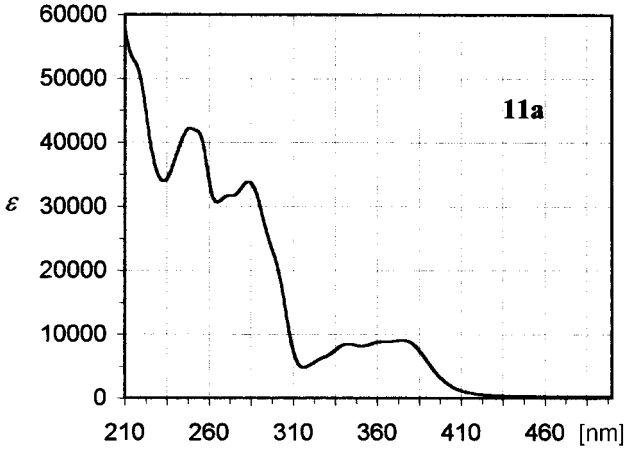

Fig. 8. *UV Spectrum* (hexane/2% CH_2Cl_2) *of dimethyl 3,6-diphenylfluoranthene-1,2-dicarboxylate* (**11a**)

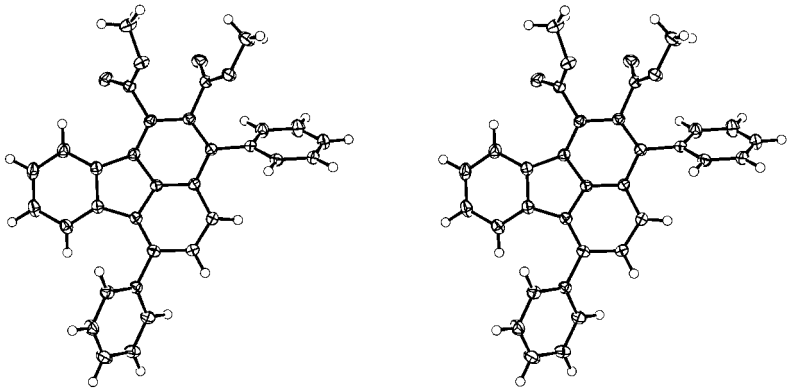

Fig. 9. *Stereoscopic view of the molecular structure of dimethyl 3,6-diphenylfluoranthene-1,2-dicarboxylate* (**11a**)

4. Concluding Remarks. – Our results, which are summarized together with some ΔH_f^0 values obtained from AM1 calculations in *Scheme 11* demonstrate that benz[*a*]azulenes behave in a similar manner to azulenes in their reaction with acetylenedicarboxylates. The main reaction path is determined with high periselectivity by the HOMO(azulene) and LUMO(acetylenedicarboxylate) interaction that leads to the reversible formation of the primary intermediates of type **2a** (**27a**) in a [4+2] manner. Other pericyclic processes do not play a significant role despite the fact that they result in the formation of products of type **12a** (**29a**) or intermediates such as **13a** (**25a**) which display much larger ΔH_f^0 differences with respect to the reactants (**1**(**24**) + ADM)[14]), whereby neither the Ph substituents on the benz[*a*]azulene (**24** → **1**) nor the

[14]) ΔH_f^0(**2a**/**27a**) – ΔH_f^0(**1**/**24** + ADM) = – 7.8/ – 12.5 and – 12.2 kcal · mol^{-1}, respectively, for the basal system; ΔH_f^0(**12a**/**29a**) – ΔH_f^0(**1**/**24** + ADM) = – 37.9/ – 35.3 and – 38.1 kcal · mol^{-1}, respectively, for the basal system; ΔH_f^0(**13a**/**25a**) – ΔH_f^0(**1**/**24** + ADM) = – 31.4/ – 35.3 and – 35.5 kcal · mol^{-1}, respectively, for the basal system.

Scheme 11

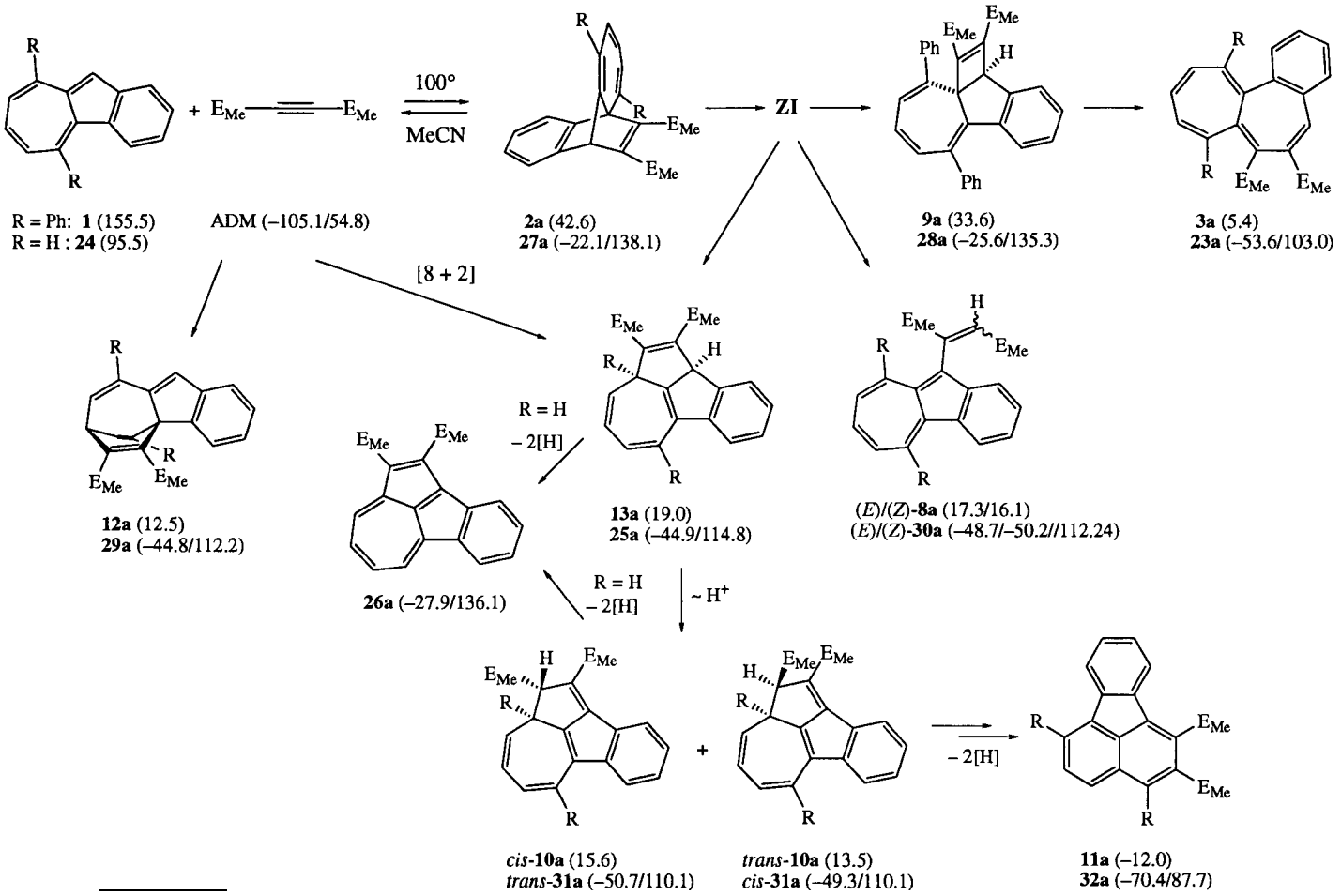

[a]) The numbers in parentheses represent the ΔH_f^0 values in kcal · mol^{-1} from AM1 calculations; second line, second-value: parent structure.

E_{Me} groups of the acetylene unit cause significant differences in the $\Delta\Delta H_f^0$ values[14]). *Fig. 10* shows the orbital coefficients for the relevant C-atoms of the HOMO and SHOMO of azulene and benz[*a*]azulene. The symmetry of azulene is disturbed by the benzo-anellation on the *a*-side. As a consequence, the pericyclic [4 + 2] reaction at the seven-membered ring of benz[*a*]azulenes, leading to compounds of type **12a** (**29a**), must no longer be SHOMO(azulene)-controlled as is necessary for azulenes, because the HOMO of azulenes have a nodal plane passing through C(2) and C(6). However, the orbital coefficients of benz[*a*]azulene are small at C(4b) and C(7) in the HOMO, as well as in the SHOMO (*cf. Fig. 10*), in accordance with the fact that we have found only trace amounts of **12a** in the reaction mixture of **1** and ADM. The pericyclic [8 + 2] reaction that leads to compounds of type **13a** (**25a**) should, according to the relevant orbital coefficients for C(9) and C(10) of the HOMO of benz[*a*]azulene, efficiently compete with the [4 + 2] reaction that finally furnishes the benzo[*a*]heptalene-6,7-dicarboxylates of type **3a** (**23a**). Indeed, the thermal reaction of **24** and ADM in mesitylene at 160° gives, under these optimized conditions, in addition to 55% of the expected benzo[*a*]heptalene-6,7-dicarboxylate **23a**, 11% of products, derived from the primary [8 + 2] product **25a** [20] (see also *Scheme 10*). That the reaction of **1** and ADM in the dark (*vide supra*) delivers only trace amounts of **13a**, which rearranges under the thermal conditions into the fluoranthene-dicarboxylate **11a**, seems to be an electronic and/or steric effect of the Ph substituent at C(9). Most of the side-products that have been isolated from the reaction mixture of **1** and ADM in MeCN result from the zwitterion **ZI** that is formed by heterolysis of the relevant C(4a)–C(11) bond in **2a**.

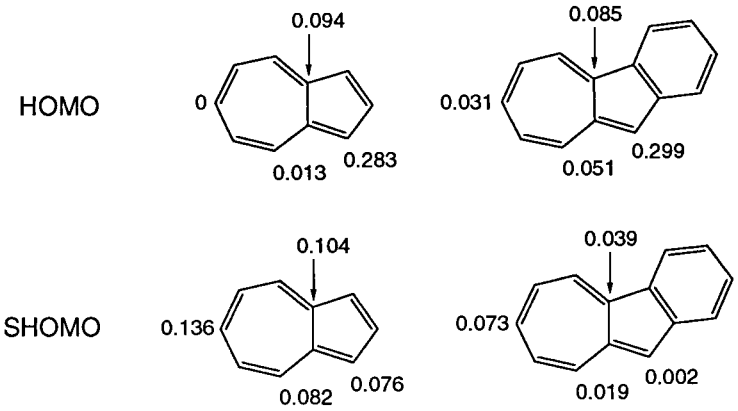

Fig. 10. *Relevant SCF orbital coefficients of the HOMO and SHOMO of azulene and benz[a]azulene* (**24**)

Two new polycyclic structures can be formed by ring closure of the zwitterions **ZI**, namely, on one hand, those of type **3a** (**28a**) and, on the other hand, those of type **13a** (**25a**), which differ markedly in their AM1-calculated ΔH_f^0, with $\Delta\Delta H_f^0$ values between 15 and 21 kcal·mol^{-1} (*cf. Scheme 11*) in favor of the latter. In other words, relaxed zwitterions **ZI** should prefer the formation of five-ring structures instead of the much more strained four-ring intermediates that yield the benzo[*a*]heptalenes by strain

relaxation[15]). However, the heterolysis of the C(4a)–C(11) bond in **2a** (**27a**) results in the formation of zwitterions **ZI** in a specific conformation. The break-down of this conformation by C–C bond formation can only lead back to the starting intermediates (**2a**/**27a**) or to the four-ring structures of type **9a** (**28a**) with slightly smaller ΔH_f^0 values. The conformation of the zwitterions has to be changed by rotation around the C(10′)–C(1) bond (equivalent to the corresponding bonds in the fumarate- or maleate-type products; *cf.* (*E*)-**8a**/(*Z*)-**8a** (**30a**) in *Scheme 11*) before the formation of the intermediates of type **13a** (**25a**) can take place. Therefore, the fate of the zwitterions **ZI** is strongly dependent on the character of the solvent (aprotic/protic; apolar/polar) and on the character of the substituents at the seven-membered ring of the azulenes and their benzo analogues (*cf. Footnote 13* and the discussion in [6]). Nevertheless, the reaction of benz[*a*]azulenes with dialkyl acetylenedicarboxylates in aromatic solvents, such as toluene or mesitylene, or in polar aprotic sovents, such as MeCN, is a valuable method for the synthesis of dialkyl benzo[*a*]heptalene-6,7-dicarboxylates, whereby catalysts such as $[RuH_2(PPh_3)_4]$ exert only a modest influence on the reaction.

We thank Prof. *M. Hesse* and his co-workers for mass spectra, our NMR Laboratory for specific NMR measurements, and our Analytical Laboratory for elemental analyses. The financial support of this work by the *Swiss National Science Foundation* is gratefully acknowledged.

Experimental Part

General. MeCN (*Fluka*, *puriss.*), DMF (*Fluka*, *puriss.*), benzene (*Fluka*, *puriss.*), ADM (*Aldrich*), ADE (*Fluka*, *purum*), ADtB (*Fluka*, *purum*) were used without further purification. ADiP was prepared according the method of *Fischer* from acetylenedicarboxylic acid. The catalysts were synthesized following the procedures of *Levison* and *Robinson* [30], and of *Giordano* and *Crabtree* [31]. The reactions of azulenes with dialkyl acetylene-dicarboxylates (ADR) were performed under Ar in oven-dried *Schlenk* vessels. MPLC: *KronLab Masterkron 4* with a *LiChroprep Si 60* (15–25 μm) column (30 × 450 mm) from *Merck*. HPLC: *Spherisorb CN* (5 μm) column (25.0 × 0.46 cm) from *Bischoff Chromatography*, and *Chiralced OD* (5 μm) or *Chiralcel OD-H* (5 μm) column (25.0 × 0.46 cm) from *Daicel Chemical Industries*. Irradiation with 8 lamps *Sylvania* (type *sterilAir BLC 8*, 366 nm, 8 watts). M.p.: *Mettler* apparatus (model *FP5* and *FP52*); not corrected. UV Spectra: *Perkin-Elmer* spectrophotometer (model *Lambda 9*); λ_{max} and λ_{min} in nm (log ε). IR Spectra: *Perkin-Elmer* spectrophotometer (model *1600* series FTIR); band positions in cm^{-1}. ^{1}H- and ^{13}C-NMR Spectra: *Bruker* instruments (model *AC 300*, *ARX 300*, *AM 400*, *AMX600*). MS: *Varian MAT 1125* for CI (NH_3) and *Finnigan MAT SSQ 700* for EI (70 eV); source temp. 250°; *m*/*z* (rel. int [%]).

1. Synthesis of 5,9-Diphenylbenz[*a*]azulene (1). – 1.1. *1,3-Diphenylcyclopent[*a*]indene-2,8(2*H*,8*H*)-dione* (**4**). Ninhydrine (48.6 g, 272.6 mmol) and 57.3 g (272.5 mmol) dibenzyl ketone were dissolved in 400 ml of hot EtOH, and 35 ml of 10% KOH/MeOH were added slowly. The dark yellow soln. became dark violet, and **4** started to crystallize. After completion of the addition of KOH, stirring was continued for another 1 h at 75°. The crystals were filtered and washed with MeOH. The product was recrystallized from toluene, the residue of the mother liquor from MeCN, to give dark violet crystals of **4** (in total 76.2 g, 84%).

Data of **4**. M.p. 205–206° (toluene). IR (KBr): 3070*w* (sh), 1703*s*, 1687*s*, 1642*s*, 1614*m*, 1590*m*, 1492*m*, 1444*m*, 1361*m*, 1306*w*, 1269*w*, 1206*m*, 1185*m*, 1166*m*, 1136*m*, 1105*m*, 994*m*, 958*w*, 888*w*, 798*m*, 776*m*, 754*w*, 732*s*, 692*m*, 660*w*, 634*m*, 565*m*, 527*w*, 507*w*, 471*w*. ^{1}H-NMR ($CDCl_3$): 8.61 (2*dd*, $^3J = 7.5$, $^4J = 2.1$, H–C(2″), H–C(6″)); 8.20 (*m*, H–C(7)); 8.07 (*m*, H–C(4)); 7.77–7.71 (*m*, H–C(5), H–C(6), H–C(2′), H–C(6′)); 7.56–7.43 (*m*, 4 H_m and 2 H_p of Ph). ^{1}H-NOE (400 MHz, $CDCl_3$): 8.61 (H–C(2″) and H–C(6″)) → 7.54–7.43

---

[15]) Indeed, the reactions of azulenes and ADM in the presence of *Lewis* acids such as Et_2AlCl or others in toluene at 0° lead exclusively to intermediates of type **13a** (**25a**) that undergo further reactions. We will report on this new type of azulene addition chemistry in this journal [15].

(*m*, H–C(3″), H–C(5″)); 8.20 (H–C(7)) → 7.75–7.71 (*m*, H–C(6)); 8.07 (H–C(4)) → 8.61 (2*dd*, H–C(2″), H–C(6″)); 7.75–7.71 (*m*, H–C(5)); 7.74 (H–C(5)) → 8.07 (*m*, H–C(4)); 7.74 (H–C(6)) → 8.20 (*m*, H–C(7)); 7.74 (H–C(2′), H–C(6′)) → 8.61 (2*dd*, H–C(2″), H–C(6″)); 7.56–7.47 (*m*, H–C(3′), H–C(5′)). ^{13}C-NMR ($CDCl_3$): 200.30 (*s*, C=O); 184.86 (*s*, C=O); 149.87, 143.44, 143.14, and 138.11 (4*s*); 135.18, 133.19, 131.17, 131.01 (4*d*); 130.79, 130.50, 129.92 (3*s*); 129.27, 128.71, 128.59, 128.53, 125.75, 124.90 (6*d*); 121.72 (*s*).

1.2. *7,10-Dihydro-5,9-diphenylbenz[*a*]azulen-10-one* (**5**). Cyclopropene was generated according to the method of *Closs* and *Krantz* [9]. $NaNH_2$ (40 g, 1 mol) was suspended in 70 ml of xylene. The suspension was heated to 80–90° under stirring. Very slowly, 86 ml (1 mol) of allyl chloride, diluted with 50 ml of xylene, were added. The developing gaseous cyclopropene was transferred with a weak stream of N_2 into a soln. of 79.85 g (238.8 mmol) of **4** in CH_2Cl_2 (500 ml). After completion of the addition of allyl chloride, heating and stirring was continued for further 2 h. The whole procedure of cyclopropene generation was repeated until the color of the soln. had changed from dark violet to orange. The yield of cyclopropene, calculated from the amount of allyl chloride, necessary for the complete conversion of **4** into **5** was 6–7%. CH_2Cl_2 was removed by distillation. The residue was recrystallized from EtOH, leading to orange crystals of **5** (68.48 g, 83%).

Data of **5**. M.p. 175–177° (EtOH). R_f(hexane/Et_2O 2:1) 0.43. IR (KBr): 3061*m*, 3023*m*, 2885*w*, 1712*s*, 1602*m*, 1490*m*, 1445*m*, 1389*m*, 1290*w*, 1242*m*, 1183*w*, 1151*w*, 1076*w*, 900*m*, 872*m*, 809*m*, 788*m*, 762*s*, 736*m*, 724*s*, 698*s*, 670*w*, 640*w*, 606*w*, 534*w*. ^{1}H-NMR ($CDCl_3$, 295 K): 7.45 (*dd*, ^3J = 6.5, ^4J = 1.4, H–C(1′7.42–7.28 (*m*, 10 H, 2 Ph); 7.12 (*td*, $^3J(1,2) \approx {}^3J(2,3) \approx 7.6$, ^4J = 1.2, H–C(2)); 7.07 (*td*, $^3J(2,3) \approx {}^3J(3,4) \approx 7.6$, ^4J = 1.4, H–C(3)); 6.33 (*dd*, ^3J = 6.7, ^4J = 1.2, H–C(4)); 5.84 (*t*, ^3J = 7.3, H–C(6)); 5.63 (*t*, ^3J = 7.1, H–C(8)); 3.13 (br., H_{exo}–C(7)); 2.20 (br., H_{endo}–C(7)). ^{1}H-NMR ($CDCl_3$, 263 K; if not otherwise stated, coupling patterns and constants are the same as above): 7.49; 7.43–7.33; 7.16; 7.12; 6.32; 5.92; 5.71; 3.19 (961.4 Hz) (*dt*, ^2J = 12.3, $^3J \approx 7.9$, H_{exo}–C(7)); 2.22 (669.4 Hz) (*dt*, ^2J = 12.3, $^3J \approx 6.6$, H_{endo}–C(7)). ^{1}H-NMR ($CDCl_3$, 320 K; if not otherwise stated, coupling patterns and constants are the same as above): 7.44; 7.41–7.27; 7.10; 7.05; 6.33; 5.77; 5.56; 2.6 (very br.; coalescence). ^{1}H-NMR ((D$_6$)acetone; 294 K): 7.50 (*m*, H–C(1), 1 H of Ph); 7.43–7.27 (*m*, 9 H of 2 Ph); 7.22 (*td*, $^3J(1,2) \approx {}^3J(2,3) \approx 7.6$, ^4J = 1.4, H–C(2)); 7.18 (*td*, $^3J(2,3) \approx {}^3J$ (3,4) ≈ 7.6, ^4J = 1.5, H–C(3)); 6.34 (*dd*, ^3J = 6.7, ^4J = 1.4, H–C(4)); 6.03 (*t*, ^3J = 7.3, H–C(6)); 5.78 (*t*, ^3J = 7.1, H–C(8)); 3.23 (br., H_{exo}–C(7)); 2.22 (br., H_{endo}–C(7)). ^{1}H-NMR ((D$_6$)acetone, 241 K; if not otherwise stated, coupling patterns and constants are the same as above): 7.47–7.28; 7.26; 7.22; 6.27; 6.05 (*dd*, ^3J = 7.6, ^3J = 7.0, H–C(6)); 5.80 (*dd*, ^3J = 7.4, ^3J = 6.8, H–C(8)); 3.20 (*dt*, ^2J = 12.3, $^3J \approx 7.9$, H_{exo}–C(7)); 2.18 (*dt*, ^2J = 12.3, $^3J \approx 6.6$, H_{endo}–C(7)). ^{1}H-NOE (400 MHz, $CDCl_3$): 7.45 (H–C(1)) → 7.12 (*td*, H–C(2)); 6.33 H–C(4)) → 7.42–7.35 (*m*, H–C(2′), H–C(6′)), 7.07 (*td*, H–C(3)); 5.84 (H–C(6)) → 7.42–7.35 (*m*, H–C(2′), H–C(6′)), 5.63 (*t*, H–C(8)), 3.13 (br., H_{exo}–C(7)), 2.20 (br., H_{endo}–C(7)); 5.63 (H–C(8)) → 7.34–7.28 (*m*, H–C(2″), H–C(6″)), 5.84 (*t*, H–C(6)), 3.13 (br., H_{exo}–C(7)), 2.20 (br., H_{endo}–C(7)). ^{13}C-NMR ($CDCl_3$): 194.97 (*s*, C=O); 153.43, 144.65, 139.86, 138.93, 136.86, 136.49, 135.25 (7*s*); 133.33 (*d*); 131.33 (*s*); 128.94 (*d*, 2 C of Ph); 128.62 (*d*, 2 C of Ph); 128.40 (*d*, 2 C of Ph); 128.36 (*d*); 128.10 (*d*, 2 C of Ph); 128.02, 127.44, 123.61, 122.96, 122.36, 117.93 (6*d*); 28.33 (*t*, C(8)).

1.3. *7,10-Dihydro-5,9-diphenylbenz[*a*]azulene* (**6**). Compound **5** (24.86 g, 71.8 mmol) was suspended in 1.5 l of Et_2O; 19.2 g (144 mmol) $AlCl_3$ and 5.45 g (144 mmol) $LiAlH_4$ were added, and the mixture was heated for 2 h under reflux. During this time, the color of the soln. changed from orange to orange-yellow, and then the soln. became clear. After cooling, the reaction was quenched by addition of conc. aq. NH_4Cl. The Et_2O layer was washed with H_2O, dried ($MgSO_4$), and then distilled. According to TLC (Et_2O/hexane 1:40), the residue contained mainly **6** (R_f 0.36) and a yellow-colored by-product (R_f 0.30). Recrystallization from Et_2O/hexane gave **6** (13.58 g) as yellow-colored crystals. The residue of the dried mother liquor was separated by CC (hexane). Recrystallization from Et_2O/hexane gave additional 2.10 g colorless crystals of **6**. The total yield of **6** was 15.68 g (66%).

Data of **6**. M.p. 143.5–144.0° (Et_2O/hexane). UV (hexane): λ_{max} 300 (1.2)[16]), 253 (2.6), 241 (2.7); λ_{min} 281 (1.0), 247 (2.5), 227 (2.4). IR (KBr): 3019*m* (sh), 2947*m*, 2892*m*, 1599*m*, 1491*m*, 1458*m*, 1445*m*, 1394*m*, 1309*w*, 1157*w*, 1075*w*, 1026*w*, 970*w*, 916*w*, 859*m*, 837*m*, 788*w*, 762*s*, 730*s*, 699*s*, 641*m*, 590*w*, 549*m*, 526*m*, 455*w*. ^{1}H-NMR ($CDCl_3$, 294 K): 7.39–7.26 (*m*, 11 H of 2 Ph, H–C(1)); 7.10 (*td*, $^3J(1,2) \approx {}^3J(2,3) \approx 7.4$, ^4J = 1.1, H–C(2)); 7.00 (*td*, $^3J(2,3) \approx {}^3J(3,4) \approx 7.5$, ^4J = 1.1, H–C(3)); 6.62 (*dd*, ^3J = 7.6, ^4J = 1.1, H–C(4)); 5.83 (*t*, ^3J = 7.2, H–C(6)); 5.73 (*t*, ^3J = 7.1, H–C(8)); 3.86, 3.66 (2 br. signals, CH_2(10)); 2.96 (br., H_{exo}–C(7)); 2.16 (br., H_{endo}–C(7)). ^{1}H-NMR ($CDCl_3$, 262 K; if not otherwise stated, coupling patterns and constants are the same as above): 7.44

[16]) UV Data from an HPLC analysis; relative absorptions in parentheses.

(*dd*, ^3J = 7.3, ^4J = 1.1, H–C(1)); 7.42–7.34; 7.17; 7.07; 6.66; 5.86; 5.76; 4.08 (1224.5 Hz); 3.53 (1059.6 Hz) (*AB*, ^2J = 23.4, CH_2(10)); 3.07 (921.7 Hz) (*dt*, ^2J = 12.4, $^3J \approx$ 7.8, H_{exo}–C(7)); 2.08 (622.4 Hz) (*dt*, ^2J = 12.4, $^3J \approx$ 6.5, H_{endo}–C(7)). ^{1}H-NMR ($CDCl_3$, 328 K; if not otherwise stated, coupling patterns and constants are the same as above): 7.35–7.24; 7.07; 6.97; 6.61; 5.82; 5.71; 3.72 (*s*); 2.54 (br.). Coalescence of the signals of CH_2(10) occurred at 296 K and for those of CH_2(7) at 300 K. ^{1}H-DR ($CDCl_3$, 260 K): 3.07 → 5.86 (*d*, ^3J = 6.7, H–C(6)); 5.76 (*d*, ^3J = 6.4, H–C(8)); 2.08 ppm → 5.86 (*d*, ^3J = 7.8, H–C(6)); 5.76 (*d*, ^3J = 7.7, H–C(8)). ^{1}H-NOE (400 MHz, $CDCl_3$, 260 K): 7.4 (H–C(1), H of Ph) → 7.10 (*d*, H–C(2)), 5.83 (*t*, H–C(6)), 5.73 (*t*, H–C(8)), 4.08 (*d*, H_α–C(10)), 3.53 (*d*, H_β–C(10)); 4.08 (H_α–C(10)) → 3.53 (*d*, H_β–C(10)); 3.53 (H_β–C(10)) → 4.08 (*d*, H_α–C(10)); 2.08 (H_{endo}–C(7)) → 5.83 (*t*, H–C(6)), 5.73 (*t*, H–C(8)), 2.96 (*m*, H_{exo}–C(7)). ^{13}C-NMR ($CDCl_3$): 146.19, 144.36, 142.20, 142.05, 141.93, 140.61, 139.74, 136.92 (8*s*); 128.84 (*d*, 2 C of Ph); 128.60 (*d*, 2 C of Ph); 128.23 (*d*, 4 C of Ph); 127.14, 127.13, 125.85, 124.79, 123.61, 123.05, 122.17, 122.07 (8*d*); 40.62 (*t*, ^1J = 130.7, C(10)); 28.02 (*tt*, ^1J = 130.9, ^2J = 4.6, C(7)).

1.3.1. endo- *and* exo-*1a,8a-Dihydro-2,8-diphenyl-1*H,*8*H-*cyclopropa[*b*]fluorene* (*endo*-**7** and *exo*-**7**, resp.). The yellow-to-orange colored fractions of the CC were collected, and their residue was recrystallized twice from Et_2O/hexane, yielding orange crystals. From the crystallization of the mother liquor, a mixture of orange and yellow crystals were obtained, which were separated mechanically. Finally, 1.21 g (5.1%) of pure orange *endo*-**7** and 0.055 g (0.5%) of pure yellow *exo*-**7** were obtained.

Data of endo-**7**: M.p. 105–110° (slowly melting). UV (hexane): λ_{max} 339 (3.91), 282 (4.06), 229 (4.27); λ_{min} 304 (3.52), 265 (3.96), 225 (4.26). IR (KBr): 3062*m*, 3025*m*, 2855*w*, 1960*w*, 1902*w*, 1801*w*, 1602*s*, 1556*m*, 1493*s*, 1450*s* (sh), 1384*m*, 1363*m*, 1347*m*, 1281*m*, 1213*m*, 1156*w*, 1132*w*, 1093*w*, 1074*m*, 1056*m*, 1029*m*, 1010*w*, 981*m*, 900*m*, 871*m*, 843*m*, 811*m*, 795*w*, 763*s*, 751*s*, 733*m*, 700*s*, 669*w*, 626*w*, 562*w*, 531*m*, 505*w*. ^{1}H-NMR ($CDCl_3$): 7.64 (*dd*, ^3J = 7.9, ^4J = 1.6, H–C(2) and H–C(6) of Ph–C(8)); 7.53–7.45 (*m*, H–C(2) and of H–C(6) of Ph–C(2)); H–C(3), H–C(4), and H–C(5) of Ph–C(8)); 7.41 (*tt*, $^3J \approx$ 7.2, $^4J \approx$ 1.5, H–C(3) and H–C(5) of Ph–C(2)); 7.33 (*tt*, ^3J = 7.1, ^4J = 1.5, H–C(4) of Ph–C(2)); 7.09 (*dd*, ^3J = 7.1, ^4J = 1.4, H–C(6)); 7.04 (*td*, $^3J(4,5) \approx {}^3J(5,6) \approx$ 7.3, ^4J = 1.1, H–C(5)); 6.95 (*dd*, ^3J = 7.7, ^4J = 1.1, H–C(3)); 6.80 (*td*, $^3J(3,4) \approx {}^3J(4,5) \approx$ 7.5, ^4J = 1.4, H–C(4)); 6.15 (*dd*, ^4J = 2.4, ^4J = 0.7, H–C(7)); 4.44 (*dd*, ^3J = 5.1, ^4J = 2.4, H–C(8)); 1.95 (*td*, $^3J \approx$ 7.8 (average value of $^3J(1_{exo},1a)$ = 8.0 and $^3J(8a,1a)$ = 7.6), ^3J = 4.1, H–C(1a)); 1.85 (*dddd*, ^3J = 8.6, ^3J = 7.6, ^3J = 6.6, ^3J = 5.1, H–C(8)); 1.58 (*td*, ^2J = 3.8, $^3J \approx$ 8.3 (average value of $^3J(1_{exo},8a)$ = 8.6 and $^3J(1_{exo},1a)$ = 8.0), H_{exo}–C(1)); 0.79 (*dddd*, ^2J = 3.8, ^3J = 6.6, ^3J = 4.1, ^4J = 0.7, H_{endo}–C(1)). ^{1}H-NOE (400 MHz, $CDCl_3$): 6.15 (H–C(7)) → 7.49 (*d*, H–C(2) and H–C(6) of Ph–C(2)), 7.09 (*d*, H–C(6)), 4.44 (*d*, H–C(8)); 4.44 (H–C(8)) → 7.49 (*d*, H–C(2) and H–C(6) of Ph–C(2)), 6.15 (*d*, H–C(7)), 1.85 (*ddd*, H–C(8a)); 0.79 (H_{endo}–C(1)) → 7.64 (*d*, H–C(2) and H–C(6) of Ph–C(8)), 7.49 (*d*, H–C(2) and H–C(6) of Ph–C(2)), 2.0–1.8 (*m*, H–C(1a), H–C(8a)), 1.58 (*td*, H_{exo}–C(1)). ^{13}C-NMR ($CDCl_3$): 149.40 (*s*, C(2)); 144.03 (*s*, C(1) of Ph–C(2)); 143.44 (*s*, C(6a)); 141.00 (*s*, C(1) of Ph–C(8)); 139.23 (*s*, C(7a)); 134.23 (*s*, C(2b)); 131.79 (*s*, C(2a)); 128.79 (*d*, C(2), C(6) of Ph–C(2); C(3) and C(5) of Ph–C(8)); 128.51 (*d*, C(3) and C(5) of Ph–C(2); C(2), C(4), and C(6) of Ph–C(8)); 126.77 (*d*, C(4) of Ph–C(2)); 126.43 (*d*, C(5)); 126.25 (*d*, C(7)); 123.73 (*d*, C(4)); 121.71 (*d*, C(3)); 119.99 (*d*, C(6)); 40.42 (*d*, C(8)); 22.40 (*t*, C(1)); 21.31 (*d*, C(1a)); 19.76 (*d*, C(8a)). Assignments of the signals were verified by ^{1}H,^{13}C-COSY spectra.

The structure of *endo*-**7** was confirmed by an X-ray crystal-structure analysis (*cf. Fig. 1,a*, and *Table 9*).

Data of exo-**7**: M.p. 167–168°. UV (hexane): λ_{max} 340 (3.98), 284 (4.13), 232 (4.26); λ_{min} 305 (3.51), 261 (4.01), 224 (4.25). IR (KBr): 3056*m* (sh), 3022*m*, 3009*m* (sh), 2874*m*, 1948*w*, 1878*w*, 1811*w*, 1753*w*, 1636*s*, 1597*m*, 1557*w*, 1490*s*, 1450*s*, 1440*s*, 1384*m*, 1352*m*, 1315*m*, 1268*w*, 1208*w*, 1096*w*, 1074*m*, 1045*m*, 1026*s*, 946*m*, 895*m*, 874*w*, 853*m*, 833*s*, 814*w*, 789*m*, 776*s*, 754*s*, 710*s*, 697*s*, 678*w*, 664*w*, 630*w*, 606*w*, 556*w*, 526*m*, 508*w*, 493*w*. ^{1}H-NMR ($CDCl_3$): 7.67 (*dd*, ^3J = 7.7, ^4J = 1.7, H–C(2) and H–C(6) of Ph–C(8)); 7.53–7.44 (*m*, H–C(3), H–C(4), and H–C(5) of Ph–C(8)); 7.34 (*dd*, ^3J = 8.0, ^4J = 1.3, H–C(2) and H–C(6) of Ph–C(2)); 7.27 (*tt*, $^3J \approx$ 7.6, $^4J \approx$ 1.6, H–C(3) and H–C(5) of Ph–C(2)); 7.17 (*tt*, ^3J = 7.1, ^4J = 1.6, H–C(4) of Ph–C(2)); 7.14 (*dd*, ^3J = 7.0, ^4J = 1.4, H–C(6)); 7.05 (*td*, $^3J(4,5) \approx {}^3J(5,6) \approx$ 7.4, ^4J = 1.0, H–C(5)); 6.99 (*d* (br. lines), ^3J = 7.7, H–C(3)); 6.81 (*td*, $^3J(3,4) \approx {}^3J(4,5) \approx$ 7.5, ^4J = 1.2, H–C(4)); 6.50 (*d*, ^4J = 0.8, H–C(7)); 4.55 (br. *s*, H–C(8)); 1.94 (*tdd*, $^3J \approx$ 7.9 (average value of $^3J(1_{exo},1a)$ = 8.2 and $^3J(8a,a)$ = 7.6), ^3J = 4.2, $^4J \approx$ 0.7, H–C(1a)); 1.79 (*dddd*, ^3J = 8.7, ^3J = 7.6, ^3J = 6.7, ^3J = 0.9, H–C(8a)); 1.62 (*td*, ^2J = 3.8, $^3J \approx$ 8.4 (average value of $^3J(1_{exo},8a)$ = 8.7 and $^3J(1_{exo},1a)$ = 8.2), H_{exo}–C(1)); 0.69 (*dt*, $J \approx$ 4.0 (average value of $^2J(1_{endo},1_{exo})$ = 3.8 and $^3J(1_{endo},1a)$ = 4.2), ^3J = 6.7, H_{endo}–C(1)). ^{1}H-NOE ($CDCl_3$): 6.50 (H–C(7)) → 7.34 (*dd*, H–C(2) and H–C(6) of Ph–C(2)), 7.14 (*d*, H–C(6)), 4.55 (*s*, H–C(8)); 4.55 (H–C(8)) → 7.67 (*d*, H–C(2) and H–C(6) of Ph–C(8)), 7.34 (*dd*, H–C(2) and H–C(6) of Ph–C(2)), 7.27 (*d*, H–C(3) and H–C(5) of Ph–C(2)), 6.50 (*s*, H–C(7)), 1.79 (*dd*, H–C(8a)), 0.69 (*dt*, H_{endo}–C(1)); 1.79 (H–C(8a)) → 7.67 (*d*, H–C(2) and H–C(6) of Ph–C(8)), 7.53–7.44 (*m*, H–C(3), H–C(4), and H–C(5) of Ph–C(8)), 7.34 (*d*, H–C(2) and H–C(6) of Ph–C(2)),

6.50 (*s*, H–C(7)), 4.55 (*s*, H–C(8)), 1.94 (*td*, H–C(1a)), 1.62 (*td*, H_{exo}–C(1)), 0.69 (*dt*, H_{endo}–C(1)); 0.69 (H_{endo}–C(1)) → 4.55 (*s*, H–C(8)), 1.94 (*m*, H–C(1a)), 1.79 (*dd*, H–C(8a)), 1.62 (*td*, H_{exo}–C(1)). ^{13}C-NMR ($CDCl_3$): 150.12 (*s*, C(2)); 147.91 (*s*, C(1) of Ph–C(2)); 143.53 (*s*, C(6a)); 141.12 (*s*, C(1) of Ph–C(8)); 138.26 (*s*, C(7a)); 133.56 (*s*, C(2b)); 130.81 (*s*, C(2a)); 128.61 (*d*, C(3) and C(5) of Ph–C(2) and C(2′)–C(6′) of Ph–C(8)); 127.23 (*d*, C(2) and C(6) of Ph–C(2)); 126.45 (*d*, C(5)); 126.10 (*d*, C(4) of Ph–C(2)); 125.95 (*d*, C(7)); 123.60 (*d*, C(4)); 121.86 (*d*, C(3)); 119.99 (*d*, C(6)); 40.48 (*d*, C(8)); 23.54 (*t*, C(1)); 20.73 (*d*, C(1a)); 20.28 (*d*, C(8a)). Assignments of the signals were verified by ^{1}H,^{13}C-COSY spectra.

The structure of *exo*-**7** was confirmed by an X-ray crystal-structure analysis (*cf. Fig. 1,b*, and *Table 9*).

1.3.2. *Reactions with* endo-**7** *and* exo-**7**. 1.3.2.1. *Treatment with* t-*BuOK*. Compound *endo*-**7** (0.011 g) was dissolved in *t*-BuOH (6 ml), and a catalytic amount of *t*-BuOK was added. The mixture was kept at 50° for 24 h, and then quenched with H_2O and neutralized with aq. HCl. After workup, TLC showed that the mixture still contained *endo*-**7**. ^{1}H-NMR Analysis revealed the presence of distinct amounts of **6** and a number of further products in trace amounts.

1.3.2.2. *Irradiation of* endo-**7** *and* exo-**7**. Solns. of *exo*-**7** and *endo*-**7** in hexane ($c = 7.6 \cdot 10^{-5}$ M and $1.11 \cdot 10^{-3}$ M, resp.) were irradiated with the light of a fluorescent tube (λ_{max} (emiss.): 366 nm) overnight. HPLC Analysis showed that the soln. of *endo*-**7** had not changed, whereas the solution of *exo*-**7** contained 10–20% of *endo*-**7**.

1.4. *Ionic Dehydrogenation of* **6**. Compound **6** (5.00 g, 15.04 mmol) was dissolved in CH_2Cl_2 (50 ml), and 5.46 g (16.54 mmol) of $Ph_3C^+BF_4^-$ were added, whereby a red soln. was obtained. Precipitation of the ochre-yellow BF_4^- salt of $\mathbf{6}^+$ started within 10 min. After 1 h stirring, hexane (12 ml) was added to complete the precipitation. The salt was filtered, washed with hexane, and redissolved in CH_2Cl_2 (*ca.* 300 ml). Et_3N (2.31 ml; 16.54 mmol) was added dropwise to this soln., whereby the green-yellow color of the soln. changed to blue. The soln. was filtered, and CH_2Cl_2 was removed by distillation. The residue was purified by CC (Alox, act. IV) with toluene/hexane 1:5. Crystallization from toluene gave **1** (4.44 g, 90%) as dark-blue-to-black crystals.

Data of **1**: M.p. 144.4–144.8° (toluene). R_f(Alox, act. IV, toluene/hexane 1:5) 0.33. ^{1}H-NMR (300 MHz, $CDCl_3$): 7.66 (*d*, $^3J(1,2) = 7.9$, H–C(1)); 7.60–7.41 (*m*, H–C(2), 10 arom. H); 7.13 (*dd*, $^3J(6,7) = 11.4$, $^3J(7,8) = 8.8$, H–C(7)); 7.11 (*s*, H–C(10)); 6.99 (*ddd*, $^3J(3,4) = 8.4$, $^3J(2,3) = 7.1$, $^3J(1,3) = 1.1$, H–C(3)); 6.86 (*d*, $^3J(6,7) = 11.4$, H–C(6)); 6.80 (*d*, $^3J(7,8) = 8.8$, H–C(8)); 6.66 (*dd*, $^3J(3,4) = 8.4$, $^4J(2,4) = 0.8$, H–C(4)).

2. Formation of Dialkyl 8,12-Diphenylbenzo[*a*]heptalene-6,7-dicarboxylates 3. – 2.1. *Dimethyl 8,12-Diphenylbenzo[*a*]heptalene-6,7-dicarboxylate* (**3a**). 2.1.1. *Formation of* **3a** *in the Presence of [$RuH_2(PPh_3)_4$]* (*cf.* [1]). Azulene **1** (0.661 g, 2.00 mmol) was dissolved in MeCN (15 ml) under Ar in a flame-dried *Schlenk* vessel, and then 2 mol-% of [$RuH_2(PPh_3)_4$] (0.046 g) were added, followed by ADM (0.74 ml, 6.00 mmol). The vessel was again flushed with Ar and then closed. The dark blue soln. was stirred for 18 h at 100°, whereby the color of the soln. changed to dark brown-yellow. The solvent was removed under reduced pressure, and ^{1}H-NMR ($CDCl_3$) was recorded from the raw residue to determine the molar ratio of the formed intermediates **2a**, **9a**, and heptalene **3a**, which was 0.95:0.32:1.00, according to the integrals of the *s* at 4.51 ppm (H–C(10) of **2a**), 4.37 ppm (H–C(10) of **9a**), and 8.42 ppm (H–C(5) of **3a**).

For the determination of the total yield of **3a**, the dark-brown residue was dissolved in DMF (20 ml) and heated for 1 h at 150°. The solvent was distilled off under reduced pressure, and the residue was purified by CC on silica gel (Et_2O/hexane 1:3, 1% Et_3N) to give a small amount of **1** (0.015 g, 5.7%), followed by **3a** as a yellow foam (0.768 g, 81%), which crystallized on treatment with Et_2O.

2.1.2. *Formation of* **3a** *in the Presence of [$RhH(PPh_3)_4$]*. The reaction was performed as described in *2.1.1* and with the same amounts of reactants. The molar ratio of **2a**/**9a**/**3a** was 0.98:0.31:1.00. The thermal reaction in DMF led to **1** (0.010 g, 3.3%) and **3a** (0.865 g, 91%).

2.1.3. *Formation of* **3a** *in the Presence of [Rh(cod)Cl]$_2$*. The reaction was performed as described in *2.1.1* and with the same amounts of reactants, but with only 1 mol-% of the catalyst (0.010 g). The molar ratio of **2a**/**9a**/**3a** was 0.62:0.06:1.00. The thermal reaction in DMF led to **1** (0.015 g, 5.7%) and **3a** (0.830 g, 88%).

2.1.4. *Formation of* **3a** *without a Catalyst*. As described in *2.1.1*, **1** (0.099 g, 0.030 mol) and ADM (0.11 ml, 0.090 mmol) in MeCN (3 ml) were stirred at 100° over 18 h. The molar ratio of **2a**/**9a**/**3a** was 1.21:0.41:1.00. The thermal reaction in DMF (5 ml) led to **1** (0.004 g, 4.0%) and **3a** (0.118 g, 83%).

Data of **3a**: Yellow prisms. M.p. 200.7–201.1° (Et_2O/hexane). R_f(hexane/Et_2O 1:1) 0.24. MPLC (hexane/CH_2Cl_2 1:2; flow rate 20 ml/min): t_R 216.0. UV and IR: see [1]. ^{1}H-NMR (300 MHz, $CDCl_3$): 8.42 (*s*, H–C(5)); 7.57 (*d* with f.s., $^3J(3,4) = 7.6$, H–C(4)); 7.31 (*td*, $^3J(3,4) = 7.5$, $^3J(2,3) = 7.6$, $^4J(1,3) = 1.1$, H–C(3)); 7.19–7.03 (*m*, 8 arom. H, H–C(2)); 6.95–6.83 (*m*, 2 arom. H, H–C(9), H–C(10)); 6.69 (*dd*, $^3J(10,11) = 10.8$, $^4J(9,11) = 0.9$, H–C(11)); 6.61 (*d* with f.s., $^3J(1,2) = 7.3$, H–C(1)); 3.77 (*s*, MeOCO–C(6)); 3.22 (*s*, MeOCO–C(7)). ^{13}C-NMR (75 MHz, $CDCl_3$; assignments *via* ^{1}H,^{13}C-correlation spectra at 600 MHz): 167.16 (C(13)); 166.90 (C(15)); 143.83 (C(7a)); 143.34 (C(5)); 139.31 (1 arom. C); 139.26 (1 arom. C); 138.48 (C(8) or C(12)); 138.18

(C(12b)); 136.21 (C(12) or C(8)); 135.96 (C(4a)); 133.42 (C(11)); 131.84 (C(10)); 131.53 (C(2)); 130.60 (C(4)); 130.47 (2 arom. C); 130.15 (C(1) and C(6)); 128.35 (2 arom. C); 128.23 (C(12a)); 127.65 (2 arom. C); 127.57 (C(3)); 127.23 (1 arom. C); 126.99 (1 arom. C); 126.81 (2 arom. C); 125.60 (C(7)); 124.60 (C(9)); 52.31 (C(14)); 51.61 (C(16)).

The structure of **3a** was confirmed by an X-ray crystal-structure analysis (*cf. Fig. 5*, and *Tables 6* and *9*).

2.1.5. *Isolation of the Intermediates* **2a** *and* **9a**. The dark brown residue of the mixture of **2a**, **9a**, and **3a** from a run, performed as described under *2.1.1*, was pre-chromatographed over a short silica gel column (CH_2Cl_2/hexane 2:1, 1% Et_3N) to remove decomposed material and a small amount of **1**, and then subjected to MPLC (CH_2Cl_2/hexane 2:1). In a first fraction, pure **2a** was obtained, followed by **9a** and **3a**.

*Data of Dimethyl 4b,10-Etheno-5,9-diphenyl-10*H*-benz[*a*]azulene-11,12-dicarboxylate* (**2a**): Yellow crystals. M.p. 111° (dec.; hexane). R_f(hexane/CH_2Cl_2 1:3) 0.24. MPLC (hexane/CH_2Cl_2 1:2; flow rate 20 ml/min): t_R 93.3. UV and IR: see [1]. ^{1}H-NMR (600 MHz, C_6D_6): 7.72–7.71 (*m*, 2 arom. H); 7.52 (*d*, $^3J(3,4) = 7.3$, H–C(4)); 7.13 (*d*, $^3J(1,2) = 7.0$, H–C(1)); 7.05–6.97 (*m*, 6 arom. H); 6.92 (*d*, $^3J_{ortho} = 7.1$, 2 arom. H); 6.81 (*td*, $^3J(1,2) = {}^3J(2,3) = 7.3$, $^4J(2,4) = 1.0$, H–C(2)); 6.77 (*td*, $^3J(2,3) = {}^3J(3,4) = 7.5$, $^4J(1,3) = 1.1$, H–C(3)); 6.53 (*d*, $^3J(6,7) = 8.2$, H–C(6)); 5.61 (*dd*, $^3J(6,7) = 8.5$, $^3J(7,8) = 11.9$, H–C(7)); 5.56 (*d*, $^3J(7,8) = 11.6$, H–C(8)); 4.84 (*s*, H–C(10)); 3.19 (*s*, MeOCO–C(12)); 2.99 (*s*, MeOCO–C(11)). ^{13}C-NMR (75 MHz, C_6D_6; assignments *via* ^{1}H,^{13}C-correlation spectra at 600 MHz): 166.15 (C(9a)); 165.97 (C(13)); 163.45 (C(15)); 161.67 (C(12)); 156.45 (C(4a)); 141.97 (C(10a)); 140.61 (1 arom. C); 140.48 (1 arom. C); 140.18 (C(11)); 136.83 (C(5)); 130.94 (C(8)); 128.68 (2 arom. C); 128.46 (2 arom. C); 128.36 (2 arom. C); 128.24 (1 arom. C); 128.11 (1 arom. C); 127.78 (1 arom. C); 127.57 (C(6)); 127.35 (1 arom. C); 126.60 (C(2)); 125.55 (C(3)); 124.99 (C(7)); 124.67 (C(4)); 122.51 (C(1)); 116.27 (C(9)); 71.39 (C(4b)); 53.88 (C(10)); 51.64 (C(14)); 51.11 (C(16)).

*Data of Dimethyl (9a*S**,10*R**)-9a,10-Etheno-5,9-diphenyl-10*H*-benz[*a*]azulene-11,12-dicarboxylate* (**9a**): Yellow prisms. M.p. 160.6–161.2° (Et_2O/hexane). R_f(hexane/CH_2Cl_2 1:3) 0.24. MPLC (hexane/CH_2Cl_2 1:2; flow rate 20 ml/min): t_R 100.2. UV (hexane): λ_{max} 340.8 (3.61), 267.2 (sh, 4.31), 257.6 (4.34); λ_{min} 340.8 (3.53), 248.0 (4.33). IR (KBr): 3061*w*, 3010*w*, 2951*w*, 1737*s*, 1721*s*, 1649*m*, 1440*m*, 1326*m*, 1270*s*, 1137*m*, 759*m*, 702*m*. ^{1}H-NMR (600 MHz, C_6D_6): 7.36 (*d*, $^3J_{ortho} = 7.4$, 1 arom. H); 7.34 (*d*, $^3J(1,2) = 7.5$, H–C(1)); 7.23–7.17 (*m*, 4 arom. H); 7.09 (*tt*, $^3J_{ortho} = 7.3$, $^4J_{meta} = 1.4$, 1 arom. H); 7.06 (*t*, $^3J_{ortho} = 7.4$, 1 arom. H); 6.79–6.95 (*m*, 3 arom. H); 6.87 (*td*, $^3J(1,2) = {}^3J(2,3) = 7.1$, $^4J(2,4) = 1.5$, H–C(2)); 6.68 (*td*, $^3J(2,3) = {}^3J(3,4) = 8.0$, $^4J(1,3) = 1.0$, H–C(3)); 6.66 (*d* with f.s., $^3J(3,4) = 8.0$, H–C(4)); 6.42 (*d*, $^3J(7,8) = 6.4$, H–C(8)); 6.37 (*d*, $^3J(6,7) = 11.5$, H–C(6)); 6.20 (*dd*, $^3J(6,7) = 6.4$, $^3J(7,8) = 11.6$, H–C(7)); 4.63 (*s*, H–C(10)); 3.43 (*s*, MeOCO–C(12)); 3.12 (*s*, MeOCO–C(11)). ^{1}H-NOE (600 MHz, $CDCl_3$): 4.37 (H–C(10)) → 7.19–7.16 (*s*); 7.28 (*s*). ^{13}C-NMR (75 MHz, C_6D_6; assignments *via* ^{1}H,^{13}C-correlation spectra at 600 MHz): 164.25 (C(15)); 161.54 (C(13)); 149.28 (C(4b)); 143.15 (C(10a)); 142.44 (1 arom. C); 142.30 (1 arom. C); 141.98 (C(4a)); 136.54 (C(11)); 136.44 (C(5)); 135.34 (C(6)); 133.50 (C(9)); 132.61 (C(12)); 129.67 (1 arom. C); 129.49 (1 arom. C); 128.98 (1 arom. C); 128.90 (C(2)); 128.80 (C(8)); 128.68 (C(7)); 128.51 (2 arom. C); 128.27 (2 arom. C); 128.00 (1 arom. C); 127.73 (1 arom. C); 127.68 (C(3)); 127.32 (1 arom. C); 127.28 (C(4)); 126.70 (C(1)); 62.62 (C(9a)); 55.38 (C(10)); 51.86 (C(16)); 51.17 (C(14)). EI-MS: 472 (20, $M^{+\cdot}$), 440 (13, $[M - MeOH]^{+\cdot}$), 312 (32, $[M - MeOH - CO]^{+\cdot}$), 381 (19, $[M - MeOH - MOCO]^{+\cdot}$), 352 (9, $[M - 2\,MeOH - 2\,CO]^{+\cdot}$), 330 (80, $[M - ADM]^{+\cdot}$). Anal. calc. for $C_{32}H_{24}O_4$ (472.54): C 81.34, H 5.12; found: C 81.36, H 5.32.

The structure of **9a** was confirmed by an X-ray crystal-structure analysis (*cf. Fig. 4*, and *Tables 5* and *9*).

2.1.6. *Isolation of the Side-Products (*E*)-***8a*** and (*Z*)-***8a***, cis-***10a*** and* trans-***10a***, ***11a***, and* ***12a***. The fractions and mother liquors of the runs *2.1.1* to *2.1.4* were combined and subjected to MPLC (CH_2Cl_2/hexane 2:1). A first fraction contained (*Z*)-**8a**, followed by fractions containing *trans*-**10a**, **11a**, *cis*-**10a**, **12a**, and (*E*)-**10a**, respectively.

*Data of Dimethyl (2*R**,2a*S**)-2,2a-Dihydro-2a,6-diphenylbenzo[*a*]cyclopent[*cd*]azulene-1,2-dicarboxylate* (*cis*-**10a**): Orange prisms. M.p. 188° (dec.; hexane/CH_2Cl_2). R_f(hexane/CH_2Cl_2 1:3) 0.24. MPLC (hexane/CH_2Cl_2 1:2; flow rate 20 ml/min): t_R 117.3. UV (hexane): λ_{max} 346.0 (sh, 3.86), 327.6 (sh, 4.01), 318.8 (4.05), 267.6 (4.48); λ_{min} 297.2 (3.88), 230.0 (4.25). IR (KBr): 3058*w*, 3023*w*, 2946*w*, 2840*w*, 1745*s*, 1715*s*, 1629*w*, 1596*m*, 1440*m*, 1332*m*, 1308*m*, 1297*m*, 1278*s*, 1254*s*, 1217*m*, 1199*m*, 1117*s*, 780*m*, 760*m*, 717*m*, 700*s*. ^{1}H-NMR (300 MHz, $CDCl_3$): 8.28 (*d*, $^3J(9,10) = 7.3$, H–C(10)); 7.38–7.33 (*m*, 4 arom. H); 7.27–7.24 (*m*, 3 arom. H); 7.16–7.08 (*m*, 3 arom. H, H–C(9)); 7.03 (*td*, $^3J(7,8) = J(8,9) = 7.6$, $^4J(8,10) = 1.1$, H–C(8)); 6.51 (*d*, $^3J(3,4) = 10.9$, H–C(3)); 6.41 (*d*, $^3J(4,5) = 6.9$, H–C(5)); 6.32 (*dd*, $^3J(3,4) = 10.0$, $^3J(4,5) = 7.0$, H–C(4)); 6.31 (*d*, $^3J(7,8) = 7.6$, H–C(7)); 4.74 (*s*, H–C(2)); 3.90 (*s*, MeOCO–C(1)); 3.14 (*s*, MeOCO–C(2)). ^{1}H-NOE (400 MHz, $CDCl_3$): 4.74 (H–C(2)) → 6.51 (*s*). ^{13}C-NMR (75 MHz, $CDCl_3$; assignments *via* ^{1}H,^{13}C-correlation spectra at 600 MHz): 171.11 (MeO*C*O–C(2)); 164.41 (MeO*C*O–C(1)); 154.56 (C(10b)); 149.54 (C(10c)); 149.16 (C(6b)); 145.00 (1 arom. C); 139.99 (1 arom. C); 139.20 (C(6)); 132.32 (C(6a)); 131.03 (C(5)); 130.30 (C(8));

130.21 (C(10a)); 129.27 (C(3)); 128.46 (2 arom. C); 128.40 (2 arom. C); 128.36 (2 arom. C, C(6)); 128.07 (1 arom. C); 127.61 (C(10)); 127.14 (C(4)); 126.93 (1 arom. C); 125.71 (C(9)); 125.51 (2 arom. C); 122.47 (C(7)); 73.22 (C(2)); 52.23 (*Me*OCO–C(2)); 52.07 (*Me*OCO–C(1)); 51.41 (C(2a)). EI-MS: 472 (15, $M^{+\cdot}$), 440 (29, $[M-\text{MeOH}]^{+\cdot}$), 412 (46, $[M-\text{MeOH}-\text{CO}]^{+\cdot}$), 381 (100, $[M-\text{MeOH}-\text{MeOCO}]^{+}$), 354 (37, $[M-2\,\text{MeOCO}]^{+\cdot}$). Anal. calc. for $C_{32}H_{24}O_4$ (472.54): C 81.34, H 5.12; found: C 81.64, H 5.05.

The structure of *cis*-**10a** was confirmed by an X-ray crystal-structure analysis (*cf. Fig. 7*, and *Tables 8* and *9*).

*Data of Dimethyl (2*R**,2a*R**)-2,2a-Dihydro-2a,6-diphenylbenzo[*a*]cyclopent[*cd*]azulene-1,2-dicarboxylate* (*trans*-**10a**): Red prisms. M.p. 201.7–203.2° (CH_2Cl_2/hexane). R_f(hexane/CH_2Cl_2 1:3) 0.31. MPLC (hexane/CH_2Cl_2 1:2; flow rate 20 ml/min): t_R 75.9. UV (hexane): λ_{max} 348.8 (sh, 3.87), 319.2 (4.04), 267.2 (4.46); λ_{min} 298.4 (3.91), 232.0 (4.28). IR (KBr): 3064*w*, 3021*w*, 2996*w*, 2947*w*, 2841*w*, 1742*s*, 1703*s*, 1636*w*, 1598*w*, 1574*w*, 1435*m*, 1340*m*, 1300*m*, 1281*m*, 1238*s*, 1199*m*, 1168*m*, 768*m*, 718*m*, 700*m*. ^{1}H-NMR (300 MHz, $CDCl_3$): 8.32 (*d*, $^3J(9,10)=7.4$, H–C(10)); 7.43–7.34 (*m*, 7 arom. H); 7.25–7.20 (*m*, 3 arom. H); 7.14 (*t*, $^3J(8,9)=^3J(9,10)=7.4$, H–C(9)); 7.04 (*t*, $^3J(7,8)=^3J(8,9)=7.6$, H–C(8)); 6.37 (*d*, $^3J(4,5)=7.2$, H–C(5)); 6.31 (*d*, $^3J(7,8)=7.5$, H–C(7)); 6.25 (*dd*, $^3J(3,4)=10.3$, $^3J(4,5)=7.2$, H–C(4)); 5.94 (*d*, $^3J(3,4)=10.3$, H–C(3)); 4.72 (*s*, H–C(2)); 3.87 (*s*, MeOCO–C(2)); 3.82 (*s*, MeOCO–C(1)). ^{1}H-NOE (400 MHz, $CDCl_3$): 4.72 (H–C(2)) → 5.94 (*w*). ^{13}C-NMR (75 MHz, $CDCl_3$; assignments *via* ^{1}H,^{13}C-correlation spectra at 600 MHz): 170.28 (MeO*C*O–C(2)); 164.79 (Me*C*O–C(1)); 153.58 (*C*(10b)); 150.90 (C(10c)); 149.04 (C(6b)); 140.72 (C(6)); 139.80 (1 arom. C); 139.04 (1 arom. C); 131.52 (C(3)); 130.96 (C(6a)); 130.72 (C(5)); 130.30 (C(8)); 129.98 (C(10a)); 128.51 (2 arom. C); 128.44 (2 arom. C); 128.06 (1 arom. C); 127.51 (2 arom. C and C(1)); 127.31 (C(10)); 127.18 (3 arom. C and C(4)); 125.64 (C(9)); 122.27 (C(7)); 73.68 (C(2)); 53.24 (C(2a)); 52.11 (*Me*OCO–C(2)); 51.47 (*Me*OCO–C(1)). CI-MS (NH_3): 490 (100, $[M+NH_4]^+$), 473 (66, $[M+H]^+$), 441 (14, $[M-\text{MeO}]^+$), 412 (42, $[M-\text{MeOH}-\text{CO}]^+$). Anal. calc. for $C_{32}H_{24}O_4$ (472.54): C 81.34, H 5.12; found: C 81.20, H 5.33.

The structure of *trans*-**10a** was confirmed by an X-ray crystal-structure analysis (*cf. Fig. 7*, and *Tables 8* and *9*).

Data of Dimethyl 3,6-Diphenylfluoranthene-1,2-dicarboxylate (**11a**): Yellow prisms. M.p. 193.2–194.0° (CH_2Cl_2/hexane). R_f(hexane/CH_2Cl_2 1:3) 0.28. MPLC (hexane/CH_2Cl_2 1:2; flow rate 20 ml/min): t_R 84.0. UV (hexane): λ_{max} 375.0 (3.96), 361 (sh, 3.95), 342.5 (3.92), 283.3 (4.53), 272 (sh, 4.50), 248.6 (4.63); λ_{min} 350.7 (3.91), 316.3 (3.68), 264.8 (4.49) 233.1 (4.53). IR (KBr): 3060*w*, 3028*w*, 2946*w*, 2843*w*, 1727*s*, 1601*w*, 1574*w*, 1436*s*, 1385*m*, 1371*m*, 1359*m*, 1300*m*, 1280*m*, 1252*s*, 1231*s*, 1149*s*, 770*m*, 756*m*, 714*m*, 705*s*. ^{1}H-NMR (300 MHz, $CDCl_3$): 8.03 (*d* with f.s., $^3J(9,10)=7.7$, H–C(10)); 7.61–7.41 (*m*, 10 arom. H, H–C(4), H–C(5)); 7.37 (*d* with f.s., $^3J(7,8)=7.7$, H–C(7)); 7.30 (*td*, $^3J(8,9)=^3J(9,10)=7.6$, $^4J(7,9)=1.0$, H–C(9)); 7.16 (*td*, $^3J(7,8)=^3J(8,9)=7.6$, $^4J(8,10)=1.0$, H–C(8)); 4.06 (*s*, MeOCO–C(1)); 3.58 (*s*, MeOCO–C(2)). ^{13}C-NMR (75 MHz, $CDCl_3$; assignments *via* ^{1}H,^{13}C-correlation spectra at 600 MHz): 168.85 (C(13)); 168.14 (C(11)); 139.87 (C(6b)); 139.62 (1 arom. C); 139.15 (1 arom. C); 137.25 (C(10a)); 136.86 (C(10c)); 134.53 (C(10b)); 133.35 (C(6a)); 133.17 (1 arom. C); 132.92 (1 arom. C); 130.98 (1 arom. C); 129.97 (2 arom. C); 129.18 (2 arom. C); 128.81 (C(3a)); 128.64 (2 arom. C); 128.47 (C(8)); 128.20 (1 arom. C); 127.91 (3 arom. C and C(9)); 126.37 (1 arom. C); 124.92 (1 arom. C); 124.37 (C(10)); 123.46 (C(7)); 52.87 (C(12)); 52.23 (C(14)). CI-MS (NH_3): 488 (86, $[M+NH_4]^+$), 470 (61, $M^{+\cdot}$), 439 (100, $[M-\text{MeO}]^+$). Anal. calc. for $C_{32}H_{22}O_4$ (470.52): C 81.69, H 4.71; found: C 81.43, H 4.86.

The structure of **11a** was confirmed by an X-ray crystal-structure analysis (*cf. Fig. 9* and *Table 9*).

*Data of Dimethyl (Z)-1-(5,9-Diphenylbenz[*a*]azulen-10-yl)ethene-1,2-dicarboxylate* ((*Z*)-**8a**): Dark green needles. M.p. 182.4–183.3° (CH_2Cl_2/hexane). R_f(hexane/CH_2Cl_2 1:3) 0.33. MPLC (hexane/CH_2Cl_2 1:2; flow rate 20 ml/min): t_R 69.6. UV (hexane): λ_{max} 409.6 (3.80), 304.0 (4.60); λ_{min} 260.0 (4.37). IR (KBr): 3055*w*, 2996*w*, 2947*w*, 2839*w*, 1726*s*, 1646*w*, 1597*m*, 1556*m*, 1433*m*, 1416*m*, 1346*m*, 1251*s*, 1197*s*, 1166*s*, 757*m*, 730*m*, 704*m*. ^{1}H-NMR (300 MHz, $CDCl_3$): 7.61 (*d* with f.s., $^3J(1',2')=8.0$, H–C(1')); 7.59–7.55 (*m*, 3 arom. H); 7.51–7.42 (*m*, 2 arom. H, H–C(2')); 7.37–7.28 (*m*, 5 arom. H); 7.15 (*dd*, $^3J(7',8')=8.5$, $^3J(6',7')=11.4$, H–C(7')); 7.02 (*td*, $^3J(3',4')=^3J(2',3')=7.7$, $^4J(1',3')=1.1$, H–C(3')); 6.963 (*d*, $^3J(7',8')=8.4$, H–C(8')); 6.958 (*d*, $^3J(6',7')=11.5$, H–C(6')); 6.59 (*d* with f.s., $^3J(3',4')=7.3$, H–C(4')); 5.80 (*s*, H–C(2)); 3.68 (*s*, MeOCO–C(2)); 3.66 (*s*, MeOCO–C(1)). ^{13}C-NMR (75 MHz, $CDCl_3$; assignments *via* ^{1}H,^{13}C-correlation spectra at 600 MHz): 166.45 (C(3)); 165.58 (C(5)); 148.86 (C(5') or C(9')); 146.94 (C(5') or C(9')); 144.67 (1 arom. C); 144.41 (1 arom. C); 141.92 (C(10'a)); 141.41 (C(4'b)); 137.97 (C(1)); 137.32 (C(9'a)); 131.54 (C(6')); 131.46 (C(7')); 130.33 (C(4'a)); 129.70 (C(8')); 129.34 (2 arom. C); 129.02 (2 arom. C); 128.31 (2 arom. C); 128.21 (C(2)); 128.16 (1 arom. C); 127.96 (2 arom. C); 127.80 (C(2)); 127.71 (1 arom. C); 124.86 (C(10')); 124.65 (C(4')); 122.74 (C(3')); 118.61 (C(1')); 52.03 (C(4)); 51.61 (C(6)). EI-MS: 472 (8, $M^{+\cdot}$), 381 (22, $[M-\text{MeOH}-$

MOCO]$^+$), 353 (8, [M – MeOH – CO – MeOCO]$^{+\cdot}$). Anal. calc. for $C_{32}H_{24}O_4$ (472.54): C 81.34, H 5.12; found: C 81.14, H 5.30.

*Data of Dimethyl (*E*)-1-(5,9-Diphenylbenz[*a*]azulen-10-yl)ethene-1,2-dicarboxylate* ((*E*)-**8a**): Dark green prisms. M.p. 182.6–183.8° (Et_2O/hexane). R_f(hexane/CH_2Cl_2 1:3) 0.21. MPLC (hexane/CH_2Cl_2 1:2; flow rate 20 ml/min): t_R 194.4. UV (hexane): λ_{max} 383.2 (3.95), 368.0 (sh, 3.98), 311.2 (4.68), 263.2 (sh, 4.47); λ_{min} 378.4 (3.94), 256.0 (4.47). IR (KBr): 3055*w*, 3029*w*, 2946*w*, 2838*w*, 1716.2*s*, 1625*w*, 1596*w*, 1576*w*, 1557*w*, 1434*m*, 1419.2*m*, 1249*s*, 1200*s*, 1176*s*, 1023*m*, 760*m*, 735*m*, 702*m*. ^{1}H-NMR (300 MHz, $CDCl_3$): 7.61–7.49 (*m*, 5 arom. H); 7.38 (*td*, $^3J(2',3') = {}^3J(1',2') = 7.5$, $^4J(2',4') = 0.7$, H–C(2′)); 7.35–7.23 (*m*, 5 arom. H, H–C(1′)); 7.09 (*dd*, $^3J(7',8') = 8.7$, $^3J(6',7') = 11.3$, H–C(7′)); 6.97 (*td*, $^3J(3',4') = {}^3J(2',3') = 7.5$, $^4J(1',3') = 0.7$, H–C(3′)); 6.93 (*d* ith f.s., $^3J(6',7') = 11.1$, H–C(6′)); 6.82 (*dd*, $^3J(7',8') = 8.8$, $^4J(6',8') = 0.6$, H–C(8′)); 6.63 (*s*, H–C(2)); 6.60 (*d* with f.s., $^3J(3',4') = 8.3$, H–C(4′)); 3.60 (*s*, MeOCO–C(1)); 3.48 (*s*, MeOCO–C(2)). ^{13}C-NMR (75 MHz, $CDCl_3$; assignments *via* ^{1}H^{13}C-correlation spectra at 600 MHz): 166.00 (C(3)); 165.03 (C(5)); 149.18 (C(5′) or C(9′)); 146.61 (C(5′) or C(9′)); 145.32 (1 arom. C); 144.95 (1 arom. C); 142.14 (C(10a′)); 140.23 (C(4b′)); 140.18 (C(1)); 136.74 (C(9a′)); 131.39 (C(7′)); 131.14 (C(6′)); 130.54 (C(4a′)); 129.29 (1 arom. C); 129.22 (1 arom. C); 128.22 (1 arom. C); 128.00 (2 arom. C); 127.81 (C(2)); 127.79 (C(2′)); 127.75 (2 arom. C); 127.71 (3 arom. C); 127.49 (C(8′)); 125.12 (C(4′)); 123.05 (C(10′)); 122.17 (C(3′)); 118.10 (C(1′)); 52.45 (C(4)); 51.58 (C(6)). EI-MS: 472 (29, $M^{+\cdot}$), 412 (6, [M – MeOH – CO]$^{+\cdot}$), 381 (17, [M – MeOH – MeOCO]$^+$), 354 (14, [M – 2 MeOCO]$^{+\cdot}$). Anal. calc. for $C_{32}H_{24}O_4$ (472.54): C 81.34, H 5.12; found: C 81.39, H 4.94.

The structure of (*E*)-**8a** was confirmed by an X-ray crystal-structure analysis (*cf. Fig. 6* and *Table 9*).

*Data of Dimethyl 9,11-Diphenyl-4b,7-etheno-4b*H*,7*H*-benz[*a*]azulene-5,6-dicarboxylate* (**12a**): The yellow compound was only obtained in soln. R_f(hexane/CH_2Cl_2 1:3) 0.23. MPLC (hexane/CH_2Cl_2 1:2; flow rate 20 ml/min): t_R 126.3. ^{1}H-NMR (300 MHz, $CDCl_3$): 7.39–7.32 (*m*, 5 arom. H, H–C(4)); 7.21 (*td*, $^3J(2,3) = {}^3J(3,4) = 7.1$, $^4J(1,3) = 1.8$, H–C(3)); 7.07–6.89 (*m*, 3 arom. H, H–C(1), H–C(2)); 6.69 (*s*, H–C(10)); 6.66 (*d*, $^3J(7,12) = 6.9$, H–C(12)); 6.58 (*d* with f.s., $J_{ortho} = 8.0$, 2 arom. H); 6.19 (*d*, $^3J(7,8) = 8.6$, H–C(8)); 4.63 (*dd*, $^3J(7,8) = 8.5$, $^3J(7,12) = 6.9$, H–C(7)); 3.80 (*s*, MeOCO–C(6)); 3.26 (*s*, MeOCO–C(5)).

2.2. *Diethyl 8,12-Diphenylbenzo[*a*]heptalene-6,7-dicarboxylate* (**3b**). 2.2.1. *Formation of* **3b** *in the Presence of [$RuH_2(PPh_3)_4$]*. Azulene **1** (0.099 g, 0.030 mmol) and ADE (0.14 ml, 0.090 mmol) were reacted in MeCN (3 ml) in the presence of 2 mol-% of the catalyst (0.0069 g) as described in *2.1.1*. The molar ratio of **2b**/**9b**/**3b** was 0.87 : < 0.01 : 1.00, according to the integrals of the *s* at 4.54 ppm (H–C(10) of **2b**) and 8.40 ppm (H–C(5) of **3b**). The *s* of **9b** was largely covered by the *s* of **2b**. The thermal reaction of DMF (5 ml), followed by CC (CH_2Cl_2/hexane 4:1), led to pure **3b** (0.116 g, 77%) as a yellow foam, which crystallized on treatment with Et_2O/hexane.

2.2.2. *Formation of* **3b** *without a Catalyst*. The reaction was performed as described in *2.2.1* and with the same amounts of reactants. The molar ratio of **2b**/**9b**/**3b** was 1.07 : < 0.01 : 1.00. The thermal reaction in DMF (5 ml) resulted in the isolation of pure **3b** (0.123 g, 82%), which was recrystallized from Et_2O/hexane.

Data of **3b**: Yellow prisms. M.p. 152.2–154.4° (Et_2O/hexane). R_f(hexane/Et_2O 1:1) 0.28. ^{1}H-NMR (300 MHz, $CDCl_3$): 8.40 (*s*, H–C(5)); 7.58 (*d* with f.s., $^3J(3,4) = 7.6$, H–C(4)); 7.33 (*td*, $^3J(3,2) = {}^3J(3,4) \approx 7.6$, $^4J(3,1) = 1.3$, H–C(3)); 7.18–7.04 (*m*, 8 arom. H, H–C(2)); 6.96–6.84 (*m*, 2 arom. H, H–C(9), H–C(10)); 6.68 (*dd*, $^3J(11,10) = 11.0$, $^4J(11,9) = 0.8$, H–C(11)); 6.60 (*d* with f.s., $^3J(1,2) = 6.9$, H–C(1)); 4.33–4.14 (*m*, MeCH_2OCO–C(6)); 3.84–3.68, 3.62–3.46 (2*dq*, MeCH_2OCO–C(7)); 1.27 (*t*, *Me*CH_2OCO–C(6)); 0.83 (*t*, *Me*CH_2OCO–C(7)).

The primary and secondary intermediates **2b** and **9b** were not isolated and characterized. Their structures are evident from the fact that they showed almost the same t_R values as **2a** and **9a** and that they rearranged completely into **3b**. The presence of the other side products analogous to those of **2a**, **9a**, and **3a** were also recognizable by TLC and chromatography.

2.3. *Diisopropyl 8,12-Diphenylbenzo[*a*]heptalene-6,7-dicarboxylate* (**3c**). 2.3.1. *Formation of* **3c** *in the Presence of [$RuH_2(PPh_3)_4$]*. Azulene **1** (1.001 g, 3.03 mmol) and ADiP (1.784 g, 9.00 mmol) were reacted in MeCN (20 ml) in the presence of 2 mol-% of the catalyst (0.069 g) for 72 h as described in *2.1.1*. The molar ratio of **2c**/**9c**/**3c** was 2.00 : < 0.01 : 1.00, according to the integrals of the *s* at 4.51 ppm (H–C(10) of **2c**) and 8.33 ppm (H–C(5) of **3c**). The *s* of **9c** was covered by the *s* of **2c**. The thermal reaction in DMF (20 ml) for 5 h, followed by CC (CH_2Cl_2/hexane 3:1), led to pure **3c** (1.303 g, 81%), which was recrystallized from hexane/i-PrOH (93:7).

2.3.2. *Formation of* **3c** *in the Presence of [$RhH(PPh_3)_4$]*. Azulene **1** (0.496 g, 1.50 mmol) and ADiP (0.892 g, 4.50 mmol) were reacted in the presence of 2 mol-% of the catalyst (0.0345 g) in MeCN (15 ml) for 41 h as described in *2.1.1*. The thermal reaction in DMF (20 ml), followed by CC (CH_2Cl_2/hexane 3:1) and crystallization from hexane/i-PrOH (93:7), gave yellow crystals of **3c** (0.238 g, 30%).

2.3.3. *Formation of* **3c** *without a Catalyst*. Azulene **1** (0.099 g, 0.30 mmol) and ADiP (0.18 ml, 0.90 mmol) were heated in MeCN (3 ml) for 38 h as described in 2.1.1. The molar ratio of **2c**/**9c**/**3c** was 0.86 : < 0.01 : 1.00. The thermal reaction in DMF (5 ml), followed by CC (CH_2Cl_2/hexane 3 : 1) and crystallization as described, led to pure crystalline **3c** (0.0436 g, 27%).

2.3.4. *Formation of* **3c** *in the Presence of LiBr*. The reaction was performed as described in *2.3.3*, however, in the presence of 20 mol-% of LiBr (0.0052 g) for 40 h. The following thermal reaction in DMF (5 ml), CC (CH_2Cl_2/hexane 4 : 1), and crystallization gave pure **3c** (0.121 g, 77%).

Data of **3c**: Yellow prisms. M.p. 160.8–162.5° (hexane/i-PrOH 93 : 7). R_f(hexane/Et_2O 1 : 1) 0.38. ^{1}H-NMR (300 MHz, $CDCl_3$): 8.33 (*s*, H–C(5)); 7.59 (*d* with f.s., $^3J(4,3) = 7.6$, H–C(4)); 7.31 (*td*, $^3J(3,2) = {}^3J(3,4) \approx 7.6$, $^4J(3,1) = 1.2$, H–C(3)); 7.18–7.03 (*m*, 8 arom. H, H–C(2)); 6.96–6.84 (*m*, 2 arom. H, H–C(9), H–C(10)); 6.67 (*dd*, $^3J(11,10) = 10.8$, $^4J(11,9) = 0.9$, H–C(11)); 6.59 (*d* with f.s., $^3J(1,2) = 7.7$, H–C(1)); 5.08 (*sept.*, Me_2CHOCO–C(6)); 4.53 (*sept.*, Me_2CHOCO–C(7)); 1.30, 1.28 (2*d*, superimp. to *t*, Me_2CHOCO–C(6)); 0.93, 0.55 (2*d*, Me_2CHOCO–C(7)).

2.3.5. *Isolation of Intermediate* **2c** *and Side-Products* cis-**10c**, (E)- *and* (Z)-**8c**. These compounds could be isolated by CC from reaction mixtures of **1** and ADiP before they were subjected to thermal rearrangement in DMF.

*Data of Diisopropyl 5,6-Diphenyl-4b,10-etheno-10*H*-benz[*a*]azulene-11,12-dicarboxylate* (**2c**): Yellow prisms. M.p. 172.6–173.9° (CH_2Cl_2/hexane/toluene). R_f(hexane/Et_2O 1 : 1) 0.46. ^{1}H-NMR (300 MHz, $CDCl_3$): 7.69–7.66 (*m*, 2 arom. H); 7.35–7.22 (*m*, 6 arom. H, H–C(1), H–C(4)); 7.12–7.06 (*m*, 2 arom. H, H–C(2)); 7.00 (*td*, $^3J(3,2) = {}^3J(3,4) = 7.5$, $^4J(3,1) = 1.2$, H–C(3)); 6.68 (*d*, $^3J(6,7) = 8.7$, H–C(6)); 5.77 (*dd*, $^3J(7,6) = 8.7$, $^3J(7,8) = 12.0$, H–C(7)); 5.61 (*d*, $^3J(8,7) = 11.9$, H–C(8)); 5.07 (*sept.*, Me_2CHOCo–C(12)); 4.50 (*s*, H–C(10)); 4.29 (*sept.*, Me_2CHOCO–C(11)); 1.24, 1.23 (2*d*, Me_2CHOCO–C(12)); 1.08, 1.02 (2*d*, Me_2CHOCO–C(11)).

The structure of **2c** was confirmed by an X-ray crystal-structure analysis (*cf. Fig. 3*, and *Tables 3*, *4*, and *9*).

The secondary intermediate **9c** could not be found in the reaction mixture.

*Data of Diisopropyl (2*R**,2a*S**)-2,2a-Dihydro-2a,6-diphenylbenzo[*a*]cyclopent[*cd*]azulene-1,2-dicarboxylate* (*cis*-**10c**): ^{1}H-NMR (300 MHz, $CDCl_3$): 8.33 (*d*, $^3J(7,8) = 7.3$, H–C(10)); 7.38–7.28 (*m*, 7 arom. H); 7.18–6.93 (*m*, 3 arom. H, H–C(8), H–C(9)); 6.29 (*d*, $^3J(4,5) = 7.0$, H–C(5)); 6.25 (*d*, $^3J(7,8) = 7.6$, H–C(7)); 6.16 (*dd*, $^3J(3,4) = 10.3$, $^3J(4,5) \approx 7.0$, H–C(4)); 5.94 (*d*, $^3J(3,4) = 10.3$, H–C(3)); 5.14–5.06 (*m*, Me_2CHOCO–C(1,2)); 4.57 (*s*, H–C(2)); 1.30–1.23 (4*d*, 2 Me_2CHOCO).

*Data of Diisopropyl (*E*)-1-(5,9-Diphenylbenz[*a*]azulen-10-yl)ethene-1,2-dicarboxylate* ((*E*)-**8c**): ^{1}H-NMR (300 MHz, $CDCl_3$): 7.51–7.16 (*m*, 10 arom. H, H–C(1′), H–C(2′)); 6.99 (*dd*, $^3J(8',7') = 8.8$, $^3J(6',7') = 11.3$, H–C(7′)); 6.88 (*t* with f.s., $^3J(3',4') = {}^3J(2',3') \approx 7.5$, H–C(3′)); 6.81 (*d*, $^3J(6',7') = 11.2$, H–C(6′)); 6.72 (*d*, $^3J(7',8') = 9.3$, H–C(8′)); 6.51 (*d*, $^3J(3',4') = 8.3$, H–C(4′)); 6.46 (*s*, H–C(2)); 4.86 (*sept.*, Me_2CHOCO–C(1)); 4.65 (*sept.*, Me_2CHOCO–C(2)); 1.12, 1.06 (2*d*, Me_2CHOCO–C(1)); 0.84, 0.66 (2*d*, Me_2CHOCO–C(2)).

*Data of Diisopropyl (*Z*)-1-(5,9-Diphenylbenz[*a*]azulen-10-yl)ethene-1,2-dicarboxylate* ((*Z*)-**8c**): ^{1}H-NMR (300 MHz, $CDCl_3$): 7.62 (*d*, $^3J(1',2') = 8.2$, H–C(1′)); 7.51–7.20 (*m*, 10 arom. H, H–C(2′)); 7.04 (*dd*, $^3J(7',8') = 8.3$, $^3J(6',7') = 11.4$, H–C(7′)); 6.93 (*t* with f.s., $^3J(3',4') = {}^3J(2',3') = 8.1$, H–C(3′)); 6.852 (*d*, $^3J(6',7') = 11.4$, H–C(6′)); 6.850 (*d*, $^3J(7',8') = 8.5$, H–C(8′)); 6.51 (*d*, $^3J(3',4') = 8.3$, H–C(4′)); 5.60 (*s*, H–C(2)); 5.00 (*sept.*, Me_2CHOCO–C(1)); 4.87 (*sept.*, Me_2CHOCO–C(2)); 1.16 (*t*-like, 2 Me_2CHOCO–C(1,2)).

2.4. *Di*(tert-*butyl) 8,12-Diphenylbenzo[*a*]heptalene-6,7-dicarboxylate* (**3d**). 2.4.1. *Formation of* **3d** *in the Presence of [*$RuH_2(PPh_3)_4$*]*. Azulene **1** (0.099 g, 0.30 mmol) and AD*t*B (0.204 g, 0.090 mmol) were reacted in the usual manner according to *2.1.1* for 40 h. The molar ratio of **2d**/**9d**/**3d** was 1.16 : 0.15 : 1.00 according to the integrals of the *s* at 4.39 ppm (H–C(10) of **2d**), 4.28 ppm (H–C(10) of **9d**), and 8.20 ppm (H–C(5) of **3d**). The thermal reaction of the mixture in DMF (5 ml), followed by filtration over silica gel with CH_2Cl_2/hexane (4 : 1), then CC (hexane/Et_2O 4 : 1), and, finally MPLC (CH_2Cl_2/hexane 4 : 1), resulted in the isolation of pure **3d** (0.0494 g, 30%) as a yellow foam.

2.4.2. *Formation of* **3d** *without a Catalyst*. The same reaction as described in *2.4.1* was performed. The molar ratio of **2d**/**9d**/**3d** was 2.50 : 0.40 : 1.00. After thermal reaction in DMF and chromatographic purification, pure **3d** (0.042 g, 25%) was obtained as a yellow foam, which crystallized on treatment with Et_2O.

Data of **3d**: Yellow prisms. M.p. 100–101° (Et_2O/hexane). R_f(hexane/Et_2O 1 : 1) 0.45. MPLC (hexane/CH_2Cl_2 1 : 2; flow rate 20 ml/min): t_R 120.0. ^{1}H-NMR (300 MHz, $CDCl_3$): 8.20 (*s*, H–C(5)); 7.56 (*d* with f.s., $^3J(4,3) = 7.4$, H–C(4)); 7.28 (*td*, $^3J(3,2) \approx {}^3J(3,4) \approx 7.5$, $^4J(3,1) = 1.2$, H–C(3)); 7.21–7.01 (*m*, 8 arom. H, H–C(2)); 6.97 (*d*, $^3J(9,10) = 6.3$, H–C(9)); 6.87 (*dd*, $^3J(10,11) = 11.3$, $^3J(10,9) = 6.3$, H–C(10)); 6.87–6.83 (*m*, 2 arom. H); 6.65 (*d*, $^3J(11,10) = 11.3$, H–C(11)); 6.56 (*d* with f.s., $^3J(1,2) = 7.6$, H–C(1)); 1.55 (*s*, Me_3COCO–C(6)); 1.00 (*s*, Me_3COCO–C(7)).

No intermediates or side products of the reaction of **1** and AD*t*B were isolated and characterized. However, the general product pattern, as recognizable by TLC and MPLC, was the same as in the other reactions with **1** and ADR.

3. Formation of Dimethyl 8-Phenylbenzo[*a*]heptalene-6,7-dicarboxylate (21a). – 3.1. *Without a Catalyst.* The reaction of 8-phenylbenz[*a*]azulene [12][32] (0.070 g, 0.27 mmol) and ADM (0.10 ml, 0.81 mmol) in MeCN (10 ml) was performed as described in *2.1.4.* The molar ratio of the corresponding primary and secondary intermediates and **21a** was 2.53 : < 0.01 : 1.00, based on the integrals of the *s* at 4.50 ppm (H–C(10) of the primary intermediate) and 8.12 ppm (H–C(5) of **21a**). The *s* of H–C(10) of the secondary intermediate was not recognizable. The thermal reaction of the mixture in DMF (5 ml), and purification by means of CC (CH_2Cl_2/hexane 4 : 1) and MPLC (CH_2Cl_2/hexane 2 : 1), followed by crystallization from CH_2Cl_2/hexane, gave pure **21a** (0.0392 g, 37%).

Data of **21a**: Orange-yellow prisms. M.p. 166.1–167.8° (CH_2Cl_2/hexane). R_f(hexane/Et_2O 1 : 1) 0.26. MPLC (hexane/CH_2Cl_2 1 : 2; flow rate 20 ml/min): t_R 212.0. ^{1}H-NMR (600 MHz, (D_6)acetone): 8.16 (*s*, H–C(5)); 7.68 (*ddd*, ^3J(4,3) = 7.6, ^4J(4,2) = 1.4, ^5J(4,1) = 0.7, H–C(4)); 7.62 (*td*, ^3J(2,1) = ^3J(2,3) = 7.5, ^4J(2,4) = 1.5, H–C(2)); 7.58 (*td*, ^3J(3,2) = ^3J(3,4) = 7.5, ^4J(3,1) = 1.4, H–C(3)); 7.22–7.20 (*m*, 2 arom. H); 7.15–7.12 (*m*, 3 arom. H, H–C(1)); 6.92 (*dd*, ^3J(9,10) = 6.6, ^4J(9,11) = 0.5, H–C(9)); 6.78 (*ddd*, ^3J(10,11) = 11.2, ^3J(10,9) = 6.6, ^4J(10,12) = 0.8, H–C(10)); 6.71 (*ddd*, ^3J(11,10) = 11.2, ^3J(11,12) = 6.2, ^4J(11,9) = 0.5, H–C(11)); 6.15 (*dt*, ^3J(12,11) = 6.2, ^4J(12,10) = ^5J(12,1) = 0.6, H–C(12)); 3.68 (*s*, MeOCO–C(6)); 3.15 (*s*, MeOCO–C(7)).

The structure of **21a** was confirmed by an X-ray crystal-structure analysis (*cf. Table 9*).

4. Formation of Dialkyl Benzo[*a*]heptalene-6,7-dicarboxylates 23. – 4.1. *Dimethyl Benzo[*a*]heptalene-6,7-dicarboxylate* (**23a**). 4.1.1. *Formation of* **23a** *in the Presence of [$RuH_2(PPh_3)_4$].* The reaction of **24** (0.089 g, 0.50 mmol) and ADM (0.19 ml, 1.50 mmol) in MeCN (15 ml) for 13 h was performed as described in *2.1.1.* The molar ratio of **27a**/**28a**/**23a** was 1.18 : < 0.01 : 1.00, based on the integrals of the *s* at 4.58 ppm (H–C(10) of **27a**) and 8.01 ppm (H–C(5) of **23a**). The *s* of H–C(10) of **28a** was not recognizable. The thermal reaction of the mixture in DMF (5 ml), followed by CC (hexane/Et_2O 3 : 1) and then MPLC (CH_2Cl_2/hexane 9 : 2), led to crystalline **23a** (0.0288 g, 18%).

4.1.2. *Formation of* **23a** *without a Catalyst* (*cf.* [2][20]). The reaction described above was repeated without the catalyst. The molar ratio of **27a**/**28a**/**23a** was 1.13 : < 0.01 : 1.00. Thermal reaction and chromatographic workup of the mixture led to 19% (0.0298 g) of crystalline **23a**.

Data of **23a** (*cf.* [2][20]): M.p. 146.2–146.7° (Et_2O/hexane) ([2]: 151° (AcOEt/pentane)). R_f(hexane/Et_2O 1 : 1) 0.28. MPLC (hexane/CH_2Cl_2 2 : 9; flow rate 20 ml/min): t_R 77.5. ^{1}H-NMR (600 MHz, $CDCl_3$): 8.01 (*s*, H–C(5)); 7.44 (*td*, ^3J(2,3) = ^3J(2,1) = 7.4, ^4J(2,4) = 1.4, H–C(2)); 7.39 (*td*, ^3J(3,4) = ^3J(3,2) ≈ 7.5, ^4J(3,1) = 1.1, H–C(3)); 7.34 (*d*, ^3J(4,3) = 7.6, H–C(4)); 7.00 (*d*, ^3J(1,2) = 7.5, H–C(1)); 6.68 (*dd*, ^3J(11,10) = 11.1, ^3J(11,12) = 6.5, H–C(11)); 6.61 (*dd*, ^3J(10,11) = 11.1, ^3J(10,9) = 6.5, H–C(10)); 6.42 (*dd*, ^3J(9,8) = 10.9, ^3J(9,10) = 6.5, H–C(9)); 6.25 (*d*, ^3J(8,9) = 10.9, H–C(8)); 6.08 (*d*, ^3J(12,11) = 6.5, H–C(12)); 3.75 (*s*, MeOCO–C(6)); 3.67 (*s*, MeOCO–C(7)).

See [20] for an X-ray crystal-structure analysis of **23a**.

4.1.3. *Isolation of Intermediate* **27a** *and Side-Products* **26a**, *(*E*)-*-**30a** *and (*Z*)-*-**30a**, *and* cis-**31a**, *and* trans-**31a**. These compounds were obtained by CC and MPLC of the above-described reaction mixtures. Except for **26a**, crystallization of the compounds was not attempted. The chromatographically determined yields after thermal rearrangement were as follows (in parentheses yields without catalyst): (*E*)-**30a**: 2% (1%), (*Z*)-**30a**: 5% (5%), *trans*-**31a**/*cis*-**31a**: 16% (21%), and **26a**: 19% (12%).

*Data of Dimethyl 4b,10-Etheno-10*H*-benz[*a*]azulene-11,12-dicarboxylate* (**27a**): R_f(hexane/Et_2O 1 : 1) 0.36. MPLC (hexane/CH_2Cl_2 2 : 9; flow rate 20 ml/min): t_R 48.0. ^{1}H-NMR (300 MHz, C_6D_6): 7.20–7.12 (2*dd*, covered by the signal of C_6D_5H, H–C(1), H–C(4)); 6.84, 6.78 (2*t* with f.s., J_{ortho} ≈ 7.3, H–C(2), H–C(3)); 6.29 (*d*, ^3J(5,6) = 12.1, H–C(5)); 5.81 (*dd*, ^3J(6,5) = 12.1, ^3J(6,7) = 7.7, H–C(6)); 5.45 (*dd*, ^3J(7,8) ≈ 11.9, ^3J(7,6) ≈ 7.8, H–C(7)); 5.25 (*dd*, ^3J(8,7) ≈ 11.8, ^3J(8,9) = 7.4, H–C(8)); 4.79 (*d*, ^3J(9,8) = 7.4, H–C(9)); 5.61 (*dd*, ^3J(6,7) = 8.5, ^3J(7,8) = 11.9, H–C(7)); 5.56 (*d*, ^3J(7,8) = 11.6, H–C(8)); 4.50 (*s*, H–C(10)); 3.39 (*s*, MeOCO–C(12)); 3.21 (*s*, MeOCO–C(11)).

The secondary intermediate **28a** could not be identified in the reaction mixtures.

*Data of Dimethyl (*Z*)-1-(Benz[*a*]azulen-10-yl)ethene-1,2-dicarboxylate* ((*Z*)-**30a**): R_f(hexane/Et_2O 1 : 1) 0.30. MPLC (hexane/CH_2Cl_2 2 : 9; flow rate 20 ml/min): t_R 65.8. ^{1}H-NMR (300 MHz, $CDCl_3$): 8.48 (*dd*, ^3J(5′,6′) = 8.5, ^4J(5′,7′) = 1.0, H–C(5′)); 8.40, 8.02 (2*d* with f.s., ^3J(1′,2′) = 8.0, ^3J(3′,4′) = 8.1, H–C(1′), H–C(4′)); 8.31 (*d*, ^3J(8′,9′) = 11.1, H–C(9′)); 7.72, 7.54 (2*dd* with f.s., ^3J(1′,2′) = 8.1, ^3J(3′,4′) = 8.0, ^3J(2′,3′) = ^3J(3′,2′) = 7.1, H–C(2′), H–C(3′)); 7.37 (*dd*, ^3J(6′,7′) = 10.8, ^3J(7′,8′) = 8.6, H–C(7′)); 7.22 (*dd*, ^3J(6′,7′) = 10.9,

$^3J(5',6') = 8.5$, H–C(6')); 7.08 (*ddd*, $^3J(8',9') = 11.1$, $^3J(7',8') = 8.5$, $^4J(6',8') = 0.7$, H–C(8')); 6.38 (*s*, H–C(2)); 3.89 (*s*, MeOCO–C(2)); 3.87 (*s*, MeOCO–C(1)).

Data of Dimethyl (E)*-1-(Benz[*a*]azulen-10-yl)ethen-1,2-dicarboxylate* ((*E*)-**30a**): R_f(hexane/Et_2O 1:1) 0.40. MPLC (hexane/CH_2Cl_2 2:9; flow rate 20 ml/min): t_R 29.5. ^{1}H-NMR (300 MHz, $CDCl_3$): 8.392 (*d*, $^3J(5',6') = 8.3$, H–C(5')); 8.393, 7.56 (2*d* with f.s., $^3J(1',2') = 7.9$, $^3J(3',4') = 7.4$, H–C(1'), H–C(4')); 7.69 (*d*, $^3J(8',9') = 11.1$, H–C(9')); 7.66, 7.50 (2*dd* with f.s., $^3J(1',2') = {}^3J(3',4') \approx 8.0$, $^3J(2',3') = {}^3J(3',2') \approx 7.0$, H–C(2'), H–C(3'); 7.34 (*s*, H–C(2)); 7.26 (*dd*, $^3J(6',7') \approx 11.1$, $^3J(7',8') \approx 8.3$, H–C(7')); 7.13 (*dd*, $^3J(6',7') = 10.9$, $^3J(5',6') = 8.3$, H–C(6')); 6.93 (*ddd*, $^3J(8',9') = 11.0$, $^3J(7',8') = 8.4$, $^4J(6',8') = 0.8$, H–C(8')); 3.75 (*s*, MeOCO–C(2)); 3.44 (*s*, MeOCO–C(1)).

*Data of Dimethyl Benzo[*a*]cyclopent[*cd*]azulen-1,2-dicarboxylate* (**26a**): Blue crystals. M.p. 188.2–189.4° (AcOEt) ([2]: 188°). R_f(hexane/Et_2O 1:1) 0.16. MPLC (hexane/CH_2Cl_2 2:9, flow rate 20 ml/min): t_R 139.0. ^{1}H-NMR: see [2].

*Data of Dimethyl (2*R**,2a*R**)-2,2a-Dihydrobenzo[*a*]cyclopent[*cd*]azulene-1,2-dicarboxylate* (*trans*-**31a**): R_f(hexane/Et_2O 1:1) 0.35. MPLC (hexane/CH_2Cl_2 2:9; flow rate 20 ml/min): t_R 50.0. ^{1}H-NMR (300 MHz, C_6D_6): 8.64 (*d*, $^3J(9,10) = 7.0$, H–C(10)); 7.12–7.01 (*m*, H–C(8), H–C(9)); 6.98 (*d*, $^3J(7,8) = 7.4$, H–C(7)); 6.47 (*d*, $^3J(5,6) = 11.0$, H–C(6)); 6.08 (*dd*, $^3J(5,6) = 11.0$, $^3J(4,5) = 7.1$, H–C(5)); 5.77 (*ddd*, $^3J(3,4) = 10.7$, $^3J(4,5) = 7.1$, $^4J(4,2a) = 2.6$, H–C(4)); 5.47 (*d*, $^3J(3,4) = 10.7$, H–C(3)); 4.18 (*d*, $^3J(2,2a) = 5.0$, H–C(2)); 3.65 (*dd*, $^3J(2,2a) \approx 4.8$, $^3J(2a,4) \approx 2.2$, H–C(2a)); 3.40 (*s*, MeOCO–C(1)); 3.33 (*s*, MeOCO–C(2)). ^{1}H-NOE (400 MHz, C_6D_6): 6.47 (H–C(6)) → 6.98 (H–C(7)) (*s*); 5.47 (H–C(3)) → 4.18 (H–C(2)) (*s*); 4.18 (H–C(2)) → 5.47 (H–C(3)) (*s*); 3.65 (H–C(2a)) → 5.47 (H–C(3)) (*s*).

*Data of Dimethyl (2*R**,2a*S**)-2,2a-Dihydrobenzo[*a*]cyclopent[*cd*]azulene-1,2-dicarboxylate* (*cis*-**31a**): R_f(hexane/Et_2O 1:1) 0.35. MPLC (hexane/CH_2Cl_2 2:9; flow rate 20 ml/min): t_R 47.5. ^{1}H-NMR (300 MHz, C_6D_6): 8.21 (*d*, $^3J(9,10) = 7.4$, H–C(10)); 7.33, 7.19 (2*td*, $^3J(8,7) = {}^3J(8,9) = {}^3J(9,8) = {}^3J(9,10) = 7.5$, $^4J(8,10) = {}^3J(9,7) = 1.1$, H–C(8), H–C(9)); 7.23 (*d*, $^3J(7,8) = 7.2$, H–C(7)); 6.71 (*dd*, $^3J(5,6) = 11.0$, $^4J(4,6) = 1.1$, H–C(6)); 6.35 (*dd*, $^3J(5,6) = 11.0$, $^3J(4,5) = 7.1$, H–C(5)); 6.04 (*ddd*, $^3J(3,4) = 10.9$, $^3J(4,5) = 7.1$, $^4J(4,2a) = 2.7$, H–C(4)); 5.23 (*d* with f.s., $^3J(3,4) = 10.9$, H–C(3)); 4.71 (*d*, $^3J(2,2a) = 9.0$, H–C(2)); 3.65 (*dt*, $^3J(2,2a) = 9.0$, $^3J(2a,3) = {}^4J(2a,4) = 2.3$, H–C(2a)); 3.91 (*s*, MeOCO–C(1)); 3.72 (*s*, MeOCO–C(2)).

4.2. *Diethyl Benzo[*a*]heptalene-6,7-dicarboxylate* (**23b**). 4.2.1. *Formation of* **23b** *in the Presence of [$RuH_2(PPh_3)_4$]*. Azulene **24** (0.101 g, 0.57 mmol) and ADE (0.40 ml, 1.71 mmol) in MeCN (16 ml) were reacted as described in *2.1.1* for 16 h. The molar ratio of **27b**/**28b**/**23b** was 1.19 : < 0.01 : 1.00, based on the integrals of the *s* at 4.48 ppm (H–C(10) of **27b**) and 7.92 ppm (H–C(5) of **23b**). The *s* of H–C(10) of **28b** was not recognizable. The thermal reaction of the mixture in DMF (5 ml) for 2 h, followed by filtration over silica gel (CH_2Cl_2/hexane 4:1) and MPLC (CH_2Cl_2/hexane 2:1), led to pure **23b** (0.0452 g, 23%) as a yellow foam.

4.2.2. *Formation of* **23b** *without a Catalyst*. Azulene **24** (0.116 g, 0.65 mmol) and ADE (0.54 ml) were reacted in MeCN (16 ml) as described in *2.1.4* for 16 h. The molar ratio of **27b**/**28b**/**23b** was 1.68 : < 0.01 : 1.00. The thermal reaction in DMF (5 ml) and the purification as described in *4.2.1* gave pure **23b** (0.0486 g, 21%) as a yellow foam.

Data of **23b**: MPLC (hexane/CH_2Cl_2 1:2; flow rate 20 ml/min): t_R 93.0. ^{1}H-NMR (300 MHz, $CDCl_3$): 7.92 (*s*, H–C(5)); 7.40–7.29 (*m*, H–C(2), H–C(3), H–C(4)); 6.94 (*d*, $^3J(1,2) = 7.5$, H–C(1)); 6.61 (*dd*, $^3J(11,10) = 10.9$, $^3J(11,12) = 6.2$, H–C(11)); 6.54 (*dd*, $^3J(10,11) = 11.2$, $^3J(10,9) = 6.0$, H–C(10)); 6.34 (*dd*, $^3J(9,8) \approx 10.9$, $^3J(9,10) = 6.0$, H–C(9)); 6.17 (*d*, $^3J(8,9) = 10.9$, H–C(8)); 6.01 (*d*, $^3J(12,11) = 6.1$, H–C(12)); 4.18–4.02 (*m*, 2 MeCH_2OCO); 1.21 (*t*, *Me*CH_{2OCo}–C(6)); 1.15 (*t*, *Me*CH_2OCO–C(7)).

4.2.3. *Isolation of Intermediate* **27b** *and Side-Products* (*Z*)-**30b**, trans-**31b**, *and* **26b**. These compounds were obtained by CC and MPLC of the above-described reaction mixtures. Crystallization of the compounds was not attempted. The chromatographically determined yields after thermal rearrangement were as follows (in parentheses yields without catalyst): (*Z*)-**30b**: 4% (3%), *trans*-**31b**: 9% (8%), and **26b**: 22% (21%).

*Data of Diethyl 4b,10-Etheno-10*H*-benz[*a*]azulene-11,12-dicarboxylate* (**27b**): MPLC (hexane/CH_2Cl_2 1:2; flow rate 20 ml/min): t_R 57.0. ^{1}H-NMR (300 MHz, $CDCl_3$): 7.29, 7.12 (2*d*, $^3J(1,2) = 7.1$, $^3J(4,3) = 6.7$, H–C(1), H–C(4)); 7.01, 6.94 (2*t* with f.s., $^3J(2,1) \approx {}^3J(2,3) \approx {}^3J(3,2) \approx {}^3J(3,4) \approx 7.5$, H–C(2), H–C(3)); 6.06 (*d*, $^3J(5,6) = 12.2$, H–C(5)); 5.89 (*dd*, $^3J(6,5) = 12.0$, $^3J(6,7) = 7.5$, H–C(6)); 5.58 (*dd*, $^3J(7,8) = 12.0$, $^3J(7,6) = 7.5$, H–C(7)); 5.43 (*dd*, $^3J(8,7) \approx 12.0$, $^3J(8,9) = 7.5$, H–C(8)); 5.07 (*d*, $^3J(9,8) = 7.6$, H–C(9)); 4.49 (*s*, H–C(10)); 4.20 (*q*, MeCH_2OCO–C(12)); 4.18–4.06 (*m*, MeCH_2OCO–C(11)); 1.24, 1.18 (2*t*, 2 *Me*CH_2OCO).

The secondary intermediate **28b** could not be identified in the reaction mixtures.

*Data of Diethyl (*Z*)-1-(Benz[*a*]azulen-10-yl)ethene-1,2-dicarboxylate* ((*Z*)-**30b**): MPLC (hexane/CH_2Cl_2 1:2; flow rate 20 ml/min): t_R 86.0. ^{1}H-NMR (300 MHz, $CDCl_3$): 8.40 (*dd*, $^3J(5',6') = 8.5$, $^4J(5',7') = 1.0$,

H–C(5′)); 8.33, 7.98 (2*d* with f.s., $^3J(1',2')=8.1$, $^3J(3',4')=7.9$, H–C(1′), H–C(4′)); 8.26 (*d*, $^3J(8',9')=11.3$, H–C(9′)); 7.65, 7.46 (2*dd* with f.s., $^3J(1',2')\approx{}^3J(3',4')\approx8.0$, $^3J(2',3')\approx{}^3J(3',2')\approx7.1$, H–C(2′), H–C(3); 7.29 (*dd*, $^3J(6',7')=10.7$, $^3J(7',8')=8.5$, H–C(7′)); 7.13 (*dd*, $^3J(6',7')=10.9$, $^3J(5',6')=8.4$, H–C(6′)); 7.08 (*ddd*, $^3J(8',9')=11.1$, $^3J(7',8')=8.6$, $^4J(6',8')=0.8$, H–C(8′)); 6.28 (*s*, H–C(2)); 4.27 (*sext.*-like, 2 MeCH_2OCO); 1.30, 1.24 (2*t*, 2 *Me*CH$_2$OCO).

*Data of Diethyl (2*R**,2a*R**)-2,2a-Dihydrobenzo[*a*]cyclopent[*cd*]azulene-1,2-dicarboxylate* (*trans*-**31b**): MPLC (hexane/CH_2Cl_2 1:2; flow rate 20 ml/min): t_R 67.0, ^{1}H-NMR (300 MHz, $CDCl_3$): 8.14 (*d*, $^3J(9,10)=7.5$, H–C(10)); 7.25, 7.10 (2*td*, $^3J(8,7)\approx{}^3J(8,9)\approx{}^3J(9,8)\approx{}^3J(9,10)\approx7.5$, $^4J(8,10)\approx{}^4J(9,7)\approx1.2$, H–C(8), H–C(9)); 7.16 (*d*, $^3J(7,8)=7.2$, H–C(7)); 6.68 (*dd*, $^3J(5,6)=11.0$, $^4J(4,6)=1.0$, H–C(6)); 6.30 (*dd*, $^3J(5,6)=11.0$, $^3J(4,5)=7.1$, H–C(5)); 6.00 (*ddd*, $^3J(3,4)=10.7$, $^3J(4,5)=7.1$, $^4J(4,2a)=2.7$, H–C(4)); 5.64 (*d*, $^3J(3,4)=10.7$, H–C(3)); 4.36–4.24 (*m*, MeCH_2OCO–C(1)); 4.18 (*d*, $^3J(2,2a)=5.8$, H–C(2)); 4.15 (*q*, MeCH_2OCO–C(2)); 3.67 (*quint.*-like, $^3J(2,2a)\approx5.0$, $^4J(2a,4)\approx2.4$, H–C(2a)); 1.33, 1.22 (2*t*, 2 *Me*CH$_2$OCO).

Data of Diethyl Benzo[a]cyclopent[cd]azulene-1,2-dicarboxylate (**26b**): MPLC (hexane/CH_2Cl_2 1:2; flow rate 20 ml/min): t_R 117.0. ^{1}H-NMR (300 MHz, $CDCl_3$): 9.31 (*d*, $^3J(3,4)=9.5$, H–C(3)); 8.28 (*d*, $^3J(6,5)=9.1$, H–C(6)); 8.19 (*t*-like, $^3J(5,4)=10.3$, $^3J(5,6)=9.4$, H–C(5)); 7.95 (*t*-like, $^3J(4,5)=10.3$, $^3J(4,3)=10.2$, H–C(4)); 7.89 (*d*, $^3J(7,8)=7.5$, H–C(7)); 7.56 (*d*, $^3J(10,9)=7.5$, H–C(10)); 7.37 (*t*, $^3J(9,8)=^3J(9,10)=7.5$, H–C(9)); 7.17 (*t*, $^3J(8,7)=^3J(8,9)=7.5$, H–C(8)); 4.51, 4.36 (2*q*, 2 MeCH_2OCO); 1.43, 1.37 (2*t*, 2 *Me*CH$_2$OCO).

5. Kinetic and Mechanistic Investigations. – 5.1. *Thermal Rearrangement of the Primary Intermediate* **2a**. Benzotricycle **2a** (6 mg) was dissolved in MeCN (2 ml) under Ar and heated at $100.0\pm0.1°$. At irregular time intervals samples were taken, diluted with MeCN, and immediately subjected to HPLC (*Spherisorb CN*; hexane/i-PrOH 93:7; flow rate 1 ml/min). Retention times (t_R): 6.2 (**9a**), 8.3 (**2a**), and 9.8 min (**3a**). UV detection at the isosbestic point of **9a**, **2a**, and **3a** (363.6 nm). The results are listed below:

Entry	Time [s]	**9a** [%]	**2a** [%]	**3a** [%]
1	0	1.729	91.328	4.473
2	3600	4.220	85.680	7.641
3	9000	6.767	79.255	11.192
4	16200	10.551	69.736	16.638
5	23400	12.131	62.918	21.472
6	30600	13.614	56.114	26.278
7	39600	14.176	48.188	33.196
8	50400	14.724	38.192	41.541
9	73800	12.686	31.080	49.473

The decrease of **2a** followed first-order kinetics with $k(-[\mathbf{2a}])=(1.68\pm0.10)\cdot10^{-5}\ s^{-1}$ ($r^2=0.996$).

5.2. *Thermal Rearrangement of the Secondary Intermediate* **9a**. *Dewar*-heptalene **9a** was dissolved in MeCN under Ar and heated at $100.0\pm0.1°$. At irregular time intervals, samples were taken, diluted with MeCN, and immediately analyzed as described above (*5.1*). Intermediate **2a** was not formed during the rearrangement of **9a**. The results are listed below:

Entry	Time [s]	**9a** [%]	**3a** [%]
1	0	100	0
2	1800	97.736	2.264
3	5400	92.551	7.449
4	9000	86.918	13.882
5	12600	81.847	17.542
6	18000	74.466	24.739
7	23400	69.545	29.440
8	30600	62.707	35.458
9	41400	43.689	53.693
10	70200	13.843	79.335

The decrease of **9a** followed first-order kinetics with $k(-[\mathbf{9a}])=(1.56\pm0.07)\cdot10^{-5}\ s^{-1}$ ($r^2=0.998$).

5.3. *Formation of* **3a** *in the Presence of [$RuH_2(PPh_3)_4$] and under Exclusion of Laboratory Light*. Azulene **1** (0.099 g, 0.3 mmol), ADM (0.11 ml), and the catalyst (2 mol-%, 0.0069 g) were dissolved in MeCN (3 ml) and

reacted in the dark as described in *2.1.1.* The molar ratio of **2a**/**9a**/**3a** was 4.03 : 1.03 : 1.00 according to ^{1}H-NMR analysis. Neither *trans*-**10a** nor *cis*-**10a** were detectable. However, traces of **11a** and **12a** were distinctly recognizable. The thermal rearrangement of the mixture in DMF (5 ml) led to 91% of **3a** (0.130 g). Trace amounts of **11a** and **12a** were still recognizable by ^{1}H-NMR, but no other compound.

5.4. *Photochemical Rearrangement of* **9a** *to* trans-**10a** *and* cis-**10a**. 5.4.1. *With Daylight. Dewar*-heptalene **9a** (1.5 mg) was dissolved in C_6D_6 (0.5 ml), and the soln. was exposed to daylight for 2 days. ^{1}H-NMR Analysis showed, besides **9a**, the presence of *trans*-**10a** and *cis*-**10a**. The molar ratio was 1.00 : 0.52 : 0.27.

5.4.2. *Irradiation with 366-nm Light. Dewar*-heptalene **9a** (2.4 mg) was dissolved in benzene (3 ml), the soln. was flushed with N_2, and then irradiated with 366-nm light of a fluorescent tube for 15 h under N_2. A mixture of *trans*-**10a**/*cis*-**10a** 1 : 1 was formed quantitatively. Irradiation for only 5 h resulted in a molar ratio of **9a**/*trans*-**10a**/*cis*-**10a** 1.00 : 0.42 : 0.54.

5.5. *Thermal Rearrangement of* trans-**10a** *and* cis-**10a** *to* **11a**. 5.5.1. *In DMF.* Photoproduct *trans*-**10a** (4.0 mg) was dissolved in DMF (1 ml), the soln. was flushed with Ar and then heated for 1 h at 150°. The fluoranthene-1,2-dicarboxylate **11a** was formed quantitatively. The same reaction, performed with *cis*-**10a**, also gave quantitatively **11a**.

5.5.2. *In Cumene.* Photoproduct *trans*-**10a** (4.9 mg) was dissolved in cumene (2 ml), the soln. was flushed with Ar and heated under reflux (152°) for 1 h. After removal of cumene, ^{1}H-NMR analysis showed a molar ratio of *trans*-**10a**/**11a** 24 : 1.

5.5.3. *In MeCN in the Presence of [$RuH_2(PPh_3)_4$]*. Photoproduct *trans*-**10a** (3.0 mg) was dissolved in MeCN (3 ml), the catalyst (1.5 mg, 20 mol-%) was added, the soln. was flushed with Ar, and then heated for 18 h at 100°. ^{1}H-NMR Analysis showed that mainly **11a** had been formed. Small amounts of *trans*-**10a** and *cis*-**10a** were still present.

5.6. *Formation of* (E)- *and* (Z)-**8a** *from* **1** *and ADM in the Presence of* CF_3COOH (TFA). Azulene **1** (0.165 g, 0.50 mmol) was dissolved in toluene (5 ml), ADM (0.213 g, 1.50 mmol) and then 10 drops of TFA were added, and the mixture was heated at 50°. After 9 days, TLC indicated that all of **1** (R_f(hexane/Et_2O 1 : 1) 0.62) had been consumed, and green spots of (*E*)-**8a** and (*Z*)-**8a** (R_f 0.33 and 0.21, resp.) were present. Toluene was removed under reduced pressure, and the products were separated by CC with hexane/Et_2O 1 : 1. After crystallization from Et_2O/hexane, (*Z*)-**8a** (0.033 g, 14%) was obtained as green needles and (*E*)-**8a** (0.193 g, 82%) in dark green prisms.

On heating in DMF (2 h, 150°) or MeCN (18 h, 100°), (*E*)-**8a** was recovered unchanged. Similarly, (*Z*)-**8a** was quantitatively recovered after heating in MeCN (18 h, 100°).

5.7. *Thermal Rearrangement of the Primary Intermediate* **2c**. 5.7.1. *In MeCN.* Benzotricycle **2c** (5.7 mg) and phenyl benzoate (6.6 mg) as an internal standard were dissolved in MeCN (8.5 ml), the soln. was flushed with Ar and then heated to 100.0 ± 0.1°. Samples were taken at irregular time intervals, diluted with MeCN, and immediately subjected to HPLC (*Spherisorb ODS2*, reversed phase; MeCN/H_2O 1 : 3; flow rate 1 ml/min). UV Detection at 260 nm. t_R: 4.5 (phenyl benzoate), 8.3 (**2c**), 10.9 (**3c**), and 17.1 min (**9c**). The results are listed below:

Entry	Time [s]	**2c** [%]	Ratio of the integrals [%][a]) **2c**/**9c**/**3c**
1	0	100	100 : < 0.01 : < 0.01
2	3600	96.4	97 : < 0.01 : 3
3	7200	93.4	95 : < 0.01 : 5
4	10800	90.8	90 : 3 : 7
5	16200	87.0	85 : 4 : 11
6	21600	81.6	81 : 6 : 13
7	28800	78.2	75 : 7 : 18
8	36000	73.3	70 : 8 : 22
9	46800	67.1	64 : 9 : 27
10	90000	59.4	55 : 10 : 35

[a]) < 0.01 means that the compound could not be detected within the range of the sensitivity of the detector.

The decrease of **2c** followed first-order kinetics with $k(-[\mathbf{2c}]) = (8.46 \pm 0.35) \cdot 10^{-6}\ s^{-1}$ ($r^2 = 0.998$).

5.7.2. *In MeCN in the Presence of LiBr.* Benzotricycle **2c** (4.1 mg), LiBr (0.13 mg, 20 mol-%), and phenyl benzoate (5.1 mg) as an internal standard were dissolved in MeCN (6.2 ml), the soln. was flushed with Ar and

Table 9. *Crystallographic Data*

Parameter	**2c**	**3a**	(E)-**8a**	*endo*-**7**	*exo*-**7**
Crystallized from	CH_2Cl_2/hexane/toluene	CH_2Cl_2/hexane	Et_2O/hexane	Et_2O/hexane	Et_2O/hexane
Empirical formula	$C_{36}H_{32}O_4$	$C_{32}H_{24}O_4$	$C_{32}H_{24}O_4$	$C_{26}H_{20}$	$C_{26}H_{20}$
Formula weight	528.64	472.54	472.54	332.44	332.44
Crystal color, habit	yellow, prism	yellow, prism	brown, prism	orange, prism	yellow, prism
Crystal dimensions [mm]	$0.23 \times 0.33 \times 0.45$	$0.35 \times 0.38 \times 0.48$	$0.15 \times 0.20 \times 0.38$	$0.14 \times 0.32 \times 0.42$	$0.12 \times 0.33 \times 0.46$
Crystal temp. [K]	173(1)	173(1)	173(1)	173(1)	173(1)
Crystal system	monoclinic	monoclinic	triclinic	monoclinic	triclinic
Space group	$P2_1/n$	$P2_1/n$	$P\bar{1}$	$P2_1/c$	$P\bar{1}$
Z	4	4	2	4	2
Lattice parameters					
Reflections for cell determination	25	23	22	24	23
2θ range [°]	36 – 40	39 – 40	34 – 40	35 – 40	38 – 40
a [Å]	9.609(2)	14.276(2)	11.037(3)	10.103(3)	9.967(3)
b [Å]	15.594(3)	11.518(2)	11.414(4)	18.782(3)	10.446(3)
c [Å]	19.638(2)	16.189(2)	10.104(5)	10.033(3)	9.917(2)
α [°]	90	90	91.16(4)	90	98.35(2)
β [°]	101.65(1)	111.613(7)	92.77(3)	110.20(2)	113.40(2)
γ [°]	90	90	77.27(3)	90	73.00(2)
V [Å^3]	2882.2(9)	2474.8(6)	1239.9(9)	1786.8(7)	905.6(5)
D_x [g cm^{-3}]	1.218	1.268	1.266	1.236	1.219
Absorption coefficient μ(MoK_α) [mm^{-1}]	0.0782	0.0773	0.0826	0.0697	0.0690
$2\theta_{(max)}$ [°]	55	60	60	55	60
Total reflections measured	7244	7823	7569	4451	5547
Symmetry independent reflections	6599	7212	7220	4089	5268
Reflections used	4437 [$I > 2\sigma(I)$]	5399 [$I > 3\sigma(I)$]	3978 [$I > 3\sigma(I)$]	2332 [$I > 3\sigma(I)$]	3618 [$I > 3\sigma(I)$]
Parameters refined	490	421	421	315	316
Final R	0.0494	0.0382	0.0495	0.0426	0.0555
R_w	0.0435	0.0372	0.0430	0.0343	0.0563
Goodness of fit s	1.753	1.971	1.753	1.737	2.515
Final δ_{max}/σ	0.0005	0.0003	0.0003	0.0006	0.0002
$\Delta\rho$ (max; min) [e Å^{-3}]	0.26; – 0.18	0.23; – 0.17	0.28; – 0.22	0.20; – 0.18	0.35; – 0.29

then heated to $100.0 \pm 0.1°$. Analyses of the taken samples as described above (*5.7.1*). The results are listed below:

Entry	Time [s]	**2c** [%]	Ratio of the integrals [%][a]) **2c**/**9c**/**3c**
1	0	100	99 : < 0.01 : 1
2	3600	98.0	97 : < 0.01 : 1
3	7200	93.6	94 : < 0.01 : 1
4	10800	90.4	86 : 3 : 11
5	16200	85.7	83 : 5 : 12
6	21600	80.8	78 : 6 : 16
7	28800	76.9	72 : 8 : 20
8	36000	71.3	67 : 9 : 24
9	46800	65.5	59 : 11 : 30
10	90000	52.5	47 : 12 : 41

[a]) < 0.01 means that the compound could not be detected within the range of the sensitivity of the detector. The decrease of [**2c**] followed first-order kinetics with $k(-[\mathbf{2c}]) = (9.24 \pm 0.45) \cdot 10^{-6}$ s^{-1} ($r^2 = 0.997$).

Table 9 *(cont.)*

9a	*cis*-**10a**	*trans*-**10a**	**11a**	**21a**	**22**
Et_2O/hexane	CH_2Cl_2/hexane	CH_2Cl_2/hexane	CH_2Cl_2/hexane	CH_2Cl_2/hexane	Et_2O/hexane
$C_{32}H_{24}O_4$	$C_{32}H_{24}O_4$	$C_{32}H_{24}O_4$	$C_{32}H_{22}O_4$	$C_{26}H_{20}O_4$	$C_{21}H_{24}O_4$
472.54	472.54	472.54	470.52	396.44	340.42
yellow, prism	orange, prism	red, prism	yellow, prism	orange, prism	yellow, prism
$0.25 \times 0.38 \times 0.43$	$0.18 \times 0.30 \times 0.45$	$0.12 \times 0.30 \times 0.33$	$0.13 \times 0.33 \times 0.52$	$0.20 \times 0.26 \times 0.50$	$0.20 \times 0.33 \times 0.43$
173(1)	173(1)	173(1)	173(1)	173(1)	173(1)
monoclinic	triclinic	monoclinic	triclinic	monoclinic	triclinic
$P2_1/c$	$P\bar{1}$	$P2_1/n$	$P\bar{1}$	$C2/c$	$P\bar{1}$
4	2	4	2	8	2
25	21	23	22	25	22
36 – 40	38 – 40	31 – 39	39 – 40	38 – 40	36 – 39
16.102(2)	11.158(2)	7.065(4)	11.438(2)	28.868(4)	9.286(3)
9.277(3)	11.536(2)	11.117(5)	11.518(2)	10.552(3)	11.711(4)
17.541(2)	10.798(2)	30.341(4)	8.998(2)	13.139(4)	9.090(2)
90	114.36(1)	90	98.25(2)	90	97.72(2)
105.789(9)	100.50(2)	96.02(4)	97.17(2)	99.04(2)	110.97(2)
90	74.27(1)	90	89.56(2)	90	88.70(3)
2521.3(8)	1214.8(4)	2370(2)	1163.9(4)	3953(2)	914.4(5)
1.245	1.292	1.324	1.342	1.332	1.236
0.0813	0.0843	0.0864	0.0878	0.0892	0.0844
60	60	55	60	55	60
7998	7412	6173	7090	4869	5629
7327	7079	5432	6778	4531	5327
4586 [$I > 3\sigma(I)$]	4888 [$I > 3\sigma(I)$]	3282 [$I > 3\sigma(I)$]	5090 [$I > 3\sigma(I)$]	3525 [$I > 2\sigma(I)$]	3679 [$I > 3\sigma(I)$]
421	422	421	414	352	322
0.0451	0.0494	0.0447	0.0434	0.0408	0.0488
0.0411	0.0462	0.0401	0.0429	0.0385	0.0489
1.754	2.218	1.843	2.090	1.814	2.158
0.0001	0.0003	0.0002	0.0006	0.0003	0.0005
0.31; – 0.21	0.31; – 0.27	0.23; – 0.20	0.32; – 0.23	0.27; – 0.18	0.33; – 0.23

6. Analytical Chromatographic Resolution of the Dialkyl Benzo[*a*]heptalene-6,7-dicarboxylates. The anal. separations were investigated on a *Chiralcel OD* column (5 μm; 4.6×250 mm). For CD spectra and absolute configurations, see [3].

6.1. *Antipodes of* **23a**. Eluant hexane/i-PrOH 93 : 7; flow rate 0.8 ml/min: base-line separation with $t_R(1)$ 15.0 and $t_R(2)$ 121.5 min; $t_R(2)/t_R(1) = 8.11$.

6.2. *Antipodes of* **21a**. Eluant hexane/i-PrOH 93 : 7; flow rate 0.8 ml/min: base-line separation with $t_R(1)$ 31.6 and $t_R(2)$ 69.1 min; $t_R(2)/t_R(1) = 2.19$.

6.3. *Antipodes of* **3**. 6.3.1. *Dimethyl Ester* **3a**. Eluant hexane/i-PrOH 93 : 7; flow rate 0.8 ml/min: base-line separation with $t_R(1)$ 18.1 and $t_R(2)$ 26.8 min; $t_R(2)/t_R(1) = 1.48$; eluant hexane/i-PrOH 95 : 5; flow rate 0.8 ml/min: base-line separation with $t_R(1)$ 20.9 and $t_R(2)$ 32.5 min; $t_R(2)/t_R(1) = 1.55$; eluant hexane/EtOH 97 : 3; flow rate 0.8 ml/min: base-line separation with $t_R(1)$ 18.1 and $t_R(2)$ 26.2 min; $t_R(2)/t_R(1) = 1.45$.

6.3.2. *Diethyl Ester* **3b**. Eluant hexane/i-PrOH 95 : 5; flow rate 0.8 ml/min: no base-line separation with $t_R(1)$ 16.5 and $t_R(2)$ 18.1 min; $t_R(2)/t_R(1) = 1.09$; eluant hexane/EtOH 97 : 3; flow rate 0.8 ml/min: no base-line separation with $t_R(1)$ 13.8 and $t_R(2)$ 14.9 min; $t_R(2)/t_R(1) = 1.08$.

6.3.3. *Diisopropyl Ester* **3c**. Eluant hexane/i-PrOH 95 : 5; flow rate 0.8 ml/min: base-line separation with $t_R(1)$ 10.01 and $t_R(2)$ 14.26 min; $t_R(2)/t_R(1) = 1.42$; eluant hexane/EtOH 97 : 3; flow rate 0.8 ml/min: base-line separation with $t_R(1)$ 9.4 and $t_R(2)$ 11.5 min; $t_R(2)/t_R(1) = 1.23$.

6.3.4. *Di(*tert-*butyl) Ester* **3d**. Eluant hexane/i-PrOH 95:5; flow rate 0.8 ml/min: no base-line separation with $t_R(1)$ 7.1 and $t_R(2)$ 7.6 min; $t_R(2)/t_R(1) = 1.07$; eluant hexane/EtOH 97:3; flow rate 0.8 ml/min: no separation of the antipodes, $t_R(1) = t_R(2)$ 7.3 min; $t_R(2)/t_R(1) = 1.00$.

7. X-ray Crystal-Structure Determinations of Compounds 2c, 3a, *endo*-7, *exo*-7, (*E*)-8a, 9a, *cis*-10a, *trans*-10a, 11a, 21a, and 22[17]). – All measurements were conducted at low-temperature on a *Rigaku AFC5R* diffractometer using graphite-monochromated MoK_α radiation ($\lambda = 0.71069$ Å) and a 12-kW rotating anode generator. The intensities were collected using $\omega/2\theta$ scans, except for *trans*-**10a**, where ω scans were employed. Three standard reflections, which were measured after every 150 reflections, remained stable throughout each data collection. The intensities were corrected for *Lorentz* and polarization effects, and, in the case of **3a** and *endo*-**7**, an empirical absorption correction [33] was applied. Each structure was solved by direct methods using SHELXS86 [34] which revealed the positions of all non-H-atoms. The non-H-atoms were refined anisotropically. The H-atoms were located in a difference electron-density map, and their positions were refined together with individual isotropic thermal parameters. All refinements were carried out on F by full-matrix least-squares procedures, which minimized the function $\Sigma w(|F_o| - |F_c|)^2$, where $w = [\sigma^2(F_o) + (0.005F_o)^2]^{-1}$. A correction for secondary extinction was applied for **2c**, *exo*-**7**, *cis*-**10a**, **11a, *and* 21a**. In the case of *exo*-**7**, five reflections were also excluded from the final refinement because of suspected extinction effects. The data collection and refinement parameters for each compound are listed in *Table 9*. Neutral-atom-scattering factors for non-H-atoms were taken from [35a], and the scattering factors for H-atoms from [36]. Anomalous dispersion effects were included in F_c [37]; the values for f' and f'' were taken from [35b]. All calculations were performed with the TEXSAN [38] crystallographic software package and the figures were produced with ORTEPII [39].

REFERENCES

[1] A. J. Rippert, H.-J. Hansen, *Helv. Chim. Acta* **1993**, *76*, 2906.
[2] R. Hunziker, D. Sperandio, H.-J. Hansen, *Helv. Chim. Acta* **1995**, *78*, 772.
[3] P. Mohler, A. J. Rippert, H.-J. Hansen, *Helv. Chim. Acta* **2000**, *83*, in press.
[4] L. A. Kapicak, M. A. Battiste, *Synthesis* **1971**, 153.
[5] Y. Chen, R. W. Kunz, P. Uebelhart, R. H. Weber, H.-J. Hansen, *Helv. Chim. Acta* **1992**, *75*, 2447.
[6] R.-A. Fallahpour, H.-J. Hansen, *Helv. Chim. Acta* **1995**, *78*, 1419.
[7] R.-A. Fallahpour, H.-J. Hansen, *High Pressure Res.* **1992**, *11*, 125; *iidem*, *Helv. Chim. Acta* **1995**, *78*, 1933.
[8] W. Ried, D. Freitag, *Chem. Ber.* **1966**, *99*, 2675.
[9] G. L. Closs, K. D. Krantz, *J. Org. Chem.* **1966**, *31*, 638.
[10] M. Oki, 'Application of Dynamic NMR Spectroscopy to Organic Chemistry', VCH Publ., Inc., Deerfield Beach, 1985, p. 287 ff.
[11] M. Karplus, *J. Am. Chem. Soc.* **1963**, *85*, 2870.
[12] M. Bühl, W. Kozminski, A. Linden, D. Nanz, D. Sperandio, H.-J. Hansen, *Helv. Chim. Acta* **1994**, *77*, 1940.
[13] A. J. Rippert, H.-J. Hansen, *Helv. Chim. Acta* **1993**, *76*, 2876.
[14] A. J. Rippert, H.-J. Hansen, *Helv. Chim. Acta* **1999**, in preparation.
[15] Y. Chen, Ph. D. thesis, University of Zurich, 1993; E. A. Lehto, Ph. D. thesis, University of Zurich, 1997; Y. Chen, E. Lehto, P. Uebelhart, H.-J. Hansen, unpublished results.
[16] K. Hafner, H. Diehl, H. U. Süss, *Angew. Chem.* **1976**, *88*, 121; *ibid. Int. Ed.* **1976**, *15*, 104.
[17] P. Brügger, P. Uebelhart, R. W. Kunz, R. Sigrist, H.-J. Hansen, *Helv. Chim. Acta* **1998**, *81*, 2201; R.-A. Fallahpour, H. Kandler, A. Linden, A. J. Rippert, P. Uebelhart, H.-J. Hansen, in preparation.
[18] P. Uebelhart, H.-J. Hansen, *Helv. Chim. Acta* **1992**, *75*, 2493.
[19] Y. Chen, H.-J. Hansen, *Helv. Chim. Acta* **1993**, *76*, 168.
[20] J. Guspanova, R. Knecht, M. Lagana, Ch. Weymuth, H.-J. Hansen, *Helv. Chim. Acta* **1997**, *80*, 1375.
[21] a) A. A. S. Briquet, H.-J. Hansen, *Helv. Chim. Acta* **1994**, *77*, 1940; b) A. J. Rippert, Ph. D. thesis, University of Zurich, 1994.

---

[17]) Crystallographic data (excluding structure factors) for the structures reported in this paper have been deposited with the *Cambridge Crystallographic Data Centre* as supplementary publication nos. CCDC-133872–133882 for **2c**, **3a**, *endo*-**7**, *exo*-**7**, (*E*)-**8a**, **9a**, *cis*-**10a**, *trans*-**10a**, **11a, 21a**, and **22**, respectively. Copies of the data can be obtained free of charge on application to the CCDC, 12 Union Road, Cambridge CB2 1EZ, UK (fax: +44-(0)1223-336033; email: deposit@ccdc.cam.ac.uk).

[22] W. von Doering, D. W. Wiley, *Tetrahedron* **1960**, *11*, 183; V. Nair, G. Anilkumar, *Synlett* **1998**, 950.
[23] K. W. Muir, G. A. Sim, *J. Chem. Soc. (B)* **1968**, 667.
[24] P. Mohler, Ph. D. thesis, University of Zurich, 1999.
[25] P. Uebelhart, A. Linden, H.-J. Hansen, Y. A. Ustynyuk, O. A. Trifonova, N. G. Akhmedov, V. I. Mstislawsky, *Helv. Chim. Acta* **1999**, *82*, 1930.
[26] A. A. S. Briquet, P. Uebelhart, H.-J. Hansen, *Helv. Chim. Acta* **1996**, *79*, 2282.
[27] A. Magnussen, H.-J. Hansen, *Helv. Chim. Acta* **1997**, *80*, 545.
[28] G. Melone, Ph. D. thesis, University of Zurich, 1999.
[29] W. F. Maddams, R. Schnurmann, *J. Chem. Phys.* **1951**, *19*, 973; F. Diederich, K. Dick, *J. Am. Chem. Soc.* **1984**, *106*, 8024.
[30] J. J. Levison, S. D. Robinson, *J. Chem. Soc. (A)* **1970**, 2947.
[31] G. Giordano, R. H. Crabtree, *Inorg. Synth.* **1990**, *28*, 83.
[32] D. Sperandio, H.-J. Hansen, *Helv. Chim. Acta* **1995**, *78*, 765.
[33] N. Walker, D. Stuart, *Acta Crystallogr., Sect. A* **1983**, *39*, 158.
[34] G. M. Sheldrick, SHELXS86. *Acta Crystallogr., Sect. A* **1990**, *46*, 467.
[35] a) E. N. Maslen, A. G. Fox, M. A. O'Keefe, in 'International Tables for Crystallography', Vol. C, Ed. A. J. C. Wilson, Kluwer Academic Publishers, Dordrecht, 1992; Table 6.1.1.1, pp. 477–486; b) D. C. Creagh, W. J. McAuley, *ibid.*, Table 4.2.6.8, pp. 219–222.
[36] R. F. Stewart, E. R. Davidson, W. T. Simpson, *J. Chem. Phys.* **1965**, *42*, 3175.
[37] J. A. Ibers, W. C. Hamilton, *Acta Crystallogr.* **1964**, *17*, 781.
[38] TEXSAN. Single Crystal Structure Analysis Software, Version 5.0. Molecular Structure Corporation, The Woodlands, Texas, 1989.
[39] C. K. Johnson, ORTEPII. Report ORNL-5138, Oak Ridge National Laboratory, Oak Ridge, Tennessee 1976.

Received August 31, 1999